UNIVERSITÀ POLITECNICA DELLE MARCHE

FACOLTÀ DI INGEGNERIA

Corso di Laurea Magistrale in Biomedical Engineering

Analysis of the spatial distribution of BOLD activations evoked in human primary gustatory area by different tastants, to build a chemiotopic map

Relatore:
Prof. **Fabri Mara**

Tesi di laurea di:
Tomaiuolo Federica

Correlatore:
Prof. **Burattini Laura**
Dott. **Marcantoni Ilaria**

A. A. 2021/2022

INDEX

INTRODUCTION

The act of eating is often thought as a means of survival, that in humans is controlled by specific hormones able to activate when we are full or hungry. Nevertheless, this mechanism does not explain why we prefer a given food with respect to another, that is a condition purely related to the concept of flavour.

Perception of flavour of food is a complex process, which involves four sensory modalities:

1. A *visual valuation* of the food gives an initial impression which allows to decide if what we are going to eat is attractive and, consequentially, tasty [1,8].
2. Then, a *somatosensory stimulation* arises from touch, proprioception and temperature, due to thermo-, mechano- and noci-receptors placed across the oral mucosa and able to identify the physical properties of the food that we are eating [8,13,14,33].
3. *Olfaction* is also stimulated by the retronasal cavity, also known as "retronasal smell", where odorous stimuli placed in the oral cavity are sampled during exhalation via the back of the throat [1, 8, 32].
4. Finally, *taste* is perceived from specific receptors of the tongue.

Once that the stimulus is inside the oral cavity, it will be ingested or rejected only after the evaluation of these multisensory attributes.

One of the most important properties of food is taste, which comes from the combination of sweet, sour, salty, bitter, and pleasant sensations coming from our tongue. The pathway through which these gustative signals are sent from the mouth to the brain and in particular which region of the brain is involved in the process of gustation is still under investigation.

Gustatory impulses originate as the response of specific cells called taste buds placed over the oral cavity and innervated by three specific cranial nerves (facial, glossopharyngeal and vagus nerve), which deliver the gustative information towards the brain as three separate pathways that converge in a region known as nucleus solitarius or gustatory nucleus. Starting from this point, gustative information is delivered in various specific districts across the outermost layer of our brain, known as grey matter or cerebral cortex. These cortical areas aimed to the integration of gustatory information are classified into two principal regions, known as primary and secondary gustatory cortex, which differentiate according to sensory inputs to be integrated.

The primary taste cortex or primary gustatory area (PGC) is mostly involved in the representation of the identity and intensity of taste [9 - 13].

The secondary taste cortex receives projections from (i) the primary olfactory cortex (involved in olfaction processing), that may be critical for flavor perception, and (ii) from a region called hypothalamus, in order to integrate taste responses with the sense of satiety [7 - 9].

In addition to the gustative information, also somatosensory information is projected from the tongue to other specific regions of the cerebral cortex [3,11].

Nevertheless, the human gustatory system, in comparison to other sensory organs (such as visual or auditory) is less studied and there are still many unknowns about the centers of the brain involved in this process.

Until the advent of neuroimaging techniques, the investigation of the human cortical gustatory area derived entirely from studies of cerebral lesions in clinical populations, even if with lack of information about the precise location of lesion. Nowadays, non-invasive clinical studies using imaging methods such as functional magnetic resonance imaging (fMRI) confirmed the importance of these regions in gustatory processing. Moreover, the multisensory capability of the mouth is unique, as many neuroimaging and electrophysiological studies suggest, where strong overlap within the brain of the different sensory modalities originating in the mouth has been showed.

This research investigates the spatial distribution of bold activations evoked in the human primary gustatory area by three different tastants (sweet, salty and water), with the purpose of building a chemiotopic map.

In order to achieve this objective, a statistical analysis has been performed across functional magnetic resonance images of a population of healthy individuals, which were stimulated during the acquisition by different tastants via a specific block protocol.

1. THE BRAIN

1.1 ANATOMY OF THE BRAIN

The **Nervous System** is the command centre of our body, able to control our movements, memory, sense and automatic responses, as well as every kind of processes performing in our body such as digestion or breathing. It can be subdivided anatomically in two main parts, known as Central Nervous System (CNS) and Peripheral Nervous System (PNS) [1, 4, 7, 31, 32].

- The **CNS** is composed of the *brain* and the *spinal cord* and consists in the centre of processing of our body.
- The **PNS** is made of all the *nerves* that connect the brain and the spinal cord to the rest of the body.

The Nervous System can also be classified functionally according to the kind of information to be processed [4,7].

- The **Somatic Nervous System** is made of all the structures of both the CNS and PNS aimed to the integration of:
  - *Sensory (afferent) information*, coming from the body, that can be conscious or unconscious and is related to vision, touch or pain.
  - *Motor (efferent) information*, coming from the brain, that refers to all those commands directed to the voluntary muscles.
- The **Autonomic Nervous System** is characterised of all the structures of both CNS and PNS involved in the processing of sensory inputs coming from the visceral organs, such as the digestive or the cardiovascular system. At the same way, it is also responsible of the motor control of the involuntary muscles (of cardiovascular system and viscera).

To maintain coherence with this work, only the CNS structures with major focus on the brain and its deeper areas will be described.

The brain is an organ that controls all the functions of our body and allows us to interact with the outside environment. Deeply, it receives inputs coming from our five senses (sight, smell, touch, taste and hearing), integrates the information received and store it in our memory, and elaborate an adequate response. In this way, it is able to control our thoughts, memory, speech, movement and all the functions of our organs.

Anatomically, the brain is enclosed into the skull and characterised of three main regions: the cerebrum, the brainstem and the cerebellum, visible on Figures 1 and 2 [4,7].

1.1.1 Cerebrum

The cerebrum is the largest part of the brain, broken up into two cerebral hemispheres (left and right) divided by means of a median segment known as *corpus callosum*.

Each hemisphere is organised in six lobes, that are all connected among each other and take their name from the cranial bone they are in contact with: *frontal, temporal, parietal, occipital, central (insula)* and *limbic*. The portion of the frontal, parietal and temporal lobes that overlie the insula is known as "operculum" [4,7].

The surface is marked through various incisures referred to as *sulci* (or sometimes fissures), among which it is important to denote the longitudinal fissure, which divides the left hemisphere from the right one. Among the several sulci across each lobe, it is also of relevance the Sulcus of Sylvius and the *Central Sulcus of Rolando*, that are placed respectively in the basal surface of the brain toward the parietal lobe and obliquely from the lateral Sylvius sulcus to the medial surface [7].

The raised ridge between two sulci is known as "gyrus". It is possible to differentiate [7]:

- The *precentral gyrus*, which is anterior and parallel to the central sulcus of Rolando.
- The *postcentral gyrus*, which is posterior and parallel to the central sulcus of Rolando.

1.1.2 Cerebellum

The cerebellum, also known as "little brain", is located under the cerebrum and acts to coordinate muscle movements, maintain posture and balance [4, 7, 32]. It is always in contact with the cerebral cortex (the outermost layer surrounding the brain, also known as "grey matter" [42]), from which it receives specific instructions, here processed in adequate responses that are sent to the motor cerebral cortex so to be translated in voluntary muscle contractions.

1.1.3 Brainstem

The brainstem is located at the base of the brain, to connect the cerebrum with the spinal cord and the cerebellum, and plays a critical role for breathing, blood pressure, heart rate and state of alert/reaction to danger [39].

It is composed of three parts here described from the top to the bottom [4, 7, 31 - 33]:

- the *midbrain* that regulates eye movements and pain suppression;
- the *pons* that controls facial movements, hearing and balance;
- the *medulla oblongata* that regulates breathing, heart rate, blood pressure and some autonomic movements (reflexes) such as swallowing, coughing and sneezing.

1.1.4 Deep structures of the brain

Deep inside the brain are the thalamus and the hypothalamus.

- The *thalamus* is an egg-shaped structure in the middle of the brain, responsible for moving information to and from the lobes like a relay station {8}. All sensory (except for smell) and motor (movement) information must be processed through the so-called *thalamic nucleus* before that is sent for further integration to the cerebral cortex. Moreover, it has also a critical role for sleeping, consciousness, learning and memory.
- The *hypothalamus* is fundamental in the homeostasis maintenance [31], due to its capability of connecting the CNS with the endocrine system. More in detail, it controls appetite, thirst and body temperature, and it is responsible of some metabolic processes, since it produces specific hormones aimed to control the pituitary gland secretions.

A detailed representation of all the anatomical structures of the brain above discussed, with focus on the cerebral cortex areas is available on Figure 1 and 1.2.

1.1.5 Cerebral cortex

The cerebral cortex is the covering of the cerebrum, constituting about the 40% of the brain and containing 100 billion of neurons. This area has been subdivided into different regions depending on several structural and functional criteria. The functions of different areas of the cortex are still under investigation, thanks also to the usage of many imaging techniques such as positron-emission tomography (PET) and functional magnetic resonance imaging (fMRI) [4,7].

One of the most common schemes used for a functional classification of the cortical regions is that of Brodmann (1909), who identified a total of 52 different areas according to a cytoarchitectural procedure, in which a microtome was used to parse the brain and link the various concentrations of neurons to specific functions and regions of the cortex [4,7].

Some researchers classify the cerebral cortex areas depending on three main types of functions (sensory, motor and association areas), as it is possible to appreciate in Figure 3.

- **Sensory areas** receive sensory information from our senses and from the external environment. This large region comprehends two distinct sub-districts denoted as *primary somatosensory cortex* (SI) and *secondary somatosensory cortex* (SII) [4,7, 42].
  - The *primary somatosensory cortex* includes the postcentral gyrus across the parietal lobe and extends up to central sulcus. This area obtains inputs from the so-called Ventral Posterior Nucleus of the thalamus (VPN), which in turn receives sensory information from the contralateral side of the head and body. More in detail, neurons located in this region receive somatic sensation related to touch, pressure, pain, temperature and gustation [4,7].

    The projection on this area has been mapped by means of a topographic representation of the sensory distribution along the surface of the postcentral gyrus of the parietal lobe, denoted as "sensory homunculus", shown in Figure 4 [4,7,42,43].
  - The *secondary somatosensory cortex* extends below the primary motor and sensory areas, and integrates inputs related to general sensory information such as touch, position sense, pressure and pain [7].
- **Motor areas** constitute the surface of the so-called precentral gyrus, located in the frontal lobe. These areas are involved in voluntary muscle movements, such as coordination, planning of complex movements and learning through imitation/empathy [4,7].
- **Association areas**, which are spread throughout all the cortex so that each one is connect to a correspondent sensory/motor area. The term "association" refers to integration of sensory and motor information. Indeed, these areas do not receive sensory inputs directly, neither generate motor commands, but (1) interpret the sensory information coming from a given area of the cortex and (2) plan and contribute to coordinate the correspondent motor output. All the integration centres elaborate information coming from association areas, in order to control complex motor activities. For example, the prefrontal cortex integrates information deriving from sensitive areas and its function is to predict a possible reaction to that given sense [4]. This explain why if, for instance, one experiences a lesion to the visive association area, he's still able to see clearly letters/number, but he's not able to interpret them anymore.

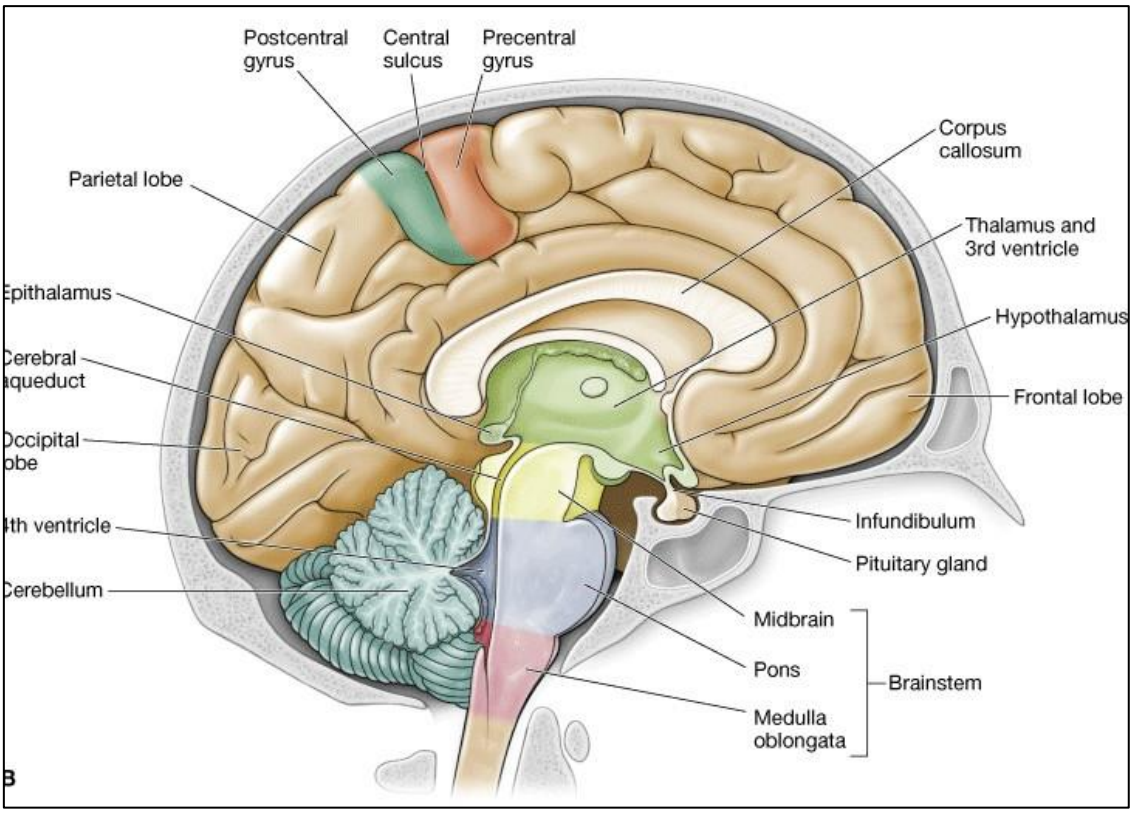

Figure 1 – *Medial view of sagittal section of the brain* {1}.

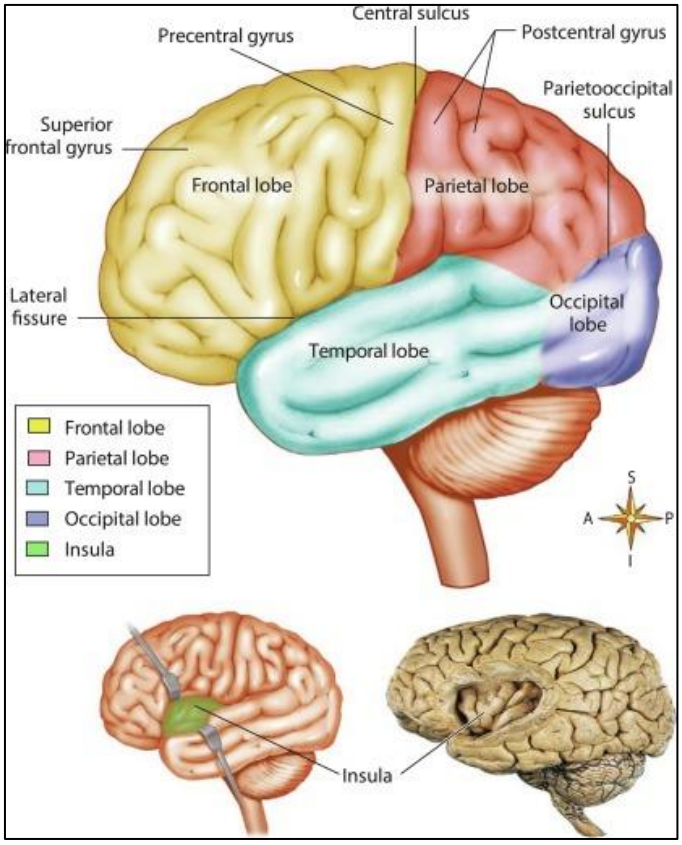

Figure 2– *Lateral view of the brain, with focus on different lobes and insula* {2}.

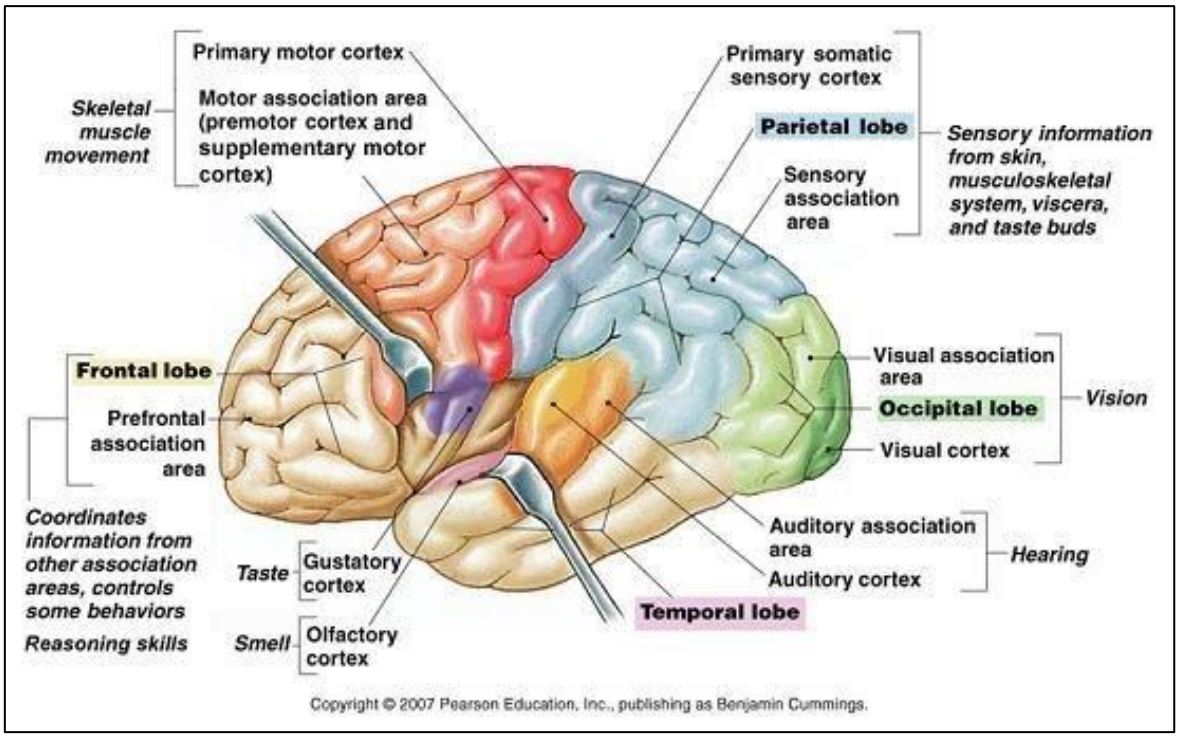

Figure 3 – *Functional areas of the cerebral cortex*: primary motor, primary sensor and association areas, with their correspondent functions [45].

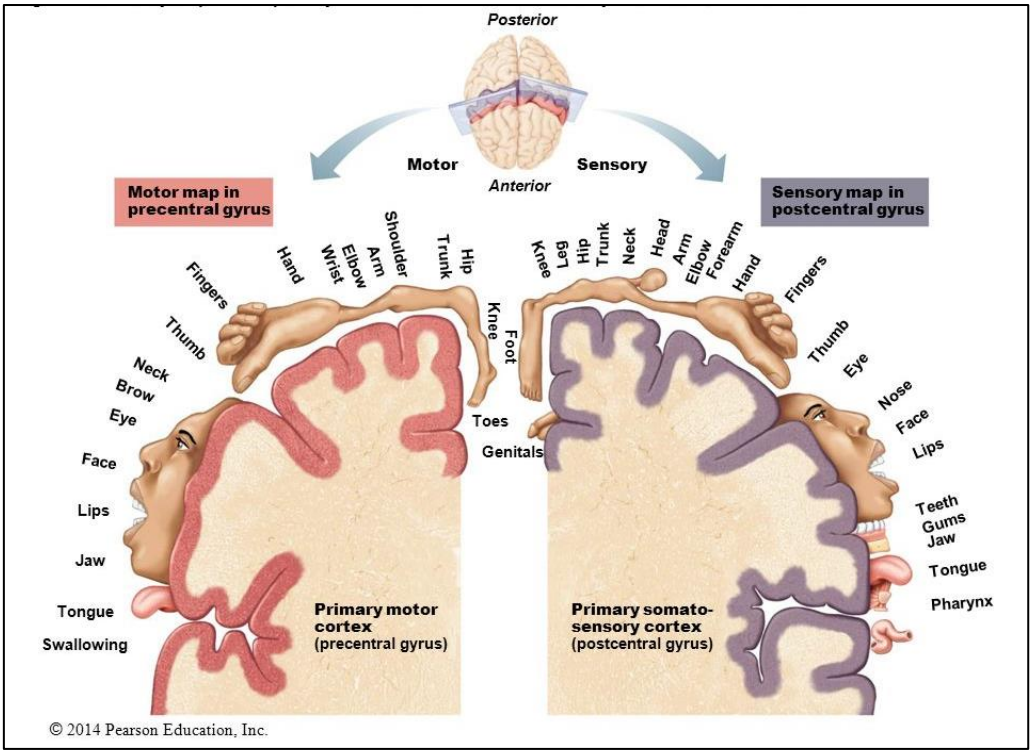

Figure 4 – *Motor and sensor homunculus*: each motor/sensory cortical region corresponds to a specific body part; proportions of the motor/sensory homunculus are completely different from the real ones of the body, because the dimension of the motor/sensory area of a specific cortical region is proportional to the sensor/motor neural units involved in the control of that region, rather than to real dimensions [4]{3}.

1.2 NEURONS AND NEUROPHYSIOLOGY

1.2.1 Architecture of a Neuron

The neuron, also known as nerve cell, is the basic unit of the nervous system, composed of three main parts, known as cell body, axon and dendrites, represented in Figure 3 [7], {13,14}.

- The **cell body** is also called *soma* and contains genetic information about the neuron, maintains its structure and plays a critical role in metabolic functions providing energy.
- The **axon** is a single nerve process with a tail-like structure that extends from the soma and through which every information is transferred; it is usually surrounded by a substance called myelin that help to conduct the information, which travels in terms of electrical signal.
- **Dendrites** are a variable number of branching processes that extend out from the cell body; their principal function is to receive and process signals coming from specific receptors or axons of other neurons.

While a neuron is usually characterized of only one axon, it is possible that it has more than one set of dendrites, depending on the specific role that it has to accomplish. For example, it is possible to find inside the cerebellum specific nerve cells known as Purkinje cells with the capability of receiving a high quantity of impulses due to the high number of dendrites that they contain {9}.

1.2.2 Neurons Classifications

Neurons can be classified according to various criteria, such as structure, function or type of information they carry {10}.

Classification according to the shape

- *Multipolar neurons*: this is the most common form of neuron in the CNS, characterised by the presence of a single axon and symmetrical dendrites extending from it.
- *Unipolar neurons:* neurons having only a single axon, usually found in invertebrate species.
- *Bipolar neurons:* neurons with two extensions (axon and dendrites placed in opposite sides).

- *Pyramidal neurons:* neurons with a single axon and multiple dendrites that generates a pyramidal shape; they are usually found in the nervous system across the cerebral cortex.
- *Purkinje neurons:* neurons with multiple dendrites aimed to release several neurotransmitters.

Classification according to the type of information carried

According to the information that the neuron is delivering, it is possible to recognize:

- *Sensory neurons (afferent):* neurons specialised to be triggered by physical/chemical inputs coming from the outside or inside the body and carry the correspondent information to specific districts in the CNS.
- *Motor neurons (efferent):* neurons specialised to carry commands from the CNS to specific effectors, such as glands or muscles.
- *Interneurons:* most common type of neurons found in the brain and spinal cord, with the aim of transferring signals from sensory neurons and other interneurons or directly to motor neurons.

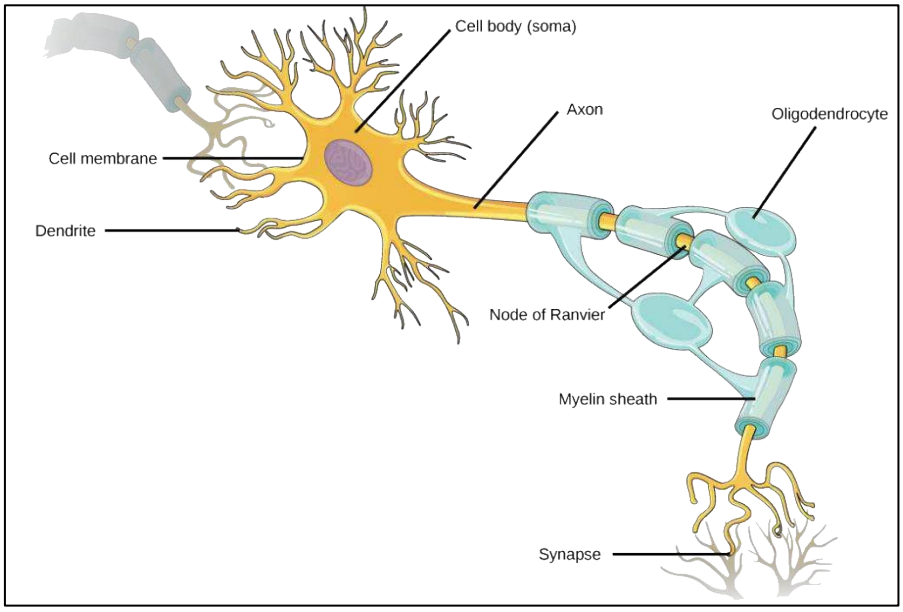

Figure 5 – *Neuron's architecture:* most organelles are in common with those of many other cells, with exception to some specialized structures (e.g. dendrites and axons). It is possible to appreciate the myelin sheath of the axon, that allows to speed up the AP transmission. The myelin cover is interrupted periodically by means of some gaps named as Nodes of Ranvier, which act as regions rich of ion channels where an AP is generated: in this way, the signal travels along the axon, "jumping" from one node to the next one {4}.

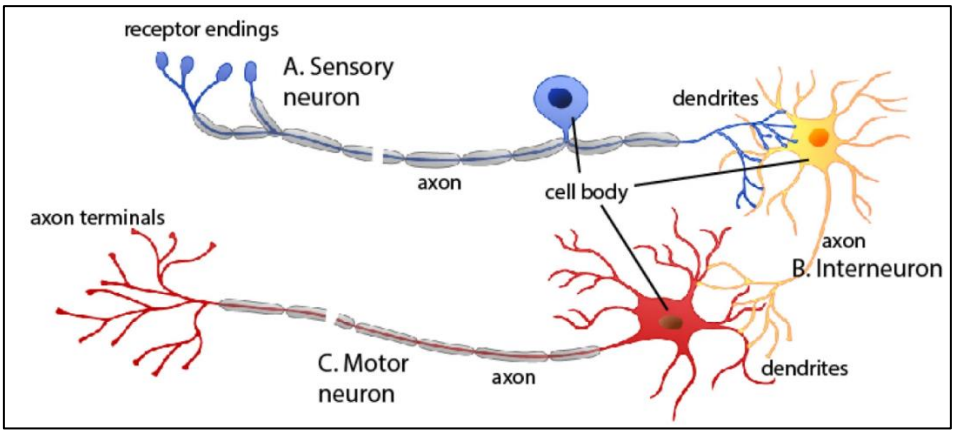

Figure 6 – *Classification of neurons depending on the type of information carried* (A: sensory neuron, B: interneuron, C: motor neuron). Each neuron is represented by means of its three main components: cell body, axon and dendrites {4}.

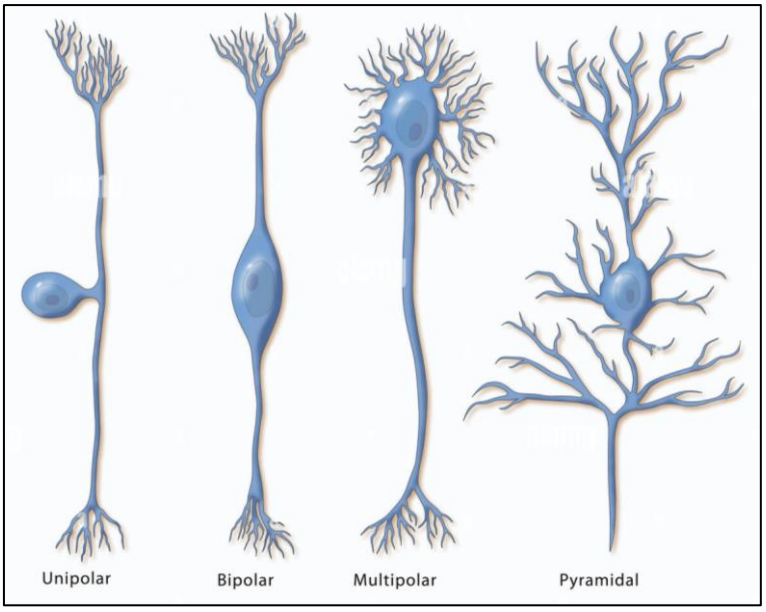

Figure 7 – *Classification of neurons depending on the shape*: from left to right: *unipolar* (one axon – one dendrite), *bipolar* (one axon, two dendrites), *multipolar* (one axon, more dendrites), *pyramidal* (one axon – multiple dendrites with pyramidal shape).

1.3 NEUROTRANSMITTERS AS CHEMICAL MESSENGER SOMATOSENSORY PATHWAY

1.3.1 Neurons Action Potential

Neurons are able to conduct sensory/motor information via electrical impulses, which are propagated throughout the axons [43]. The Action Potential (AP) occurs as a response of the neural cell to an electrical change of specific ionic gradients across their *plasma membrane*, a flexible structure consisting of two layers of lipid molecules, so that it is able to (i) block the diffusion of water-soluble molecules, (ii) be selectively permeable to specific molecules (ions)

by means of specialized channels, (iii) transduce information to chemical/physical stimulation by neurotransmitters [7].

Usually, the distribution of specific ions (Sodium Na^+, Potassium K^+ and Chloride Cl^-) across the neural membrane is such that the interior part of the neural cell is electrically in a negative state of about (-60/-75) mV, defined as *resting membrane potential*.

Each neuron is usually characterised of a several number of ion channels which allow a passive flow of ions, i.e. a movement of charged particles in/out the membrane whose direction is determined by the electrochemical driving force. These channels are usually closed in rest modality, and open only when activated due to the binding of a ligand or a change in the membrane potential [4,7].

The electrical signals used for delivering the information are expressed as deviations from the normal value of the resting membrane potential. These voltage changes at the neural membrane are called "graded potentials" and can derive from sensory stimuli from the environment (*receptor potentials*) or from another neuron (*synaptic potentials*). This electrical activity induces in turn the generation of an AP, that travels along the axon of the neuron until it produces a synaptic potential in the next neuron [4,7,43,46].

A typical generation of an Action Potential can be described as a cascade of events, divided in the following stages, each one related to the perturbation of specific ion channels located across the plasmatic membrane (K^+/Na^+ channels, where K^+ and Na^+ indicate, respectively, Potassium and Sodium ions).

1. During the initial *resting phase*, a transmembrane protein known as sodium-potassium pump (Na^+/K^+ pump) is active, expelling 3 Na^+ ions for every $2K^+$ ions entering, so that the neuron's membrane potential is kept in equilibrium (-70 mV).
2. As soon as a sensory receptor is triggered, sodium channels open, leading Na^+ ions to come inside the neuron's cell. This influx causes the membrane potential to enter in the *depolarization phase*: K^+ channels close, while adjacent Na^+ channels open progressively, leading the membrane potential to rise up to (-55/-50) mV. During this stage, more and more Na^+ channels continue to open according to a positive feedback mechanism (i.e. the opening of the initial Na^+ channels induces in turn the opening of more Na^+ channels), until the membrane potential passes from negative to positive values, reaching a maximum of about 30 mV that generates a wave of depolarisation that spread along the neuron's axon.

3. After reaching the maximum value, the membrane potential goes into a *repolarization phase*, during which Na^+ channels become inactive, while the K^+ channels re-open, allowing a positive electrical current to flow from the inside to the outside of the neuron. This ions flow makes the membrane potential to return to its resting value.
4. Due to the fact that some K^+ channels remain open, the voltage experiences an *undershoot phase*, in which it reaches more negative values than that of equilibrium. After this, it comes back to the resting condition of -70 mV [4,7].

A representation of the generation of an Action Potential, with references to the different phases of ion channels opening/closing for each phase is available on Figure 8.

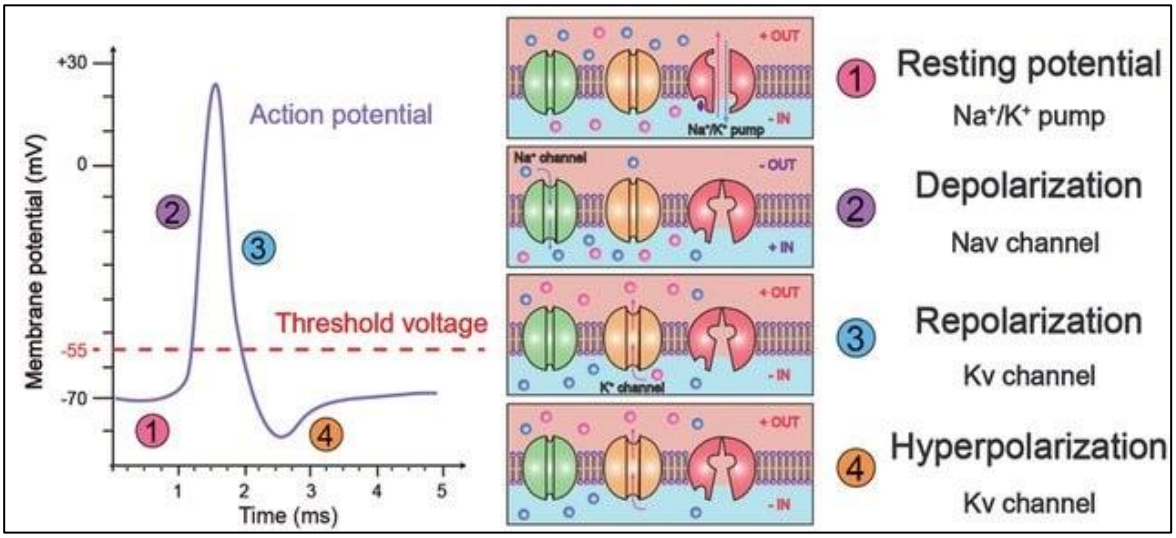

Figure 8 – Generation of an Action Potential in a Neuron, where each phase is described as an electrical consequence of the opening/closing of a specific ion channel: *Resting Potential* (opening of the Na+/K+ pump, membrane potential at equilibrium), *Depolarization* (closure of Na+/K+, opening of voltage gate channels Nav), *Repolarization* (closure of Nav, opening of the voltage gate channels Kv), *Hyperpolarization* (Kv still open) [55].

1.3.2 Synapses

A synapse is referred to the neural termination of dendrites, crucial for the neural communication, since it works as a junction region between the presynaptic neuron and the postsynaptic one. There exist two different kinds of synapses, according to the type of information to be delivered.

- *Electrical synapses* consist in physical junctions presented as a channel between the presynaptic and the postsynaptic neuron, where information can move in both directions

(pre ⇆ post). In this case, the electrical transmission is mediated by clusters of intercellular channels called gap junctions that connect the interior of two adjacent cells, allowing the bidirectional passage of the electrical ionic current (visible on Figure 9 – right side).

- *Chemical synapses* are made such that there is no contact between the pre and post synaptic neuron (visible on Figure 9 – left side). In this case, a neurotransmitter (a specific compound used for neural communication) is released at the presynaptic membrane level inside the external environment via specific vesicles; then, it binds with a selective receptor of the postsynaptic membrane, inducing a momentary change of the postsynaptic membrane potential. Since only the presynaptic membrane is allowed to release neurotransmitter, the direction of information is forced to be unidirectional (pre →post). [4].

1.3.3 Neurotransmitters as chemical messenger of somatosensory pathway

As already introduced, neurons are used to communicated with each other by means of action potentials and chemical compounds denoted as *neurotransmitters*. At the junction between two neurons, the presynaptic neuron releases a neurotransmitter into a gap called "synaptic cleft", placed between the *presynaptic* axon terminal and the *postsynaptic* dendrite. At this level, the neurotransmitter binds to specific postsynaptic receptors, causing the activation of a given ion channel: according to the gate that has been activated, it is possible either to excite or inhibit the postsynaptic neuron from firing its own action potential {14}.

There are multiple types of neurotransmitters specifically related to the functions to be accomplished. For example, glutamate is one of the most important excitatory neurotransmitters in the brain, also responsible of the nervous system plasticity (i.e. the ability of neural networks in the brain to change through growth and reorganization). On the contrary, gamma-aminobutyric acid (GABA) and glycine are the main inhibitory neurotransmitters [46].

A general description of how a (chemical) synaptic transmission via neurotransmitters works is reported in Figure 10.

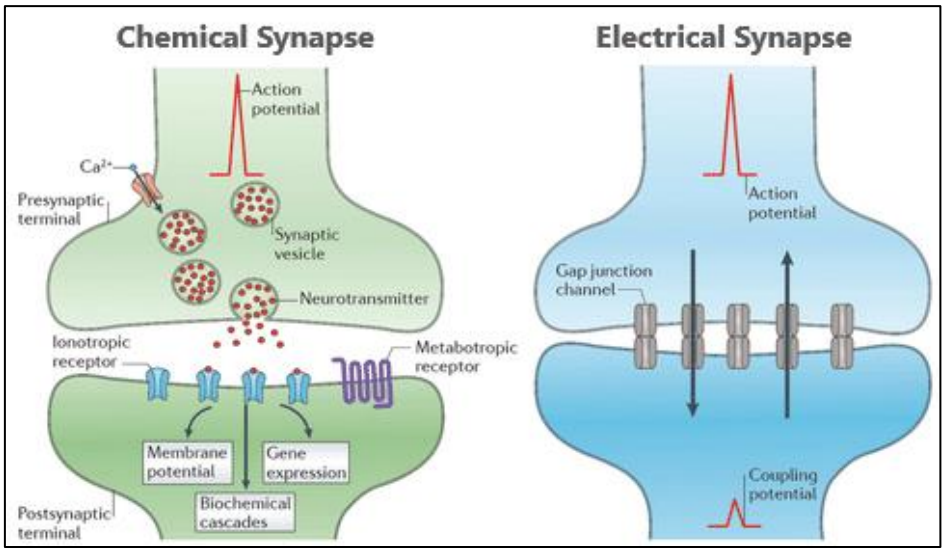

Figure 9 – *Main modalities of synaptic transmission*: on the left chemical synapse (signal transmission mediated via neurotransmitters and receptors), on the right electrical synapse (electrical signal travelling through gap junction channels) [56].

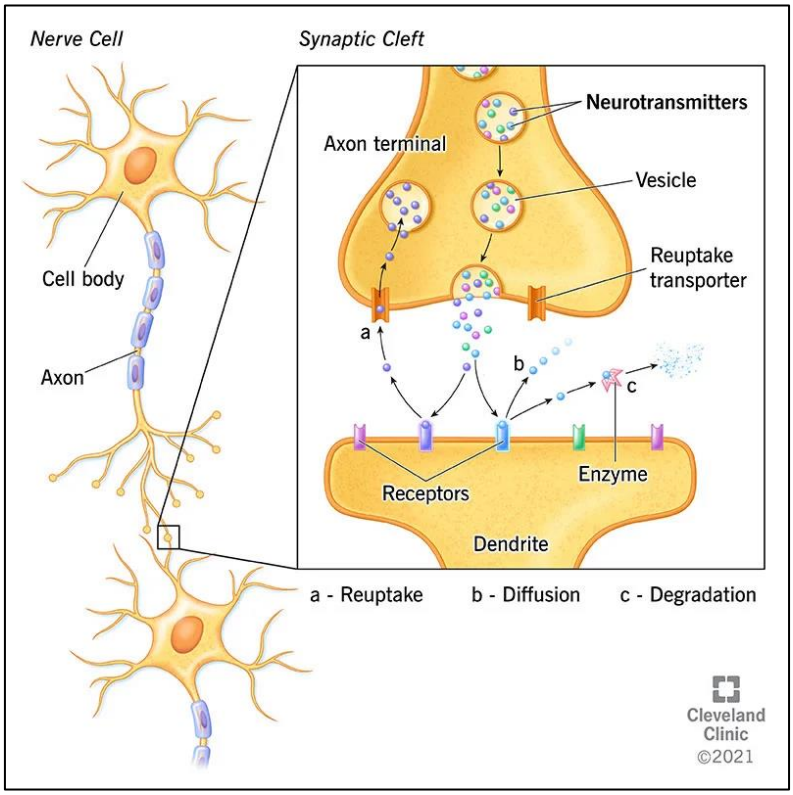

Figure 10 – *Representation of a chemical signal transmission*: neurotransmitters carry chemical compounds from the pre-synaptic neuron to the post-synaptic one, where the correspondent specific receptors detect the receiving signal {5}.

1.4 CRANIAL NERVES

A vast network of nerves sends electrical signals to and from other cells, glands, and muscles all over our body. These nerves receive and interpret information of different nature and control the body response. To maintain coherence with the aim of the researcher, this work will focus only on the principal cranial nerves.

The cranial nerves are identified according to their position along the longitudinal axis of the brain, by adopting roman numbers with the prefix CN [4]. Every nerve is connected to the brain via:

- *Sensitive nuclei*, which function as integration centres of the information carried by the nerve.
- *Motor nuclei*, which receives commands from the upper districts of the brain.

The brain is composed of twelve pairs of peripheral nerves: two pairs arise from the cerebrum, while the other ten are nerves of the brainstem (with exception of the spinal accessory nerve CN XI). Their fibers communicate with the brain passing through the cranial cavity, canals and fissures in the skull, supplying the head and neck [4, 7].

It is possible to classify the cranial nerves according to their function [4, 7]:

- *Afferent nerves* (input): special nerves which convey to the brain sensory information (smell, sight, taste, hearing and balance) received at the level of specific receptors.
- *Efferent nerves* (output): motor nerves that send from the brain the commands aimed to control voluntary skeletal muscles, voluntary somatic muscles of the eye and tongue and involuntary muscles of the eye.
- *Visceral nerves:* either afferent or efferent nerves with mainly autonomic functions.

In addition to this main function, it is common to use also other terms to describe deeper the components of these nerves:

- *General*: term referring to the extensive areas of the head.
- *Somatic*: term referring to head, body wall and extremities.
- *Special*: term referring to specialised sensorial function of gustation, olfaction, vision, audition and equilibrium.

According to these characteristics, it is possible to classify the cranial nerves components as general somatic afferent (GSA), general visceral afferent (GVA), general somatic efferent

(GSE), general visceral efferent (GVE), special somatic afferent (SSA), special visceral afferent (SVA) and special visceral efferent (SVE) [7].

A general description of main functions and components for each cranial nerve is available on Table 1 below. It is also possible to appreciate their location and projections within the brain in Figure 11.

Name	*Components*	*Main Function*
I. Olfactory Nerve	SVA	Sensitive (smell)
II. Optic Nerve	SSA	Sensitive (vision)
III. Oculomotor Nerve	GSE, GVE	Motor (movement of eyes, pupillary constriction)
IV. Trochlear Nerve	GSE	Motor (movement of eyes)
V. Trigeminal Nerve	SVE, GSA	Sensitive (general sensation of face, nose and mouth) Motor (muscle of mastication and eardrum tension)
VI. Abducent Nerve	GSE	Motor (movement of eyes)
VII. Facial Nerve	SVE, GVE, SVA, GVA	Motor (muscles of facial expression, lacrimation and salivation) Sensitive (taste, visceral sensory)
VIII. Vestibulocochlear Nerve	SSA	Sensitive (hearing and equilibrium)
IX. Glossopharyngeal Nerve	SVE, GVE, SVE	Motor (swallowing, salivation and laryngeal control) Sensitive (taste, visceral sensory)
X. Vagus Nerve	GVE, SVA, GVA	Parasympathetics functions to thoracic and abdominal viscera Sensory (taste, visceral sensory)
XI. Spinal Accessory Nerve	SVE	Motor (movements of shoulder and head)
XII. Hypoglossal Nerve	GSE	Motor (movements of tongue)

Table 1 – *Cranial Nerves and functional components* [4,7].

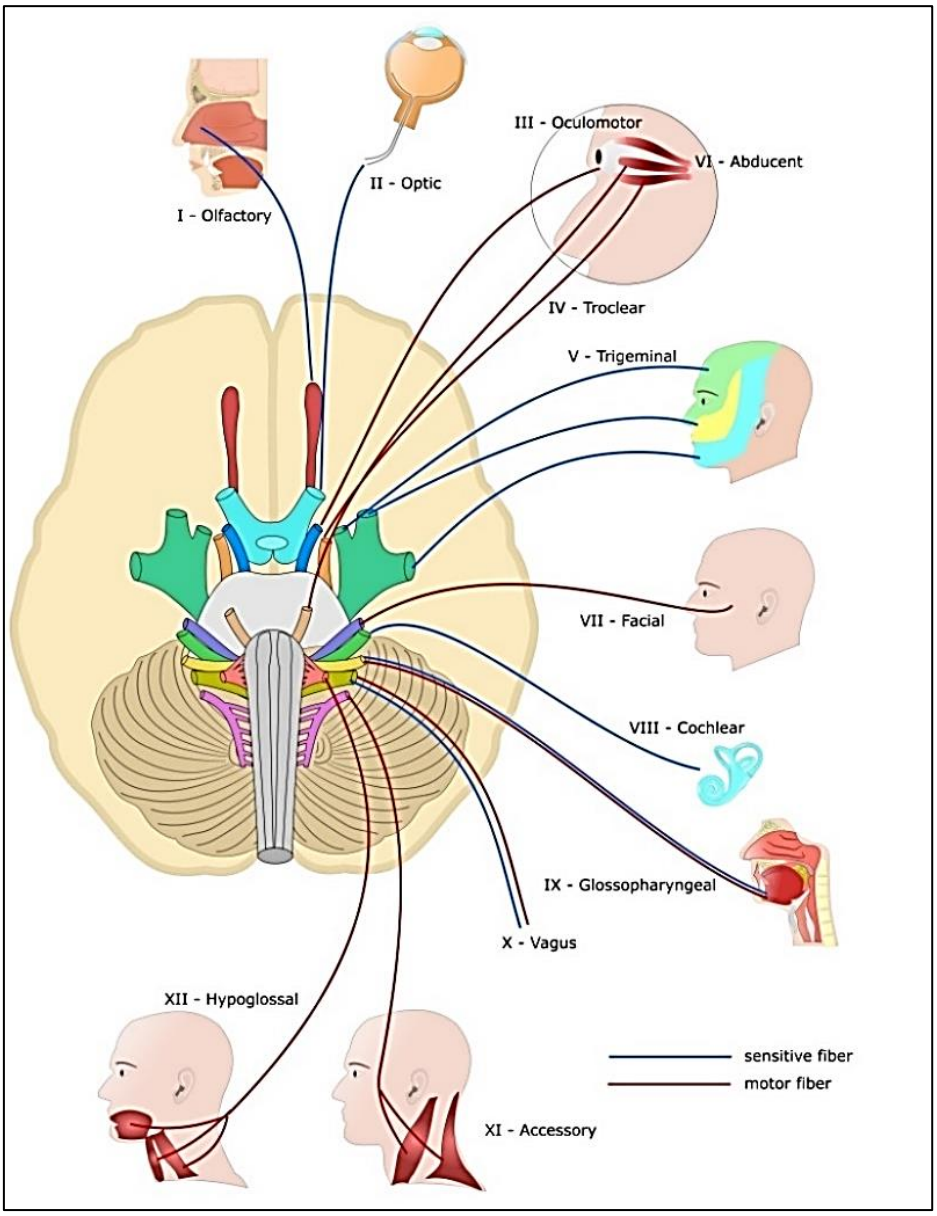

Figure 11 – *Location and afferent/efferent fibers of cranial nerves with projection across the brain districts* {6}

1.5 SENSITIVE PATHWAYS

A neural pathway or tract is a bundle of axons that connects two or more different neurons, allowing the transfer of information between them. Each pathway runs bilaterally, one for each side of the cerebral hemisphere [4]. Despite the existence of both motor (descending) and sensitive (ascending) neural pathways aimed to carry information between the periphery and the SNC, this work will focus only on the functioning of the sensitive pathways and the cranial nerves associated.

In general, a typical ascending pathway starts at the level of the sensitive receptors which are triggered by internal or external conditions and induced to carry the correspondent information

to the SNC, in terms of AP delivered via afferent sensitive fibers [4]. This suggests that tracts are generated by neurons synapsing one onto the other, and, according to their location within the tract, it is possible to recognize three different types of neurons:

- *1st order sensitive neurons* are afferent fibres conveying information towards the SNC; their body cell is located in a peripheral - spinal or cranial - ganglion (group of neuron cell bodies).
- *2nd order sensitive neurons* are usually interneurons that the 1st order axons synapse with; their somas are located in the spinal cord or may ascend in the thalamus.
- *3rd order sensitive neurons* are usually located in the spinal cord or in the thalamus and receive the information from the 2nd order neuron that synapse with them. Then, their axons deliver the sensitive stimulus to the correspondent cerebral cortex area, where it is processed [4].

Depending on the type of information to be integrated by the SNC, there exist three different ascending pathways:

1. The *dorsal column system*, that carries information about proprioception, vibration sensations from the skins and joint [40].
2. The *spinothalamic tract*, that delivers information about pain, temperature and general tactile sensations [41].

Generally, the axons of 1st and 2nd sensory neurons decussate, i.e. during the ascend they cross to the contralateral (opposite) side. Therefore, sensitive stimuli coming from the left side of the body are sent to the right side of the cerebral cortex and vice versa. This process occurs at the level of the medulla [4].

After the decussation, the 2nd order fibers convey the sensitive information to the contralateral side in a specific region known as Ventral Posterolateral (VPL) nucleus of the thalamus. Finally, according to the nature of the stimulus, this is projected to the correspondent area of the cerebral somatosensory cortex [4, 7].

On Figure 12 it is possible to see how the 1st order, 2nd order and 3rd order cooperate for the functioning of the somatosensory pathway.

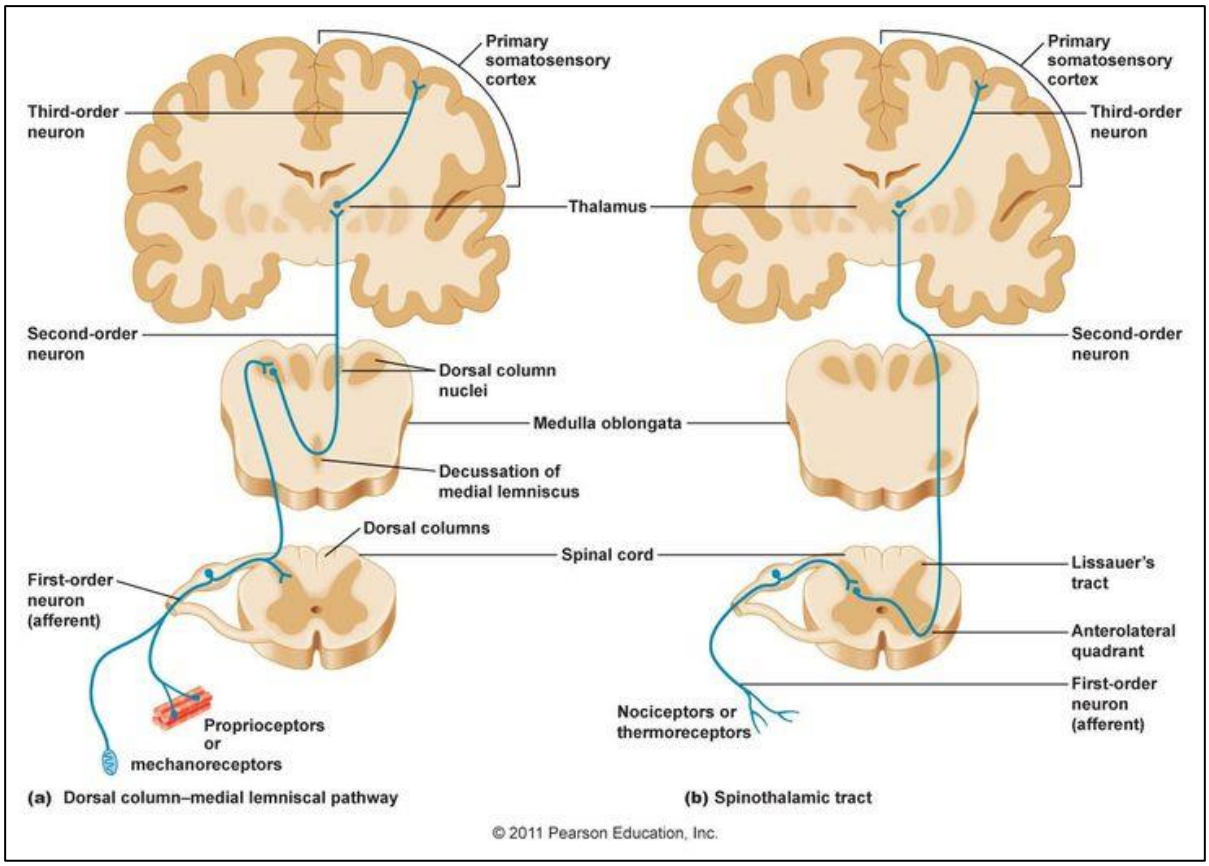

Figure 12 – *Somatosensory (afferent) pathways from receptors to cerebral cortex*: the 1st order neuron (afferent) delivers sensory inputs detected at receptors level and synapses with the 2nd order neuron at the medulla level, where decussation occurs; then, 2nd order neuron synapses with the 3rd order neuron at the VPL (Ventral Postero Lateral) region of the thalamus; finally, the 3rd order neuron send the signal to the correspondent area of the primary somatosensory cortex [57].

2. TASTE PERCEPTION IN HUMANS

2.1 SOMATOSENSORY AND TASTE INPUTS FROM THE TONGUE

The mouth plays a critical role in the somatosensory system, due to its rich somatosensory innervation, and the large variety of tissue types (skin, muscle, teeth) that is made of. Haggard et al. provide several different levels of oral somatosensory awareness, starting from individual sensations, to finally obtain a theoretical model of the 'mouth image', that allows to understand the differences between oral somatosensory awareness and that one of any other part of the body [16].

Indeed, neuroimaging and electrophysiological studies have demonstrated a robust overlap within the brain of various sensory modalities (mechanical, thermal, chemical, sensory) originating in the mouth [2,3,8,11,14,15].

In order to focus on the somatosensory and gustative projection from the mouth to the brain, it is necessary to introduce some general aspects concerning the gustative receptors placed across the oral cavity.

2.1.1 Taste Buds

The human tongue is an epithelial sac composed of skeletal or voluntary striated muscles and connective tissue, characterised by several protrusion known as taste papillae [19,35-37]. There are three main types of taste papillae:

- *Fungiform taste papillae*, located in the anterior two-third of the tongue;
- *Circumvallate taste papillae*, located in the posterior one-third of the tongue;
- *Foliate taste papillae*, placed on the lateral sides of the tongue [36].

Taste buds are organs made of clusters of columnar sensory cells, located mainly inside the taste papillae of the epithelium of the tongue, even if they are also placed across the oral cavity (palate and epiglottis). Each taste buds contains three different types of cells, each one with specific functions [35]:

- *Type I* cells usually identify salty stimuli,
- *Type II* cells are usually aimed to detect bitter, sweet and umami (i.e. pleasantness) stimuli,
- *Type III* cells usually detect sour stimuli.

In general, each gustatory stimulus is detected and processed by specific taste buds through chemo sensitive receptors of different nature, such as protein-receptors or ion channels that can either interact with a given gustative impulse to generate a second messenger, or deliver the stimulus itself directly into the cytoplasm of the taste bud cells (Figure 13). Taste receptors activate specifically when chewed food comes in contact with some taste papillae: during this process, each given receptor detects and matches with a specific food substance of one of the four basic tastes (sweet, sour, salty and bitter), reporting the correspondent taste cell that a taste substance has been detected [35].

Taste cells have normally a negative internal charge, similar to neurons. The interaction between the taste receptors and the food particles causes an increase of positively charged particles inside the taste cells, which in turn generates electrical changes inducing a depolarization. Under such condition, the depolarized taste cell is forced to release selective neurotransmitters in terms of chemical signals directed to specific gustatory neurons {15}.

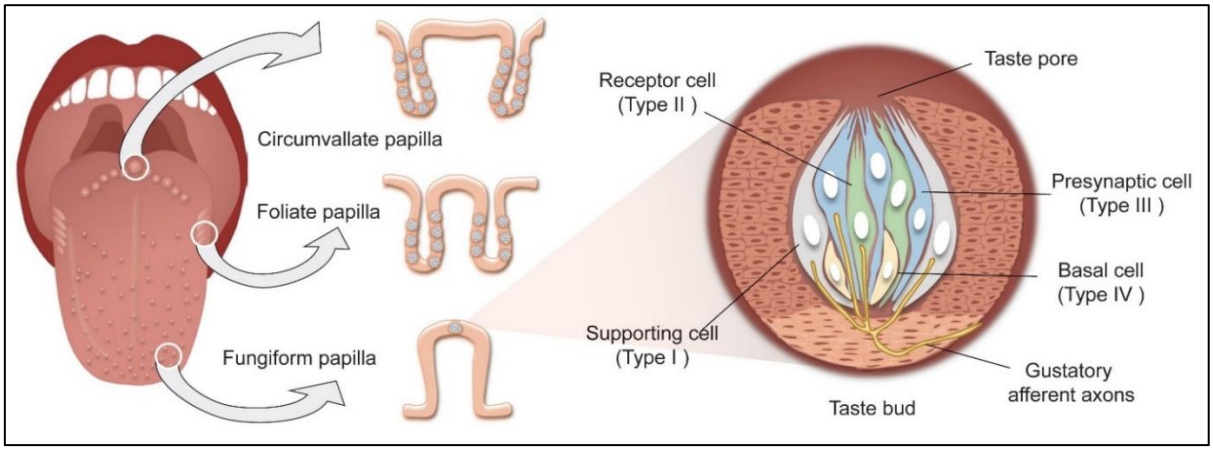

Figure 13 – *Peripheral gustatory system*: on the left, it is possible to distinguish the three different locations of circumvallate, foliate and fungiform papilla; on the right, a focus of the composition of a typical taste bud cell, with its receptors {7}.

2.2 SENSITIVE NERVES AS PATHWAYS OF GUSTATIVE INFORMATION

Somatosensory (touch and temperature) and gustatory (taste) information from the tongue are delivered to the brain by means of three principal cranial nerves: the *trigeminal nerve* (CN V), the *facial nerve* (CN VII), the *glossopharyngeal nerve* (CN IX) and the *oropharynx or vagus nerve* (CN X) [2 -7, 17, 22, 29].

In order to better understand which are the branches of these nerves functioning as somatosensory or gustative pathways to the CNS, it is necessary to provide some general information concerning their anatomical placement.

- The *trigeminal nerve* (CN V) is the most complex of the cranial nerves, due to its capability of being characterised either of a sensory or a motor division [26],{12}. Anatomically, the trigeminal nerve originates in the CNS from three sensory nuclei and one motor nucleus; in correspondence of the pons, the sensory nuclei generate a single sensory root, while the motor nucleus continues as a motor root. The sensory root expands at the level of the cavernous sinus (a depression on the temporal bone, located at the sides and base of the skull, lateral to the temporal lobes of the cerebral cortex), to generate the trigeminal ganglion, i.e. a group of neurons cell bodies outside the CSN. From the trigeminal ganglion, three divisions develop across the face: ophthalmic (V1), maxillary (V2) and mandibular (V3).

  To keep in line with the object of this research, only the sensory pathways will be taken under consideration, which are aimed to provide touch-position and pain-temperature information.
- The *facial nerve* (CN VII) arises intracranially from the pons, in the brainstem, as composed of a motor and a sensory root which fuse together, forming the geniculate ganglion (i.e. a collection of cell bodies); then, three branches are generated: the *greater petrosal nerve* that innervates the soft palate, and the *chorda tympani*, special sensory fibers innervating the anterior two-thirds of the tongue.

  Extracranially, it is subdivided into five different motor branches: temporal, zygomatic, buccal, marginal mandibular and cervical branch, all aimed to control the muscles of facial expression [39]{11}.
- The *glossopharyngeal nerve* (CN IX) is a mixed nerve that arises from the brainstem and provides fibers to the posterior one-third of the tongue, delivering either sensory or motor information. This nerve originates in the medulla oblongata and exits through the jugular

foramen, where it is possible to find the cell bodies of the sensory fibers; then, the nerve descends the neck, until it ends in the pharynx, where it is subdivided in the lingua, pharyngeal and tonsillar branches [7,38,39]

- The *oropharynx* or *vagus nerve* (CN X) is placed immediately under the glossopharyngeal nerve and provides specific taste fibers - known as special visceral afferent - to the epiglottis region of the oral cavity and the root of the tongue {13}. This nerve originates from the brainstem and exits the cranium via the jugular foramen**,** with the glossopharyngeal and accessory nerves (CN IX and XI respectively).

2.2.1 Lingual Somatosensory pathways

Lingual somatosensory inputs are carried to the brain through the glossopharyngeal nerve (CN IX) for the posterior part of the tongue, and the trigeminal nerve (CN X) for the anterior part. More in detail, the trigeminal nerve receives sensitive information resulting from temperature and tactile stimulation, as well as chemical stimuli. Then, the sensory fibers (organized in three main divisions – ophtalmic (V1), maxillary (V2) and mandibular (V3) -), converge in the trigeminal ganglion at the base of the middle cranial fossa and finally from here pass to the trigeminal nuclei in the brainstem, so to the thalamus and somatosensory cortex [14,26].

The glossopharyngeal nerve carries general sensory information from the upper part of the pharynx and the posterior one-third of the tongue [2, 4, 6, 7, 11, 38]{11}. According to Onoda et al. [18], fibers carrying sensitive information from the lips and tongue project into the ventral posteromedial nucleus in the thalamus (VPM), in the posterior corona radiata (white matter sheet of axons that carry info from\to the cerebral cortex), in the parietal operculum that cover a region of the cerebral cortex known as insular cortex. Since, as it will be described later, some of these regions overlap with those ones of the gustatory projections, there may be the possibility that the central gustatory pathway and the somatosensory pathway travel in association to each other [18]. This theory has been confirmed with the discovery of "*bimodal neurons*" in correspondence of the Nucleus Solitarius Tract (NTS), in the brainstem. These neurons are capable to give a bimodal response, which can be either somatosensory or gustatory [2]. For these reasons, many studies in recent years have been made to further investigate the brain projection of oral sensations and discriminate these areas with respect to those ones of pure gustatory information.

2.2.2 Gustatory pathways

Cranial nerves CN VII, CN IX and CN X provide the afferent taste fibers needed to acquire gustative information from the taste bud cells [2 -7, 11, 14, 15 17, 19, 22, 29].

The 1st order neurons or "gustatory neurons" originate as peripheral taste chemoreceptors placed across the papillae. The given taste triggers cellular depolarization, and the primary sensory axons travel along the chorda tympani and greater superior branches of the facial nerve (dorsal surface of the tongue), the lingual branch of the glossopharyngeal nerve (soft palate and pharynx) and the vagus nerve (upper part of esophagus) [30]. The gustatory information travels passing through the jugular foramen to enter the brainstem. As entering the medulla, the 1st order gustative fibers ascend centrally to the rostral nucleus of the solitary tract (rNST) [3, 19, 20, 22, 29], where they are joined by the oral somatosensory projection from the spinal trigeminal nucleus [30].

At the level of the rNST the 1st order gustatory neurons synapse, and the ascending 2nd order neurons originated project bilaterally to the ventral posteromedial (VPM) nuclei of the thalamus via the central tegmental tract [1-3,8,16,17,19,20, 22, 30]. In rodents, 2nd order neurons coming from the NST project ipsilaterally to the so-called gustatory parabrachial nuclei in the pons (PBN), before reaching the VPM nuclei in the thalamus. By the way, the PBM circuitry in primates seems to be aimed only to deliver general visceral information (from the vagus nerve) to the correspondent specialized thalamic nuclei, whereas gustatory fibers bypass this region, conveying directly to the VPM nuclei [9].

Finally, 3rd order neurons from the thalamus project via the posterior limb of the internal capsule to the inferior one-third of the primary sensory cortex (the gustatory cortex of the parietal lobe) and various centres of the forebrain [3, 6 – 8, 19]. The entire gustatory pathway from receptors to cerebral cortex is visible on Figure 14.

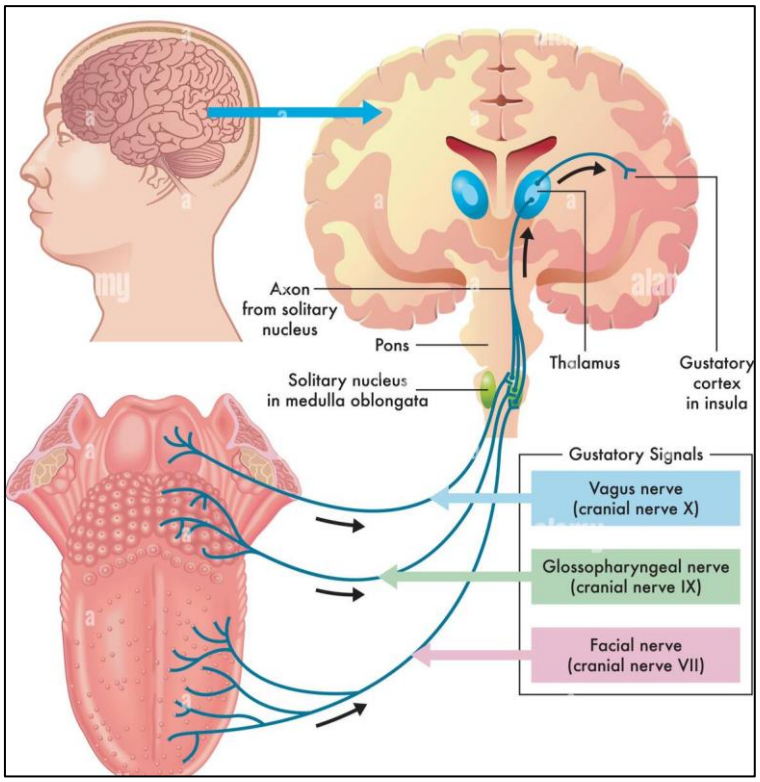

Figure 14 – *Gustatory pathway*: CN X, CN IX and CN VII conduct gustative information from tongue receptors to the solitary nucleus in the medulla oblongata; then, 2nd order fibers convey the received information to the Ventral Posteromedial nucleus of the thalamus; finally, 3rd order neurons deliver the signal to the correspondent area of the gustative cortex {}.

2.3 GUSTATIVE PROJECTIONS IN THE CEREBRAL CORTEX

2.3.1 Primary and Secondary taste cortex

The cerebral cortex is composed of two different regions (primary and secondary cortex), each one with specific functions.

The primary cortex comprehends all those cerebral areas that receives motor/somatosensitive information directly from the thalamus. In the case of gustatory information, the exact position of the **primary taste (or gustatory) cortex (PGC)** is still under debate. Until the advent of neuroimaging techniques, knowledge of human cortical gustatory representation derived entirely from studies of cerebral lesion sites in clinical populations [2]. Most of them reported gustatory disturbances when the damage affected different region of the insular cortex (mostly the rostral and left posterior areas). More recent studies, based on neuroimaging techniques such as functional magnetic resonance (fMRI), positron emission tomography (PET), magnetoencephalography (MEG) or electroencephalography (EEG), confirmed the role of those regions in the elaboration of gustative information and reported also activations in the

parietal opercular region, in the postcentral gyrus adjacent to the somatosensory representation of the tongue [2, 8, 16].

On these bases, it is common to associate the primary taste cortex to the *frontal operculum* and *rostral insula*. Furthermore, it is possible to associate the neural activations related to the elaboration of taste in correspondence of some *Brodmann Areas (BA)*, regions of the cerebral cortex originally defined and numbered by the anatomist Korbinian Brodmann according to the cytoarchitectural organization of neurons. Precisely, most of the studies have shown a neural activation in correspondence of the following areas*:* *BA43*, a transition region of the fronto-parietal operculum along the post-central gyrus and *BA13*, which defines the insula location, just above the lateral fissure. Nevertheless, other neural activity after taste stimulations has been also found in correspondence of the so-called Broca's areas, regions situated in *BA44* and *BA45*, along the posterior inferior frontal gyrus (pars triangularis) of the brain [2,3,7-9,10, 12, 15-20, 22, 23]. A schematic representation of the BA in both left and right hemisphere is shown in the following Figure 15.

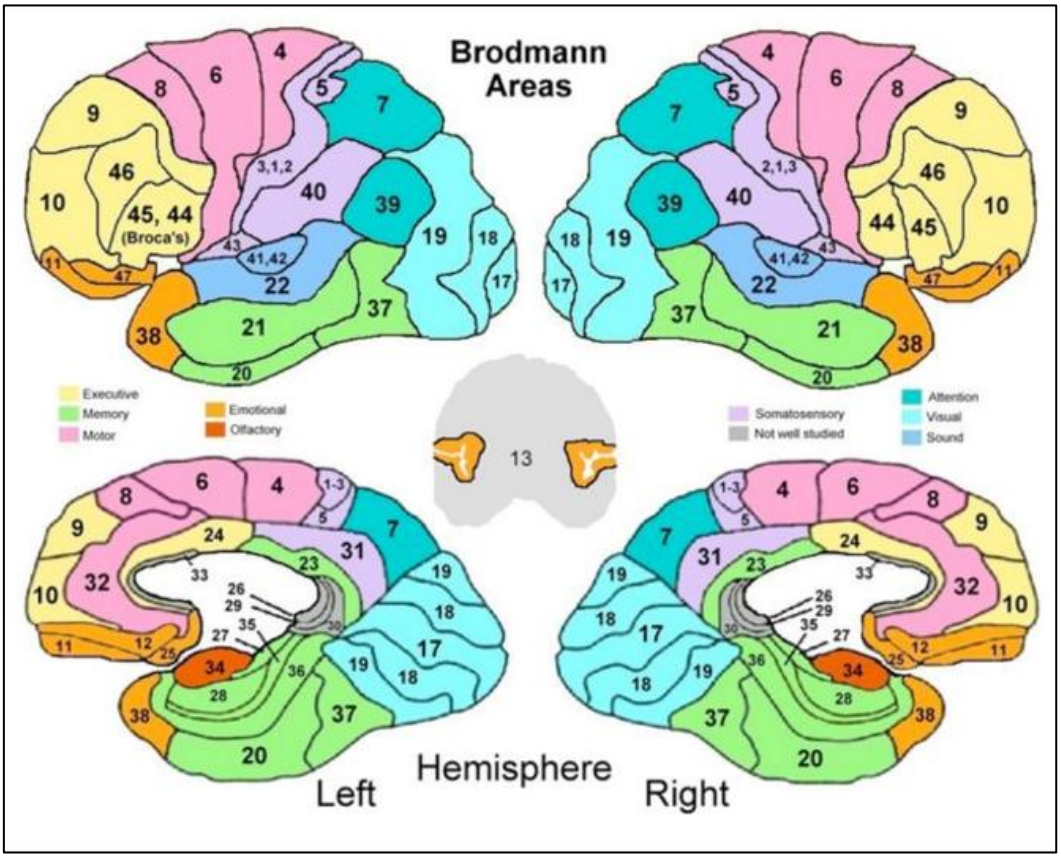

Figure 15 – *Schematic representation of Brodmann areas in the left and right hemispheres* [58].

In primates, the primary taste cortex is mostly involved in the representation of the identity and intensity of taste [9 - 12], and in particular, several fMRI studies have shown that the PGC in the insula is responsive to at least two associated levels of representation: taste qualities and their palatability [23].

A **secondary taste (or gustatory) cortex (SGC)**, located in the caudolateral region of orbitofrontal cortex, also elaborates taste stimuli [9,16,19]. More in detail, this region receives projections from (i) the primary olfactory cortex (OFC), that may be critical for flavour perception, and (ii) the hypothalamus, in order to integrate taste responses with the sense of satiety. This supplemental region is mostly addicted to represent the reward-related or affective aspect of taste [7 – 9, 22].

In addition, many studies have demonstrated that the elaboration of flavour results from the interaction of different modalities of senses. For example, Rolls and Baylis proved that the flavour integration in the orbitofrontal cortex comes from a combination of gustatory and olfactory inputs [18].

2.3.2 Somatosensory region of the tongue

In addition to the gustative information, the thalamus project also multiple somatosensory information of the tongue to other specific regions of the parietal, insular and frontal cortex [3,8,11,26].

A deeper investigation of these areas, however, is challenging, due to many problems that usually arise during experiments. In particular, the stimulator chosen to trigger the sensory response from the tongue may cause technical problems or noise during scanning, since it is difficult to fix it on the tongue stably. Another issue is related to the fact that tactile stimulation on the tongue may stimulate vomiting reflexes [11].

By the way, neurophysiological studies based on EEG and MEG techniques with somatosensory stimulation have reported electrical activity mostly in the postcentral gyrus in the primary somatosensory cortex (in particular, it was found an ipsilateral projection within the so-called area 3b) [11,24], while tongue areas in the secondary somatosensory cortex have been detected only in small regions [11].

Precisely, several fMRI studies have showed that the Rolandic operculum, being located anteriorly to the cortical somatic tongue representation, plays a critical role in the elaboration of somatosensory information of the tongue [2, 3, 11, 12].

2.3.3 Gustatory pathways organization

Recent studies have examined the pattern of somatosensory and taste projections from each side of the tongue to the ipsilateral or contralateral cerebral hemisphere in humans [53,54]. The most common result is that there is a bilaterality of the cortical representation of the tongue in both the somatosensory and taste modalities, probably due to the existence of crossed/uncrossed projection for each side of the tongue in the ascending pathway, but there is a predominance depending on the sense modality taken into consideration. More in detail, it seems that:

- The *taste modality* induces a predominance of the **ipsilateral representation** with respect to the contralateral.
- The *somatosensory modality* induces a predominance of the **contralateral representation** with respect to the ipsilateral [3].

There results arise from various studies applied on taste disturbances coming from unilateral lesions in the SNC. Among these, Onoda et al. examined a total of 38 cases of patients with taste disorders due to central lesions, reporting that from the medulla to pons taste disorders were ipsilateral to the lesion, whereas for lesions above the midbrain the ipsilateral disorder decreased, with an increase of contralateral and bilateral cases of taste disorders. According to these results, Onoda et al. proposed a model in which the gustatory pathway ascends ipsilaterally until the medulla, and at the level of the pons, precisely in correspondence of the PNB, it branches and proceeds bilaterally to the cerebral cortex, shown in Figure 17 [18].

These interhemispheric differences may be due to many factors, here reported:

- **Large inter-individual variability**

  It is commonly known that different subjects perceive the same intensity of a given tastant in a different way, inducing a large inter-individual variability in terms of neural gustatory representation. To solve this issue, Schoenfeld et al. performed, in an fMRI study of the primary gustatory cortex for both the single-subject and the multi-subject analysis, an additional multi-session analysis [9].

- In the *individual analysis*, each of the four tastants used (sour, bitter, salty, sweet) was contrasted to all the others, in order to detect those voxels that were more active for the given taste with respect to all the other ones.
- In the *group analysis*, the conjunction approach was adopted, according to which a first analysis was performed to identify the contrast of one specific taste vs all the others, obtaining a cluster of voxels which detect the area mostly activated by that taste; after that this process was repeated to all the tastants, a conjunction among all these clusters was applied, in order to find all the voxels able to activate after more than one specific stimulus. In this way, an overlap of some regions across subject was revealed.

  Since it seems that inter-variability may be linked to differences of the cortical folding across people, some recent approaches are trying to unfold the cortical surface, so to be able to investigate deeper the precise anatomical location of such regions of the gustatory cortex. Nevertheless, another factor that may contributes to inter-variability is the intensity needed for a given taste stimulus to be detected by the correspondent gustatory neuron: some neurons, in fact, may be activated after a given threshold for identifying a given taste but may need a higher input to be triggered for the identification of another taste [9].

- **Intra-individual variability**

  This problem is related to the existence of the probability that the same person, even if perfectly healthy, may sense the same taste in different sessions with different intensity (so, this is a variability linked to different cycles of experiments for the same subject).

- **Hand predominance**

  Some researches have found a correlation between interhemispheric differences and hand predominance. One of the first results was provided by Faurion et al. in 1996, showing a functional lateralization of brain processing involved in taste perception (related to handedness) in the lower part of the insula [25].

  Several studies suggested that cognitive function is less lateralized in left-handers rather than right-handers [17]. Faurion et al. disproved this theory through a study based on a whole tongue stimulation performed on 10 healthy subjects (five right-handed and five left-handed), whose results showed a main stronger activity at the level of the dominant hemisphere in correspondence of the inferior insula, according to the subject's handedness: for the right-handers a greater cluster of voxels was identified in the left hemisphere, whereas for the left-handers a bigger activity was detected in the right one [44].

  Iannilli et al. supported this theory introducing the so-called *relative brain hemispheric activity index (H)*, which is defined as the number of the activated voxels in the

corresponding hemisphere, weighted by the relative statistical Z score and normalized to the whole activity in both hemispheres [17]. Mathematically:

$$H_{L(R)} = \frac{\sum L(R)(activated\ voxelsxrelativeZscore)}{\sum L{+}R(activated\ voxelsxrelativeZscore)} \quad (1)$$

By computing this index on their study, results showed that a stimulation of the right tongue induced a greater H_L than H_R, whereas a stimulation of the left tongue leaded to a greater H_R.

- **Differences between right and left tongue stimuli**

  Going deeper in the concept of left/right tongue, Stevenson et al. examined fourteen patients with unilateral insular lesions (seven right-sided and seven left-sided damaged) by applying unilaterally to the tongue tip four tastants: sour, bitter, salty and sweet. Results stated that taste discrimination was better if administered across the right side of the tongue rather than the left one, and that the quality of tastant was better judged when is applied to the left tongue tip rather than the right one [3,21].

2.3.4 Models of gustatory information flow from tongue to primary taste cortex

To explore deeply the organization of the gustatory information pathway, Stevenson et al. analysed and compared four different models of flow from tongue to primary taste cortex [21], schematized on Figure 16.

- The **1st model**, proposed by *Iannilli et al.*, shows an information flow with ipsilateral connections directly from tongue to the primary taste cortex.
- The **2nd model**, proposed by *Lee et al.*, suggests an ipsilateral information flow that decussates at the level of the midbrain, from which it proceeds contralaterally until the primary taste cortex.
- The **3rd model**, proposed by *Pritchard et al.* as results of a gustatory impairment study, presents an ipsilateral flow to the primary taste cortex in both sides, followed by a further unidirectional flow of information from the right to the left insula.
- The **4th model**, proposed by *Onoda et al.*, derives from the study introduced in the previous chapter and shows two parallel flows from tongue to cortex: a first ipsilateral pathway on both sides, and an additional flow generated by some afferent fibers that decussate at the level of the midbrain, sending to the primary cortex information related to the contralateral side of the tongue. More in detail, according to the researchers, it seems that the corpus

callosum (the slice of nerve fibers that connect the two halves of the cerebral cortex), has a critical role in the interhemispheric transfer of gustatory information. This theory has been explored by Aglioti et al., whose study showed that callosotomized patients took more time in identifying and naming the administered tastant. This gave an idea of the corpus callosum as an "equalizer" between the ipsilateral and contralateral input, allowing each hemisphere to receive inputs of equal intensity [3,16].

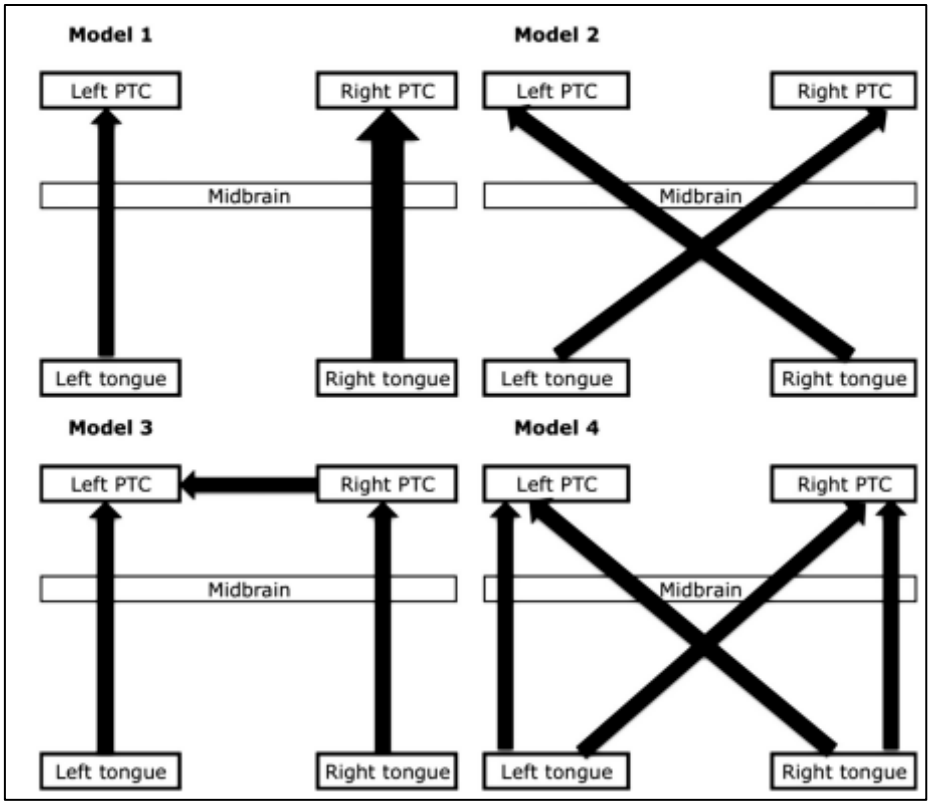

Figure 16 – *Schematic representation of the four possible lateralization models according to Stevenson et al* [21].

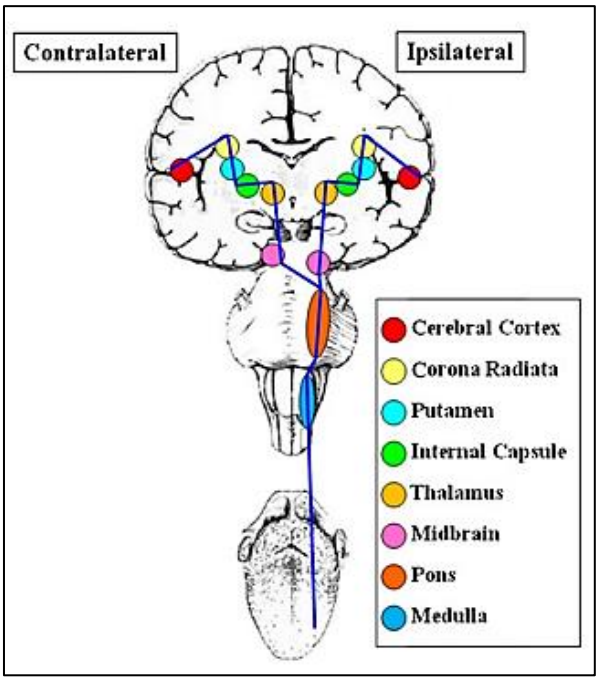

Figure 17 – *Lateralization model proposed by Onoda et al.*

2.3.5 Four Taste Modality

Taste combines the recognition and response to several chemical compounds such as salts, sugars, acids, and other substances. Taste and smell interact in order to induce chemosensory perceptions such as flavor, which can be improved by trigeminal chemical sense input and temperature. For long time, it has been believed that taste receptors are able to clearly discriminate only four common types of tastants: sweet, salty, sour and bitter [1]. During the middle part of the 20th Century, a theory was diffused according to which the gustatory receptors responsible for coding different basic taste properties were asymmetrically placed over the surface of the tongue [37]. According to this, the so-called "*tongue map*" have been developed, where sweet receptors were thought to be on the tip of the tongue, salt and sour receptor on the sides and bitter receptors on the back (Figure 8). Nowadays, several researchers have refused this myth, proving that all taste receptors able to identify the basic tastants are distributed in equal manner across the overall surface of the tongue, the soft palate (roof of mouth toward the back of the oral cavity) and the pharynx [37]. This means that sensitivity to each tastant in the specific location of the tongue is similar, whereas the discrimination capability occurs only at the level of the cerebral cortex. In this context, there are two different theories [1]:

1. *Pattern theory:* taste receptors cells should respond with different sensitivities to the basic tastants, producing a pattern for each different taste.
2. *Labelled line theory*: the basic tastes are sensed by means of different kinds of receptors, each one delivering the gustative information to the brain via its own pathway.

Currently, several researchers suggest a collaboration between both ways of taste perception.
Most of the studies aimed to the investigation of the gustatory pathway are based on the administration of the four basic tastants (sweet, salty, bitter and sour) applied to only one or both sides of the tongue. However, a fifth tastant has been added called umami ('delicious' in Japanese), which represents the flavor of MSG (monosodium glutamate) used in cooking and it is usually associated to meat, fish, tomatoes, cheeses and other dishes based on proteins. It is still not completely clear which is the pathway travelled by the umami substances and which are the cortical regions tuned by this kind of tastant. A study conducted by Schoenfeld et al., for instance, showed an individual representation of the umami taste (non-overlapping with the other taste regions) within the primary taste cortex of each subject [9]. However, this area does not match with that one found by De Araujo et al., where the umami taste region was identified within the same area associated to glucose [46]. These two results, together with other similar controversial studies, make the join of umami to the basic four tastes still under debate.
Another argument that arouses conflicting opinions is that inherent in the inclusion of water as a separate taste instead of neutral. Indeed, in some studies even a "water sense" is indicated, as occurs in that one of Schoenfield et al., as well as in De Araujo et al., where water is considered to activate specific cortical area (when subtracted from activation produced by saliva) and consequentially it should not be considered tasteless [8,9,46]. However, also in this case, the concept of water as an independent taste is still a point of criticism for many researchers.

In this research, only three of the four (five) basic tastants have been take into consideration: *salty, sweet and water.*

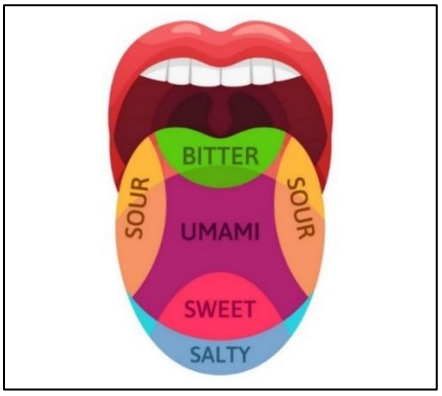

Figure 18 – *Representation of the "tongue map".*

3. FUNCTIONAL MAGNETIC RESONANCE IMAGING

The Magnetic Resonance Imaging refers to the application of nuclear magnetic resonance (NMR) to radiological imaging. The terms 'magnetic' and 'resonance' are related respectively to the use of different magnetic fields and to the need of matching the (radio)frequency of an oscillating magnetic field to the 'precessional' frequency of the spin of some nuclei (hence the 'nuclear') in a tissue molecule {16}.

Magnetic resonance imaging is a relatively new discipline and is thought to be a powerful imaging modality because of its flexibility and sensitivity to a broad range of tissue properties. One of the major advantages of MRI is that it does not require ionizing radiation, since it is based on the usage of RF electromagnetic radiation and magnetic fields, which do not have the associated potentially harmful effects {17}. Contrast resolution, moreover, allows visualization of soft tissue with similar characteristics, such as liver–spleen or white matter–gray matter.

3.1 THE BASICS OF MAGNETIC RESONANCE IMAGING

3.1.1 Fundamental interaction of a Proton Spin with the Magnetic Field

The primary origin of the MR signal relies on the fundamental law of physics of *spinning:* charged masses are able to induce a magnetic field about themselves. More in detail, hydrogen nuclei (consisting of a single proton) contained within free water or lipid molecules of the human body, exhibit an intrinsic property known as nuclear spin that gives rise to a small magnetic field for each proton, known as a magnetic moment.

Normally the magnetic moments (spins) are randomly oriented but in the presence of the externally applied B_o field, they tend to align either toward or against the externally applied magnetic field. An equilibrium state is quickly attained, where there is a small excess of spins aligned with the field as this is the more energetically favorable direction of alignment. This excess of proton magnetic moments generates the net magnetic field, aligned at equilibrium along the positive z axis (along B_o) with the value M_o, and often shown as a vector as shown in Figure 19. The size of this net magnetization is one of the key determinants of the maximum signal intensity that can be generated and used to form images. The greater the applied magnetic field strength, B_o, the greater the excess of protons aligned with the magnetic field and the greater the size of the net magnetization. In order to generate a MR signal from the net magnetization, the radiofrequency (RF) magnetic field is generated by the integral rf transmitter

coil and used to deliver energy to the population of protons. This field is applied at a particular frequency, known as the Larmor frequency (ω_o) that is proportional to the strength of the magnetic field, according to the Larmor equation:

$$\omega_0 = \gamma \times B_0 \tag{2}$$

where γ is a constant known as *gyromagnetic ratio*, with a value of 42.6 MHz/Tesla for the proton {18}.

The Larmor frequency is also known as the resonant frequency, as it is the characteristic frequency at which the protons only absorb energy (or resonate).

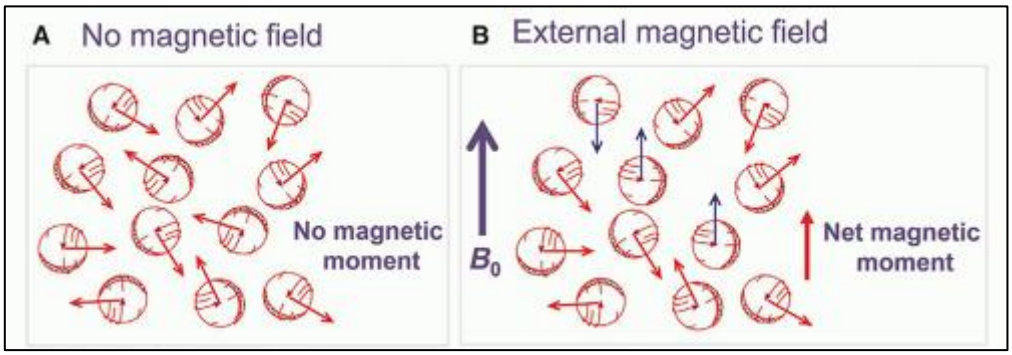

Figure 19 – *Representation of hydrogen protons without and with magnetic field:* with no magnetic field (A), protons are free of assuming random orientations; in presence of magnetic field (B), some protons (blue vectors) change their orientation to be parallel or antiparallel to Bo {18}.

3.1.2 MRI Signal Localization and Magnetic Field Gradients

The process of localization of each point in space is denoted as "Spatial Encoding" and is like placing an XYZ coordinate system on the imaged object. To do so, a magnetic resonance imaging (MRI) system comprises three main electromagnetic components [47] {22,23,24}: a set of main magnet coils, three gradient coils and an integral radiofrequency transmitter coil, visible on Figure 20. Each of these components generates a different type of magnetic field that, when applied to a patient, produces spatially encoded magnetic resonance signals, used to form MR images.

- A strong, uniform magnetic field B_o is generated by the ***main magnet coils***. The strength of this field, measured in units of Tesla (T), has the purpose of aligning the H spins. A reference coordinate system of three orthogonal axes, x, y and z is used to define the

magnetic field direction, with the z-axis normally chosen to be parallel to the direction of B_o.

- A ***gradient system***, composed of simply loops of wire on a cylindrical shell placed within the magnet, produces a time-varying magnetic fields in the X, Y and Z directions. These gradients, superimposed over the strong uniform magnetic field Bo, allow to localize the tissue signal during the examination.
- ***Radiofrequency coils*** or RF coils are key components because work as the *"antennae"* of the MRI system, serving as the transmitter as well as receiver in the formation of the final images.
  - ⇨ When used as *transmitters*, the RF-coils generate an oscillating magnetic field B_1 perpendicular to the static main magnetic field B_0. If the oscillation of B_1 closely matches the natural precession of nuclear spins near the Larmor frequency, energy is deposited into the spin system, causing a change in its net alignment. The B_1 field is typically turned on for only brief periods of time (a few milliseconds), called "RF-pulses": by adjusting the duration or the magnitude of these pulses, the nuclear spin can be rotated of an angle of 90° or 180°.
  - ⇨ When used as *receivers*, RF-coils are responsible for detecting the MR signal, which consists in the oscillating net magnetic flux returning from the excited spin. This flux is captured by the coil, generating an electric current which is then amplified, digitized, and filtered.

Finally, an imager system, including the computer, reconstructs and displays the final images.

As already anticipated, each MR scanner usually applies three types of gradients for 3D localization: *slice selection* (Gz) along z-axis, *phase encoding* (Gx) along x-axis, *frequency encoding* (Gy) along y-axis.

Amplitude and duration of these gradients, related to the magnitude of the applied current in each coil set, determine a specific final type of position in three-dimensional space. The three gradients are sequenced in a specific order, usually denoted as *pulse sequence* and depending on the kind of information one is interested to obtain.

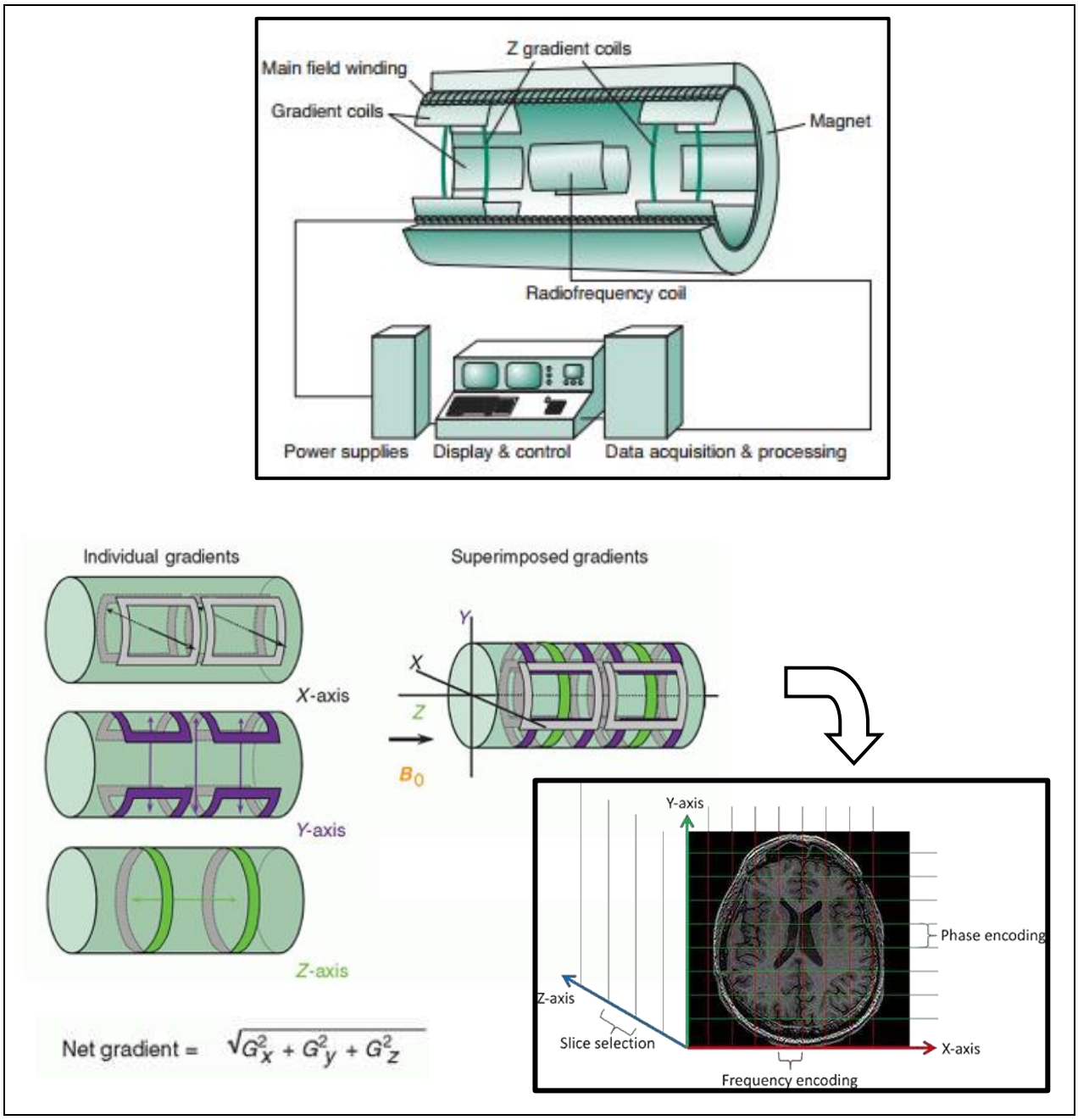

Figure 20 – *On the top (A), representation of the main components of an MRI scanner {19}; below (B) a schematization of how superimosed gradients work for spatial encoding {18}:* each three-dimensional axis is identified via the superimposition of a given gradient field; then, the final image is reconstructed by means of three steps (slice selection alog Z-axis, phase-encoding along y-axis, and frequency encoding along x-axis).

3.2 FMRI BASIC PRINCIPLES: BOLD signal in brain activity

In order to function, the brain requires energy that is given in terms of nutrients, specifically oxygen delivered from the blood flow. More in detail, when specific neural cells are active, there is an increase of energy request from these cells, leading to a consequent increase of oxygenated blood flow in the surrounding area. This concept suggests that changes in brain activity is strictly related to changes in the blood flowing through the correspondent area. The oxygen flows through capillary red blood cells bounding with a specific protein known as hemoglobin (Hb).

In 1936, Linus Pauling from the California Institute of Technology [48] discovered two different conditions of the hemoglobin, as shown in Figure 21:

- *Oxygenated hemoglobin* or *oxyhemoglobin* (HbO2), reflecting diamagnetic properties with no unpaired electrons and magnetic moments equal to zero: this causes a minimal impact on the applied magnetic field and, consequentially, no distortion in the MRI signal.
- *Deoxygenated hemoglobin* or *deoxyemoglobin* (dHb), reflecting paramagnetic properties, with unpaired electrons and non-null magnetic moment: this leads to an interaction with the magnetic field applied from the MR scanner, causing a distortion of the MR signal.

This difference in magnetic properties leads to small differences in the MRI signal of blood, according to the stage of oxygenation. Thus, since blood oxygenation varies according to the intensity of neural activity, this information can be used to detect and quantify brain activity.

The contrast between these two levels of blood oxygenation used in brain activity studies is known as BOLD imaging (i.e. Blood Oxygenation Level Dependent), and measures the ratio between oxygenated and deoxygenated hemoglobin concentration in the blood. More in detail, in 1990 Ogawa observed that the BOLD effect within blood vessels became more visible as blood oxygen decreasing. Combining the magnetic properties of the hemoglobin with the MRI imaging technique, he was then able to provide the first functional brain activity map (i.e. the first fMRI images), by using deoxyhemoglobin as contrast agent, instead of the radioactive agents used until that time [49].

The BOLD signal, detected by means of the fMRI, is coupled to the underlying neuronal activity that gives rise to the Haemodynamic Response (HR) via a process called *neurovascular coupling* [50].

It is important to underline that the BOLD signal gives a method of indirect measure of brain activity, which can be described in the following steps:

- As soon a stimulus occurs, it is transduced by the sensory organs into nerve impulses, which in turn stimulate neuronal firing in the brain
- The increase of firing neurons leads to an increase of oxygen demand that is delivered by the blood, triggering the hemodynamic response. This causes a rapid rise of HbO_2 and a consequential decay of dHb at capillary level of cortical regions.
- The decrease of dHb concentration leads to an increase of hydrogen molecules of water in that cortical area, that is, a consequential increase of the MRI signal, finally detected by the MRI scanner [50,51].

The final brain images are characterized by coloured patches correlated to the areas activated during the given stimulus (or task), represented in Figure 22. These activation maps known as *functional images*, are 3D images (x for left/right, y for anterior/posterior, and Z for superior/inferior direction) or sometimes 4D when the time is also considered.

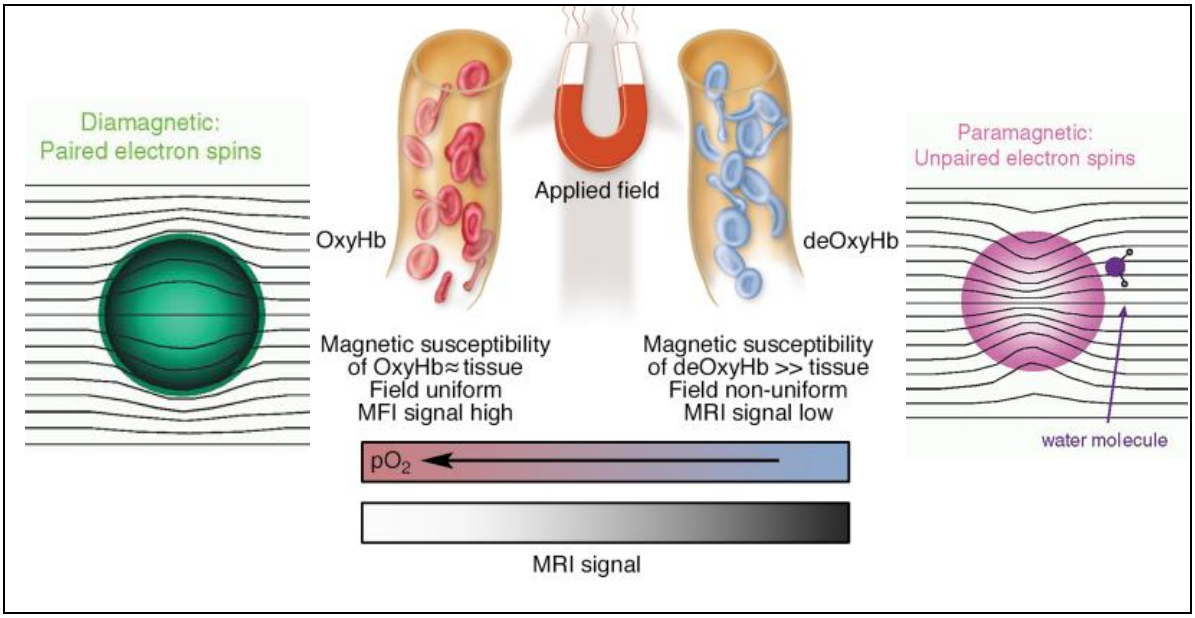

Figure 21 – *The central figure shows a schematic illustration of the origins of the BOLD effect in fMRI [51]; on the lateral sides, how the different magnetic properties of oxygenated/deoxygenated hemoglobin affect the local magnetic field applied {18}.*

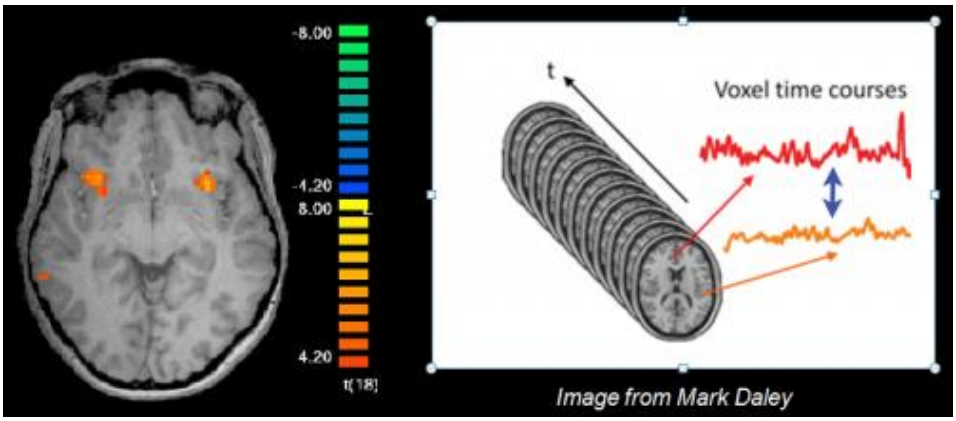

Figure 22 – *Final Brain image with different coloured areas according to the intensity of activation of the correspondent cortical area.*

A typical MRI BOLD response model can be represented as a signal in which it is possible to identify three main stages, shown in Figure 23 {20}:

1. An initial dip, occurring after 1-2s after the stimulus, usually more visible at very high fields (>7 T). It is thought to be due to a sudden decrease of dHb concentration within the cerebral region triggered, even if sometimes it is associated to the increase of local cerebral blood volume (CBV).
2. A positive dominant peak, that is reached around 5-6 s after the stimulus and constitute the bulk of the BOLD response. Here cerebral blood flow (CBF) increases unproportionally with respect to the metabolic demand, causing an increase in the HbO_2/dHb ratio and, consequentially, into the MR signal.

   In those experiments based on multiple stimuli, the dominant peak is transformed into a broad plateau, that remains constant until the end of the stimulus (and sometimes anticipated by a small initial overshoot).
3. A post-stimulus undershoot stage finally occurs, with variable duration; this is mainly due to the consumption of oxygen from the activated neurons, which in turn leads to an increase in dHb concentration and, consequentially, to a decrease of the MRI signal until a minimum. After that point, the signal increases again to reach the basal level until new cortical neurons are activated.

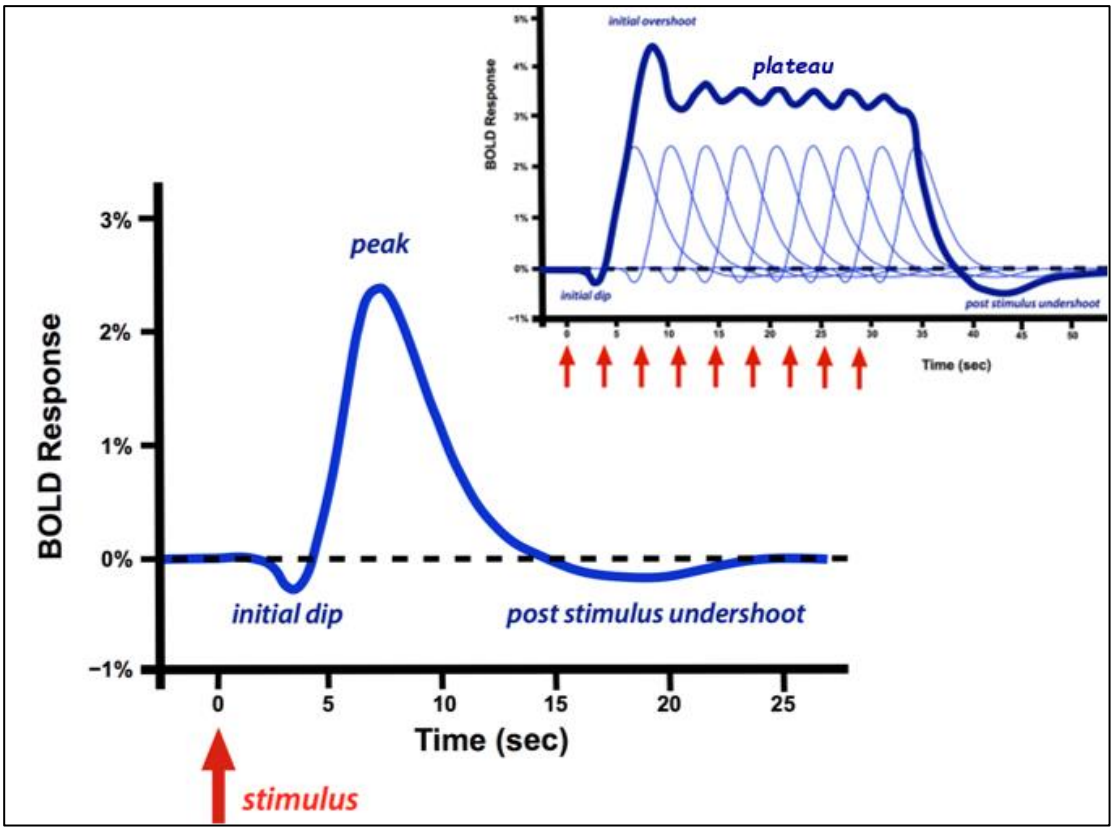

Figure 23 – *A typical MRI BOLD response; on the top right, an example of BOLD response in case of repeated stimuli {20}*

4. MATERIALS AND METHODS

This chapter illustrates the experimental procedure adopted for the MRI acquisition and the pre-processing steps used to analyse the fMRI images of the subjects recruited for the study. This thesis work was performed at the Department of "Information Engineering" at Università Politecnica delle Marche, in collaboration with the Department of "Scienze Cliniche Specialistiche ed Odontostomatologiche" of Università Politecnica delle Marche and the Riuniti Hospitals of Ancona.

4.1 EXPERIMENTAL PROCEDURE

4.1.1 Participants and Lingual Stimulation

To obtain the topographic map of the BOLD effect elicited by salty, sweet and distilled water stimuli in the cerebral cortex, unilateral stimulation of the tongue was applied to 11 healthy subjects aged 23 to 38 years old (mean 28.7 ± 4.3; 7 women). All of them gave their informed consent and the experimental protocol was approved by the Ethical Committee of Università Politecnica delle Marche. All participants but two were right-handed as determined by the Edinburgh handedness inventory [52].

Some preliminary behavioural experiments have been performed to find an appropriate threshold magnitude for the salty stimulus, and to establish the duration of the sensation induced by the salty, sweet and water stimuli. The concentration values of salty, sweet and neutral stimuli applied during the experiment are available in Table 2 [3].

Stimulation was performed by placing a soft cotton pad (tip diameter of 3 – 5 mm), on one or the other margin of the protruded tongue, at least 2.5 cm from the tongue tip. Additionally, checks based on the spatial spread of a dye, was used to ensure that both the salty solution and the water remained lateralized to the application side, as devised in Aglioti et al.'s work [53]. It has been also carefully avoided stimulation of the tip of the tongue, due to bilateral innervation of the tip from the chorda timpani.

Stimulus	***Evoked by***
Salty	NaCl 1 M
Sweet	Sucrose 10%
Neutral	Distilled water

Table 2 – *Concentration values used for salty, sweet and neutral stimuli.*

4.1.2 MRI Data Acquisition: Imaging Protocol

Taste stimuli were applied initially to the left and then to the right side of the tongue, during two different scan session and according to two similar block-design experimental paradigms.

- The first stimulation paradigm lasted 5 min, of which 60 s of rest, 30s of stimulation, 90 s of rest, 30 s of stimulation and the last 90 s of rest.
- The second stimulation paradigm was characterized by 30 s of initial rest, followed by ten alternating period of stimulation (each one lasting 15 s) and rest (each of lasting 45 s).

In this analysis, only those subjects who underwent the second protocol were taken into account. The taste stimuli responses analysed were those coming from water, salt and sweet solutions administration. More in detail:

- The neutral stimulus analysis was performed on four subjects (S1, S2, S3, S4).
- The salty stimulus analysis was performed on four subjects (S1, S2, S4, S5)
- The sweet stimulus analysis was performed on six subjects (S1, S2, S3, S4, S5, S6, S7).

More details concerning the physical characteristics of the healthy volunteers, such as hand predominance (with related individual's Oldfield Handedness Questionnaire Scores) are available on Table 3.

Subject	***Age***	***Gender***	***Hand Predominance (Oldfield score)***
S1	26	F	Right (13)
S2	26	M	Right (18)
S3	35	F	Left (46)
S4	30	F	Right (19)
S5	23	M	Right (16)
S6	26	M	Right (26)
S7	28	F	Left (41)

Table 3 – *Physical characteristics of the healthy volunteers.*

The scanning sessions were performed by means of a 1.5 Tesla scanner (Signa LX NV/i, General Electric Medical System, Milkwaukee, WI) equipped with 50 mT/m gradients, with the head restrained in a circularly polarized head coil. Once inside the scanner, patients were instructed to find and keep a comfortable position, with eyes closed, while holding their tongue out of the mouth in order to perform simultaneously the taste stimulation.

The experimental procedure for fMRI was organised of four different scans:

1. An anatomical sagittal localized (T1 FLAIR, 2D, TR=1675 ms, TE= 24 ms, Field Of View= 30 x 30 cm, slice thickness 5 mm, Matrix 416 x 320, 2 Nex, scan time 1:56 min) selected 10 (20 in more recent studies) axial section levels.
2. A 3D dataset (IR Prep Fast SPGR 3D, TR= 15.2 ms TE= 6.9 ms, TI= 500 ms, Flip Angle= 15 degrees, FOV = 29 x 29 cm, slice thickness = 1 mm, Matrix = 288 x 288, 1 Nex, scan time = 8:20 min) was then acquired.
3. Ten high-resolution axial anatomical images were then obtained (T1 FLAIR, 2D, TR= 1700 ms, TE= 24 ms, FOV = 24 x 24 cm, slice thickness = 5mm, Matrix = 256 x 256, 1 Nex, scan time = 2:25 min), on which the functional acquisitions were overlaid.
4. Finally, fMRI acquisitions according to the same axial planes were taken by means of a single-shot T2*-weighted gradient-echo EPI sequences (TR=3000 ms, TE= 60 ms, Flip Angles= 90°, FOV= 24 x 24 cm, Matrix= 64 x 64, 1 Nex, scan time 5:12 min).
   In this way, after the stimulation, 1000 (2000 in more recent studies) axial functional images have been acquired (100 images per section, 1 image/ 3 ms), from the 10 (20 recently) contiguous 5-mm-thick axial sections obtained in the first step.
   These functional images have been acquired following the BOLD contrast method.

4.2 DATA ANALYSIS

The images acquired during the experiment were collected inside of a Unix workstation (General Electric Advantage Windows 4.2) and then transferred to a personal computer in DICOM format.

The resulting data have been processed and analysed by means of FSL software (standing for FMRIB Software Library), developed by Stephen Smith and colleagues at Oxford University, UK, and released in 2000 [59,60]. It functions as a library/analysis tool for MRI, fMRI and DTI Brain Imaging data. It can be installed on Mac and Linux, but it is also possible to use it on Windows 10 via a virtual machine (WSL – Windows Subsystem for Linux), that is able to execute a Linux environment directly in Windows. Then, it is possible to run the software and visualize all the results by using a Graphical User Interface (GUI): in this case, Xlaunch was used with this purpose.

4.2.1 FSL software

FSL software has been much used for the management of fMRI data, principally due to its ability in [59,60]:

- Developing several types of statistical modelings and estimations via various tools such as FEAT or FLAME.
- Performing a strong Independent Component Analysis (ICA), usually for modeling of resting-state fMRI data.
- Analysing diffusion tensor imaging data, via a powerful visualization tool termed FSLView.

By default, FSL works with Nifti_GZ image format, that corresponds to the compressed NIfTI file (.nii or .nii.gz), nowadays considered one of the most used standard format for medical data. Since the MRI brain images are instead acquired in terms of DICOM format, it was necessary to perform a conversion so to make them able to be used in FSL environment. Thus, an additional software termed MRIcron has been used, able to perform the conversion from DICOM to Nifti {21}.

4.2.2 Pre-Processing

Before the statistical analysis, it is mandatory to perform a series of pre-processing steps, aimed to remove artefacts and noise components in the fMRI data [60]. These steps, together with those used for the statistical analysis, are performed via three specific FSL tools which are called BET (Brain Extraction Tool), FLIRT (FMRIB's Linear Image Registration Tool) and FEAT (FMRI Expert Analysis Tool), shown in Figure 24.

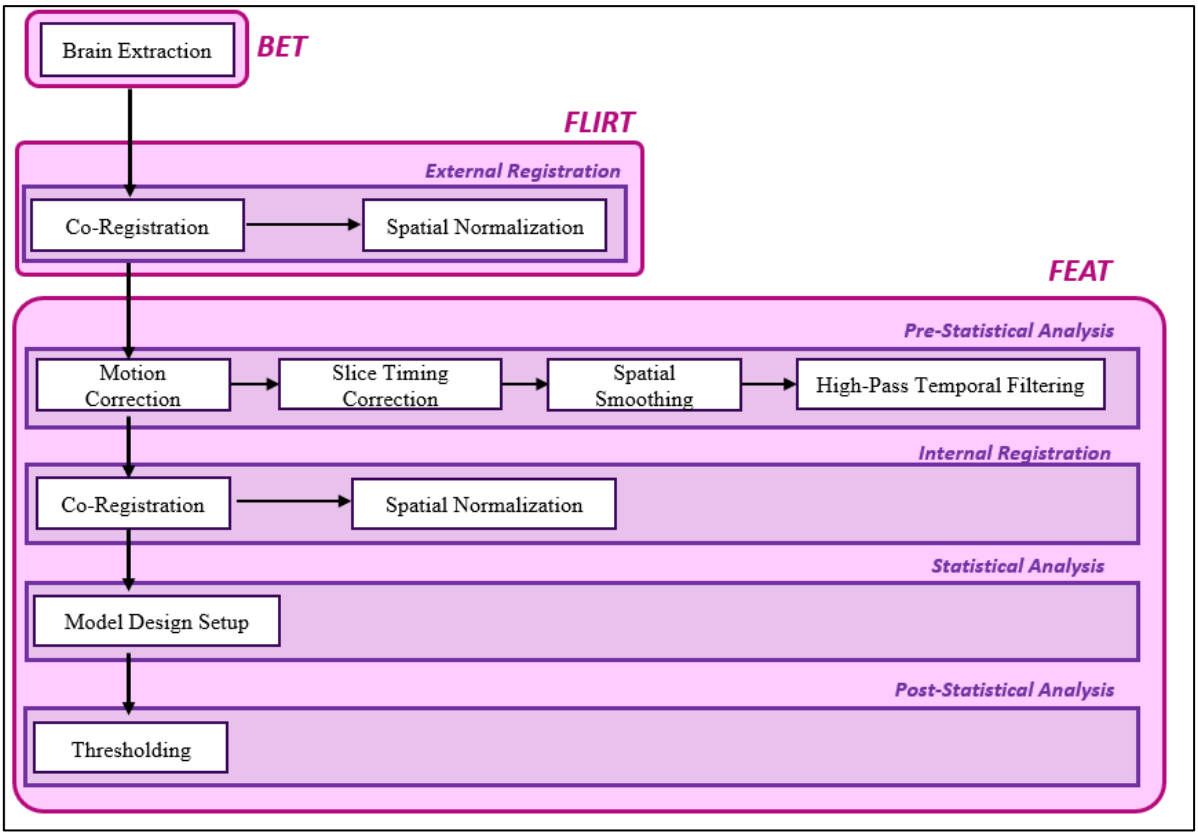

Figure 24 – *Principal FSL steps, with main focus on the most common fMRI pre-processing steps, reported in Pre-Statistical Analysis*

4.2.2.1 Brain extraction

The first pre-processing step is aimed to differentiate brain from non-brain tissue. In order to accomplish this objective, the BET (Brain Extraction Tool) function of FSL has been used [60, 61], which provides an automatic algorithm able to extract from the T1-weighted structural images only the brain tissue, thus removing parts such as skull, eyes and neck, that are not useful for the registration process. Due to the unicity of each brain image, the BET tool offers the possibility to manage the removal of the non-brain tissues by setting some parameters according to the brain under investigation. More in detail, the most important parameter to be properly set is the so-called *fractional intensity threshold parameter* (-f option), corresponding to the threshold taken into account during the brain extraction. Its value is variable depending on the brain image and should be set carefully (which means low values rather than too much high values) so to avoid the removal of also some of the brain tissue. More in detail, the default value is 0.5 and the valid range is from 0 to 1, so that the higher the value, the more the tissue removed. In the case of this experiment, a threshold value of 0.14 was originally chosen, due

to the particularity of the brain image of being already cut in a section of interest of the brain (illustrated in Figure 25). Then, the resulting image was carefully checked via the FSL's visualization tool named FSLeyes, to verify if non-brain tissues were correctly removed without losing also brain components. In those cases in which was considered necessary, the -f option was increased/decreased to obtain better results. The final image was automatically renamed as "initial name_brain" and used later during the registration process. An example of structural brain image before and after BET is available on Figure 26.

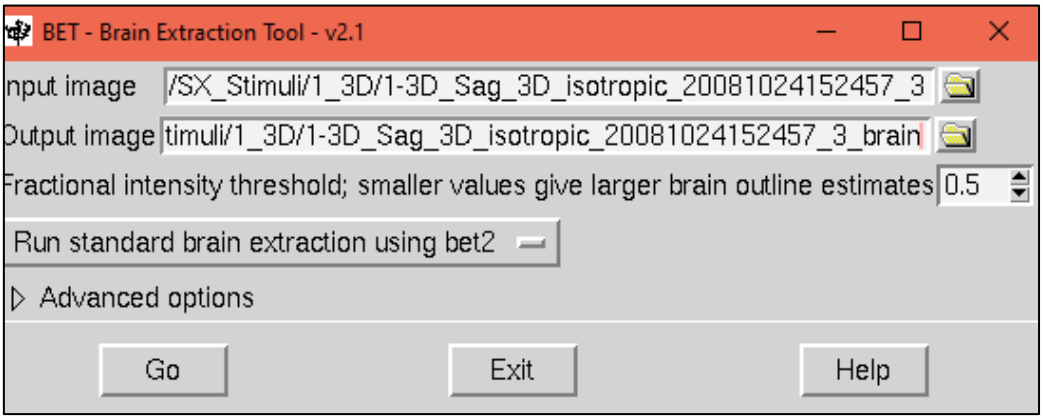

Figure 25 – *Brain Extraction Tool (BET) layout.*

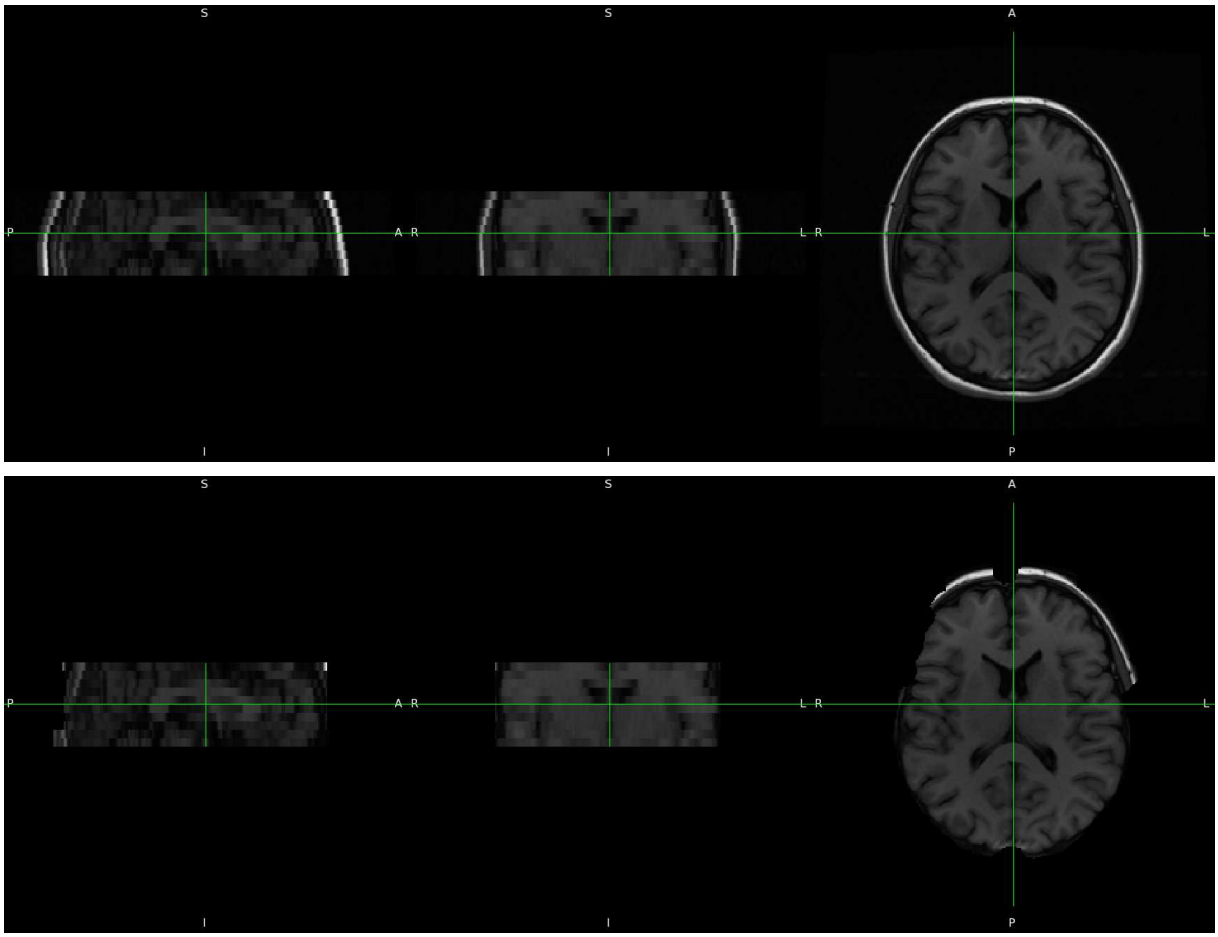

Figure 26 – *Example of non-brain tissue removal after BET on 2D structural MRI image.* On the top image, the initial 2D structural image; on the bottom, the resulting image after non-brain tissue removal with f-value equal to 1.4.

4.2.2.2 External Registration

In most of fMRI cases, there is the necessity of generalizing a given brain image across individuals. Nevertheless, since individual brains are highly different with respect to their sizes and shapes, it would be more appropriate for them to undergo firstly a transformation, so that they can be subsequently aligned one to the other [60]. This spatial transformation of the fMRI data into a reference space prior to the analysis is denoted as Registration and can be subdivided into two steps [62]:

1. *Co – registration*

This step is aimed to reach an anatomical voxel-correspondence between each functional image and the T1-weighted structural image of the same subject. In this way it is possible to conduct a proper analysis and precisely recognize the anatomical position of any region of interest, *i.e.*, that one in which it is possible to appreciate more voxel activity in the functional image.

2. *Spatial Normalization*

In order to localize and interpret the resulting localizations, it is necessary to make use of an *atlas*, that is defined as a guide for the location of anatomical features in a certain coordinate space. As anticipated, due to the high variability of human brains, it is necessary to align all the acquisitions (both the functional and structural) to a *template*, which is a specific atlas representation that allows to perform a proper spatial normalization of the MRI data [60].

There are several kinds of atlases, among which it is appropriate to mention:

- ***Talairach atlas***

The Talairach atlas is the best world-wide known brain atlas, created by Jean Talairach in 1976 and then updated in 1988. This results from a specific spatial normalization method known as Landmark-based method, in which Talairach provided a set of anatomical landmarks to align brains across individuals: the anterior and posterior commissures (AC and PC), the midline sagittal plane and the exterior boundaries of the brain at each edge, illustrated on Figure 27.

Even though it was highly adopted during the neuroimaging development period, nowadays its usage is controversial, mainly because of the absence of an accurate MRI scan for the individual on whom the atlas is based. Indeed, according to Poldrack et al., this atlas is based on the single brain of a 60-years-old woman, and therefore it is not able to represent neither the population nor a single individual. Moreover, the construction of the atlas results from the reflection of the left hemisphere to model the other hemisphere, which consequentially leads to some errors due to the asymmetries which are normally present in each human brain. According to these reasons it is thought more preferrable to adopt other automated registrations methods which use image-based templates. Nevertheless, it is still spread out the tendency of using the term "Talairach space" when indicating any stereotactic space [60].

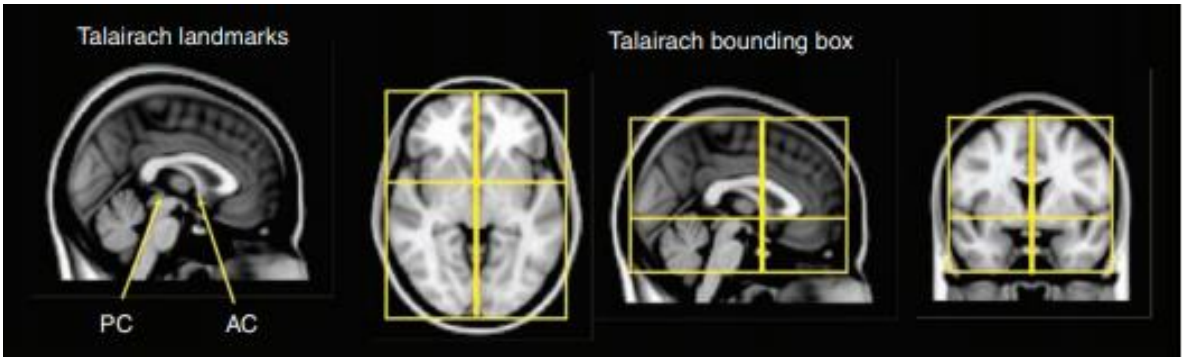

Figure 27 – On the left, *Talairach space with the correspondent landmarks*: anterior commissure (AC) and posterior commissure (PC). On the right, the *bounding box for the Tailarach space* determined by the AC and PC along the midline sagittal plate, and the superior and inferior boundaries of the cortex [60].

- ***MNI atlas***

This is a population-based atlas which provide an automated registration, with respect to the landmark-based registration given by the Talairach one. The resulting templates have been created at the Montreal Neurological Institute (MNI) and are the most common used in fMRI studies [60]. These set of templates includes:

- The *MNI305*, resulting from the alignment of a set of 305 images to the Talairach atlas using the landmark-based registration, giving a mean on which each of the initial images are then aligned using a 9-parameter registration [63].
- The *ICBN-152 templates*, that consist in a set of higher-resolution images registered to the previous MNI305 template, using a 9-parameter affine transform. Most of the nowadays neuroimaging tools use the MNI152 as the standard space for normalization, leading the International Consortium for Brain Mapping (ICBM) to choose this atlas as the "standard" for neuroimaging experiments [60].

- ***Probabilistic atlases***

With respect to the previous ones (that are based on single individuals' brains), these kinds of atlases give a description of the variability in the localization of specific anatomical structures within a stereotactic space across a large number of individuals [60]. One of the most common is the *Harvard-Oxford atlas*, which is considered the most reliable in the study of activation locations. This is available in terms of two atlases which cover 48 cortical (cortical atlas) and 21 subcortical (subcortical atlas) structural areas, derived from structural data and segmentations provided by the Harvard Center for Morphometric Analysis {22}.

The FSL software package provides a set of different atlases, such as the Harvard-Oxford probabilistic anatomical atlas (cortical and subcortical), or *the MNI152 standard-space T1-weighted average structural template*, which derives from 152 structural images averaged together after high-dimensional nonlinear registration into the common MNI152 coordinate system. This last one template belongs to the 152 nonlinear 6^{th} generation healthy human atlases available from the NeuroImaging & Surgical Technologies (NIST) Lab, according to the McConnel Brain Imaging Centre {23}.

The two previously described steps (Co-Registration and Spatial Normalization) are usually performed directly in FEAT, prior the Statistical Analysis. Nevertheless, in this case it was necessary to perform an initial external Registration, to ensure a correct re-alignment and re-

orientation of either the structural or functional images inside the Standard Space. To accomplish this step, the FLIRT tab was used, available in the FSL initial GUI prior the FEAT tab.

FLIRT (FMRIB's Linear Image Registration Tool) is a fully automated robust and accurate tool for linear (affine) intra-and.-inter-modal brain image registration. [64,65]

There are two different modes of operation within FLIRT:

- Registration of two single volumes together (*Input image → Reference image*): this is the simplest use of FLIRT and gives as output a normalized image saved in the appropriated output image box.
- Two-stage Registration (*Low-res image → High-res image → Reference image*): in this case, the low-resolution input is initially registered to the first target high-resolution image and then this result is registered to the final Reference image. These two transformations are concatenated and then applied to the original low-res image, giving as output a new version of it, transformed and/or re-sliced to the reference image space {24}.

Within the FLIRT tab, in correspondence of each target image, there are two dropdown menus:

- The *Search* window, that gives to the FSL tool how much to search for a good alignment between the low-res or input image and the high-res or reference image. There are three possible choices (*No search, Normal Search, Full Search*) for selecting the angular range over which the optimisation search stage is performed.
- The *Degrees Of Freedom* window, it is possible to choose between 3,6, and 12 degrees of freedom, according to the kind of transformation one is going to perform: for 3D-to-3D mode, the DOF can be set to 12 (affine), 9 (traditional), 7 (global rescale) or 6 (rigid body), while for 2D-to-2D mode, only 3 DOF (rigid body) transformations are allowed.

In this case, an external registration was executed using FLIRT using a two-stage registration mode, which uses as input the low-resolution image, and two target images *(low-res image → high-res image → reference image)*. In this case, the functional image was used as low-res image, while the 3D-ISO acquisition was chosen as high-res image. More in detail, the registration process can be described via the two following steps

1. Firstly, the low-res functional data was registered to the high-res 3D – ISO image, by using 7 DOF.

2. Then, the high-res 3D-ISO was registered to the final Reference image, which can be any standard template available in the FSL library (in this case, the MNI_T1weighted_2mm template), by using 7 DOF.

The two-resulting transformations were then concatenated and applied to the original low-res functional image in order to normalized it with respect to the standard MNI space, giving the final output image. Moreover, the FLIRT GUI offers the possibility to extend the estimated transform to another (secondary) image, which was originally aligned with the input image, in order to align both to the standard space. Thus, the 2D anatomical axial sections were selected as secondary images during the registration process of each correspondent functional image. In this way, both the functional and anatomical images maintained their alignment during their normalization to the reference space. Then, the two images, aligned one to the other and both to the template, were given as functional normalized output and a new 2D structural normalized output, available as .nii files. Further Advanced Options are also available in the bottom of the FLIRT GUI. More in detail, a main focus was involved in the choice of the interpolation method to be used in the final transformation: according to the data analysis adopted by Mascioli et. al [3], the trilinear interpolation was selected. Furthermore, also the angular range over which the initial optimisation search stage is performed was selected (in correspondence of Search Option), by choosing the maximum range [min= -180, max=+180].

In Figure 28 it is possible to appreciate the different modes of FLIRT, in the case of 3D transformation. The final output image, once saved in the appropriate folder chosen within the output box inside the FLIRT tab, will be the input of the FEAT GUI.

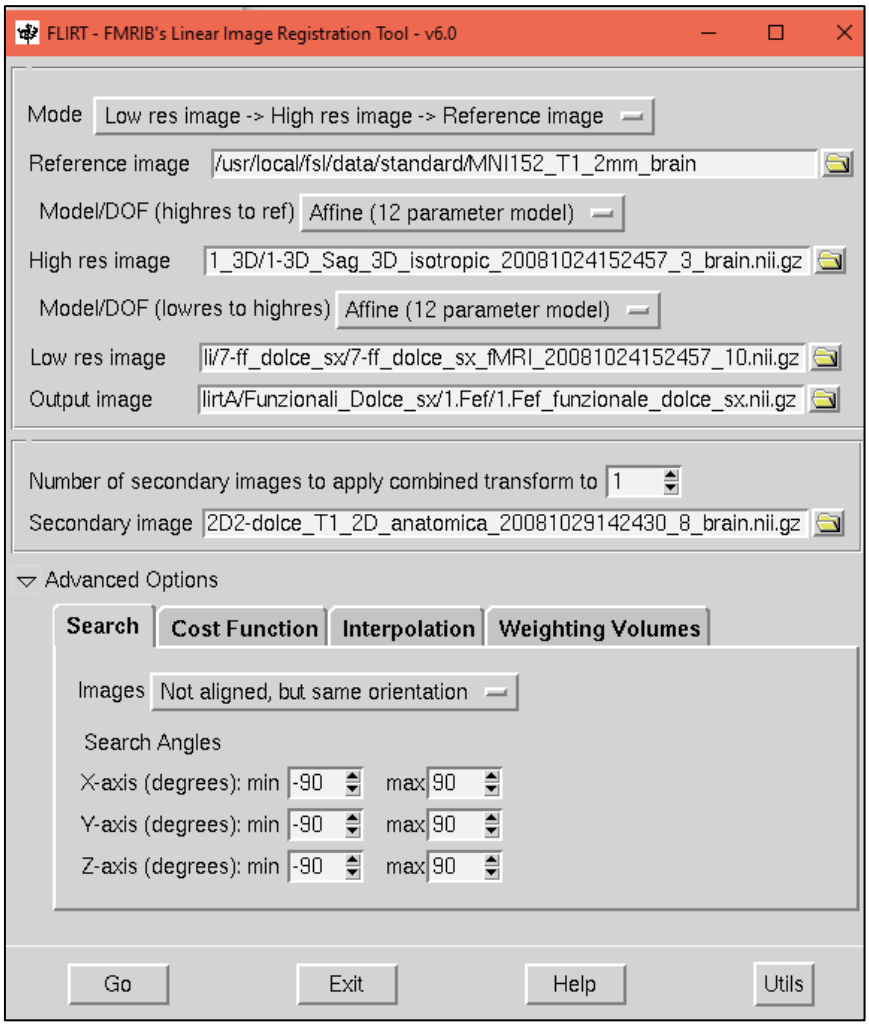

Figure 28 – *Different modes of FLIRT*: (a) *input → reference image*, using as input the 3D structural image and reference the MNI152 template; (b) *low res → high res → reference image*, where low res stands for functional image, high res as structural (in this case the previously normalized 3D image) and reference as MNI152 template.

4.2.2.3 Data Selection

Once the first registration process has been successfully completed, the proper fMRI input should be given to the FSL FEAT tool.

To do so, it is necessary to move to the FEAT GUI, and choose on the top "*First-Level Analysis*": this panel allows to analyse each session's data, which means the time-series analysis of each subject's 4D fMRI data. The "Higher-level analysis" alternatively proposed will be then selected to compare the different first-level analyses across all the subjects.

At this point it is possible to run a "Full" analysis (pre-processing and statistics) or each step separately. In this work the "Full" analysis has been chosen, since all the steps were required for a complete investigation.

The first step is the selection of the input data. Once the "Data" section of the FEAT GUI has been opened, the 4D fMRI functional data (previously registered via the FLIRT tool) has been given as input. This makes the Repetition Time (TR) and the number of total volumes automatically set: this information is critical for a correct choice of volumes deletion, a procedure that should be done prior to any type of analysis aimed to delete the so-called "dummy scans", which are the number of acquisitions coming from those cycles that the machine has to perform after receiving the RF pulse, until it reaches the steady-state magnetization. Since these acquisitions have no clinical significance, can be easily removed. The proper number of volumes to be deleted is usually related to the value of TR and the total volumes. Since in this experiment 100 volumes have been taken, with TR=3 s, it has been chosen to delete only the first two volumes.

4.2.2.4 Pre-statistical Analysis

At this point, it is necessary to perform all the pre-processing steps needed to obtain a proper Registration, as it can be appreciated in Figure 29.

- **Motion correction (realignment)**

One of the most important artefacts to manage is related to (involuntary) head movements, which often lead to significant changes in BOLD signal intensity, most of times at the edge of the brain and at tissue boundaries. The main consequence is a misalignment of successive slices that in turn results in an incorrect representation of a given anatomical part of the brain, by associating, for instance, a specific voxel to an improper anatomical brain area. The standard method of correction is based on the choice of (1) a center of mass as the center of transformation (or initial alignment) and (2) the parameterization of the transformations as three Euler angles, three translations and three scales. More in detail, head motions should be described via 6 parameters, 3 of translations (x, y, z) and 3 of rotations (roll, pitch, yaw) that are used in Euler convention to describe rigid body motion in a three-dimensional space [66].

The method proposed by FSL to correct motion effect is denoted MCFLIRT (Motion Correction FLIRT) and consists in a traditional intra-modal motion correction algorithm designed for fMRI time series [65]. MCFLIRT considers the entire time-series, in which the

middle functional volume is selected as the common reference volume, and all the other volumes are aligned with it via an iterative procedure using a specified cost function. Here, a series of optimizations are performed, that use trilinear interpolation with the purpose of minimizing the cost function.

❖ Slice time correction

Functional MRI acquisitions are performed via echo planar imaging (EPI), where multiple two-dimensional slices are acquired and then stacked together in order to construct the final three-dimensional volume. The timing of the entire process, previously defined as Repetition Time (TR) ranges between 0.5 and 4 seconds, according to specific parameters such as the pulse sequence chosen, the Field-Of-View (FOV) and the total number of slices. This means that fMRI data are considered as 2D scans, in which the singular slices cannot be obtained simultaneously, but only at different timings, leading to an accumulation of delays between the first and the last slice, that must be corrected to perform a proper analysis. These are also known as "slice-dependent-delays", since they are usually specific to the type of modality of slice acquisition selected. The most used pre-processing step aimed to adjust this problem is the so-called Slice Time Correction (STC), which works by shifting the time series of each slice to align all the slices to a single reference time point [67]. More in detail, it is usually common to consider one slice as the reference one and all the others are then temporally shifted to match the reference-slice acquisition time. Nevertheless, the efficiency of this method is strictly related to many factors, such as the subject's brain size, the head position and orientation in the scanner, and the temporal shift size itself.

The Slice timing correction implemented by FSL has the purpose of correcting each voxel's time series by assuming that all slices were acquired exactly half-way through the relevant volume's TR, even though the acquisitions are taken at different timings. To do so, FSL FEAT uses a low-order Hanning windowed sinc interpolation, for shifting each time-series of a fraction of TR. The requirement is the knowledge of the order through which the slices were acquired and select it on the panel: it is possible to choose a sequential order of acquisition (ascending or descending), or an interleaved mode (in which first all the odd slices and then the even ones are acquired, or vice versa). In the case of this experiment, the correction chosen has been Regular up (0, 1, 2 … n-1), in which the acquisitions are considered as taken from the bottom to the top.

❖ Spatial smoothing

Another step needed during the pre-processing stage is the so-denoted Spatial smoothing, which requires the application of a filter to the image, with the purpose of removing high-frequency regions of the signal (that's the reason why it is usually compared as a low-pass filter), leading to many benefits [60]:

- ✓ It allows to increase the Signal-to-Noise ratio (S\N) in case of larger features, compensating the eventual loss of some smaller features.
- ✓ It contributes to reduce the mismatch due to the variability of the anatomical location of some functional regions, that rises when data are combined across individuals.

Spatial smoothing can be performed in various modalities The most popular method adopts the convolution of the functional 4D image with a 3D Gaussian (or Kernel) filter, which establishes an amount of smoothing according to the width of its distribution (known in statistics as "standard deviation σ"). Precisely, the degree of smoothing is proportional to the "Full Width at Half-Maximum" (FWHM) of the Gaussian distribution, which measures the width of the distribution in correspondence of the point at which it is at half of the maximum value, and it is related to the standard deviation via the equation:

$$FWHM = 2\sigma\sqrt{2\ln(2)} \tag{3}$$

According to this, the larger FWHM, the greater the smoothing, and consequentially, the more blurring of an image is, as can be seen in Figure 29.

It is important to note that, while the smoothing represents how much the filter is applied to the image, the smoothness indicates the correlation between neighbouring voxels. This relationship can be expressed mathematically as:

$$FWHM = \sqrt{FWHM_{intrinsic}^2 + FWHM_{applied}^2} \tag{4}$$

where the first contribution indicates the smoothness related to the intrinsic correlations in the image, while the second one is due to the application of the Gaussian filter. Due to this relationship, it is always recommended to make some considerations before deciding how much smoothing to apply. For example, if the purpose is to reduce noise in the image, it is suggestible to adopt a filter which should not be larger than the signal of interest.

Since the objective of this work was to find very small activation areas, a FWHM = 1mm was definitely selected to perform spatial smoothing on the functional data. In this way, the

possibility of obtaining more separated clusters of activations was ensured, with respect to the standard value of 5mm which instead gave a minor number of clusters composed of a greater amount of activated voxels.

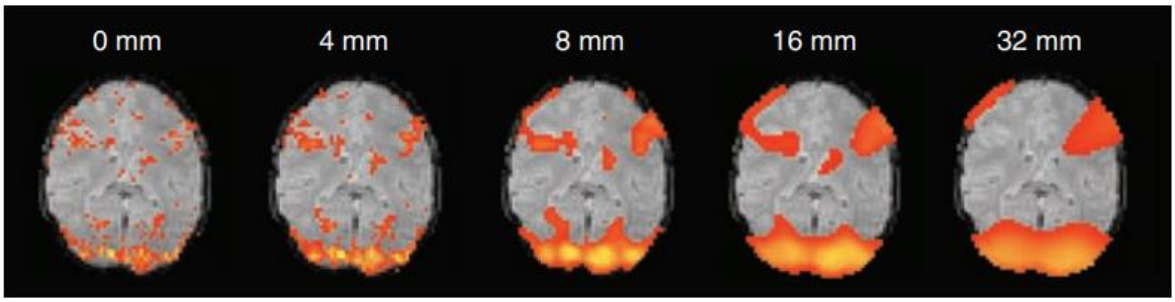

Figure 29 – *Example of the effects of spatial smoothing on activation* [60]*:* it is possible to appreciate how the FWHM value affect the quality of the final image. More in detail, as the FWHM value increases, there is a greater detection of larger cluster activity. On the other hand, this leads to a decrease of smaller cluster activity detection.

❖ Temporal filtering

Temporal filtering is the last step required to complete the pre-processing phase of the fMRI data. Indeed, when dealing with task responses, what one is looking for are changes in neuronal activity as a response to a certain stimulus. This means that the fMRI signal rises from the hemodynamic response to a given neuronal activity, and not the activity itself, leading to important implications for what concern the temporal characteristics of the signal. More in detail, temporal filtering has the purpose of removing/attenuating frequencies of the raw signal which are not of interest, that in fMRI data are usually far from the task-frequencies. For instance, if the experiment is based on a repetition of a stimulus every 10 s, the response signal should have a task-frequency around 0.1 Hz. Moreover, noise in fMRI data is usually present in low frequencies, which means that most of times temporal filtering consists in the application of a high-pass filter, expressed usually via a cut-off period (seconds), even though it can be also easily computed in terms of cut-off frequency (Hertz). What is challenging in this context is the appropriate choice for the cut-off period: for task-data, a good solution could be setting the high-pass filter as the longest temporal period allowed, without attenuating the task waveform. For this reason, in case of an rArA (r= resting phase, A=stimulus) experiments, the FSL guide suggests adopting a cut-off period of (r+A) seconds {25}. By the way, it is also possible to let the tool itself to compute the appropriate cut-off period once that the fMRI data has been given as input. For this reason, it was decided to select the button “Estimate High-Pass Filter”, which changed the appropriate cut-off period from the 100 s default value to 90 s (or 0.01 Hz), as shown in Figure 30.

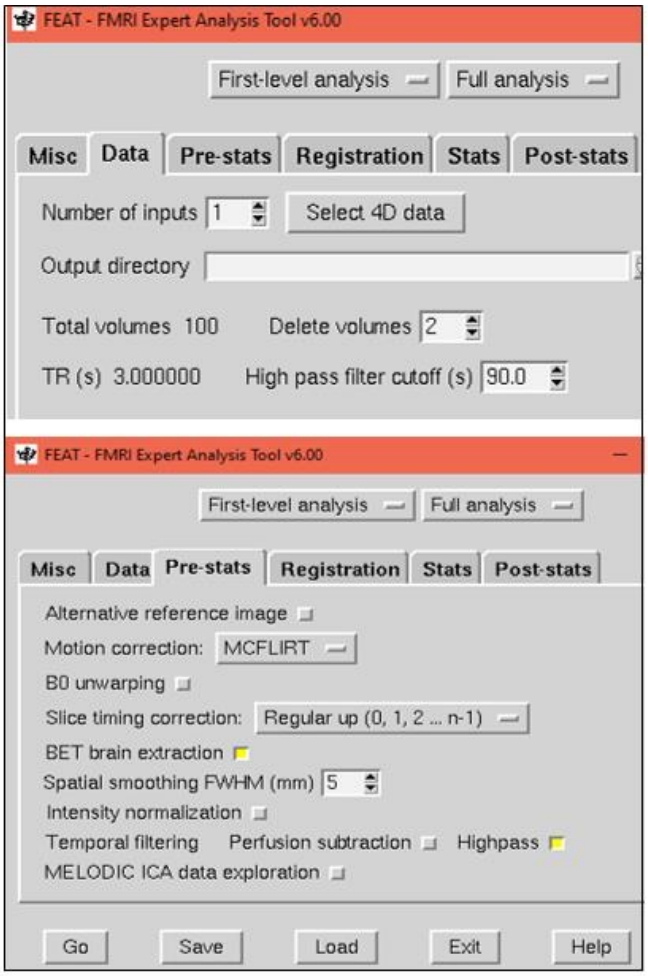

Figure 30 – *Example of pre-processing steps adopted in FEAT:* in the top panel, deletion of volumes according to TR value and estimation of the High-pass filter cut-off of 90s; in the bottom panel, Slice-Timing correction and Spatial smoothing options.

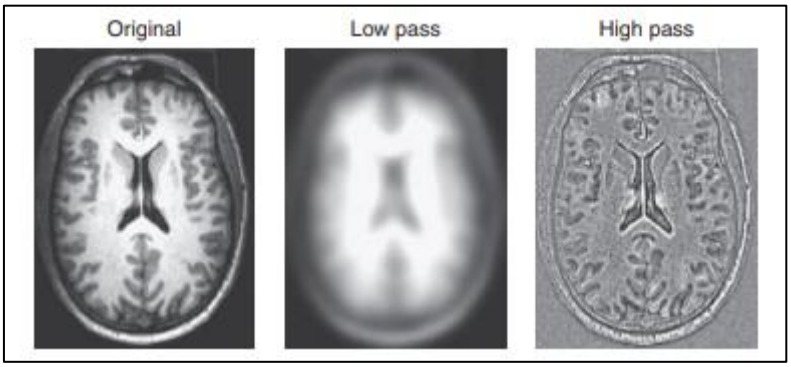

Figure 31 – *Examples of filters applied to a T1-weighted MRI image* [60]: the low pass filter blurs the image whereas the high-pass filter enhances the edges in the image.

4.2.2.5 Registration

Once that Slice-Timing Correction (STC), Motion Correction and Temporal filtering have been performed for attenuating artifacts effects, the last phase before the statistical analysis was a further internal registration of the input functional data onto the standard MNI template. This final step was necessary despite the already-externally-applied registration, because allows the standardization of the statistical results of the cortical activations onto a normalized brain.

The FEAT GUI provides also in this case a two-steps Registration: first co-registration of the functional input data onto the correspondent structural image, and successive normalization of the resulting data onto a standardized template.

The two main buttons of interest within the Registration tab are the *Main structural image*, that should be selected and requires as input the structural (2D anatomical or 3D) image of the single subject under investigation (*i.e.*, the subject whose functional image is under analysis), and the *Standard Space*, on which it is possible to manage the options for normalizing the anatomical image to the template image.

Since, despite the initial external registration, the functional data appeared still not properly aligned to the standard template, a second normalization was applied at this level. More in detail, (as can be seen reported on Figure 32):

- The *Main Structural image* was set as the normalized 2D structural image obtained as output after the two-stage registration process performed in FLIRT. Since this image was still aligned to the functional data, only 3DOF were selected, with Normal Search.
- The *Standard Space* was set as the MNI T1weighted_2mm template, with Full Search and 7 DOF, in order to guarantee a proper alignment for those images which were not completely resliced to the template in the previous step.

Despite the pros of standardizing the resulting image into a Standard Space, a common problem when normalizing a functional image is related to a lack of a unique process which allows to make an instant translation from one standard space to another one without introducing some noise. Therefore, after the statistical analysis has been performed, an extra-step is needed to convert the MNI coordinates obtained after the statistical analysis in Talairach coordinates. Some ways to proceed could be the following ones:

- A MATLAB function can be used (*Mni2atlas*), that takes a Region Of Interest (ROI) or a vector of coordinates in MNI space and returns labels from different FSL atlases (among which the Talairach one) [68], {25}

- An automatic algorithm can be adopted, available as a simple tool that allows a user to map from MNI to Talairach coordinates and back {26}.

In this work, the resulting MNI coordinates of the activated voxel locations were converted using the automatic algorithm provided by the mni2tal tool previously cited. It is important to underline that the MNI linear transform is not able to perfectly match its brains to the Talairach brain. In fact, the MNI brains are about 5 mm taller (from the AC to the top), 10 mm deeper and 5 mm longer than the Talairach one [68]. As a consequence, it is possible to note an important difference in terms of localizations of areas; for instance, if considering a set of coordinates equal to (x=-8, y=-76. z=-8), this will be located in the occipital cortex in the MNI brain, but in the Talairach atlas will correspond to the CSF. For this reason, a correct translation from one coordinate space to the other one is critical for a proper activation analysis {27}.

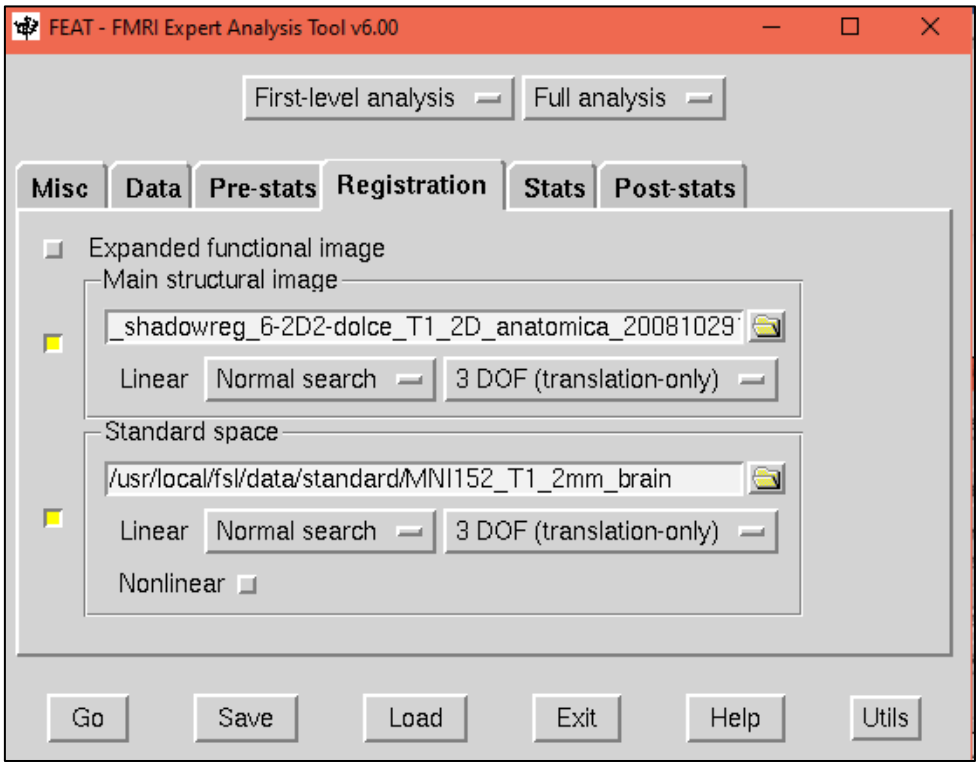

Figure 32 – *Registration options chosen in FSL FEAT GUI.*

4.2.3 Single-Subject Statistical Analysis (First-Level)

Once all the previous steps have been successfully completed, the Statistical Analysis can be performed. Since it was initially selected "First-Level Analysis", in this context the purpose is to guide a statistical study of the cortical activation locations within a single subject. To do so, the last two tabs of the FEAT GUI have to be set.

4.2.3.1 General Linear Model (Stats)

In order to improve the quality of the final statistical results, a reliable model should be given to the Stats tab. With this aim, the FEAT GUI uses the General Linear Model, which allows to describe one or more stimulation types.

For each voxel, a linear combination of the modelled response to the correspondent stimulation type is found, which minimises the unmodelled noise in the fitting {28}. More in detail, the General Linear Model sets up a model and fits it to the input 4D data. If the model is derived from the experimental procedure used for the stimulation of the subject in the MRI scanner, then it is possible to reach a proper fit between the model itself and the functional data. The GLM used in FEAT is univariate, that is the model is fit to each voxel's time course separately, instead of all the times courses at the same time (like, for example the Independent Component Analysis – ICA).

The GLM is usually formulated in matrix notation, where all the parameters are grouped into a vector A, and all the model timecourses into a matrix X, characterised of a certain layout denoted as Design Matrix. For example, if the subject experiences two different stimuli (such as vision and auditory), then there will be two model timecourses, represented each one as a column, with time going down the image vertically. Each of this column is denoted as *Explanatory Variable (EV)* and represent a different stimulus type, so that, when the model is fit to the data, for each voxel there will be found an estimate of "how good is the fit" of each EV to that voxel's timecourse. Each EV in the design matrix should result in a Parameter Estimate (PE) image. In order to convert the value of the parameters estimates (PEs) into a statistical map, the actual value of PE is divided by the correspondent error. The results is a *t* value that is then converted into a probability (*P*) or *Z* statistic via statistical transformations: thus, t, P and Z indicate how the data is related to a specific EV of the model. More in detail, it is possible to obtain images of Z (denoted also as "Gaussianised t") meaning how much each voxel is related to each EV, leading to make a comparison among the various parameter estimates in order to find out that one representing the best the data. This process, also known as "producing contrasts" is performed by substracting each parameter to the other one, in order to evaluate a standard error.

The simplest design that can be generated derived from the conversion of a single EV into a Z-statistic image, by setting up a contrast value for that EV (usually this value is equal to 1), and leaving all the other EVs to 0. Starting with this concept, it is then possible to compare, for example, two different stimuls (EV1 and EV2) by simply substracting one to the other, and the

operation is made by setting one contrast value to -1 and the other one to 1. It is important to underline that all the EVs must be independent of each other, that is, no EV should be a sum of other EVs in the design, otherwise the matrix used to model the data is not able to properly work.

It is possible to setup the Model by pressing the "*Model Setup Wizard*" button for simple rest-A-rest-A experiment, or "*Full Model Setup*" button for more complex models (or to adjust the setup created by the wizard). In the case of this experiment, where the duration of each stimulus, as well as the rest period, are not always the same (*e.g.*, the initial rest period is longer than the middle ones), the second option was chosen. Then, since each fMRI data refers to the single subject's response to a single taste, a simple Design Matrix with only one EV was adopted, named S (where S stands for "Stimulus"), as shown in Figure 31.

Then, the GLM tab allows the possibility to choose the basic shape of the waveform describing that stimulus. It is possible to choose among the following options:

- *Empty* (all zeros), if one need an EV to be ignored;
- *Square* wave, if the model should fit an on/off experiment;
- *Sinusoid* wave, for sinusoidal modelling, where it is also possible to choose the number of harmonics to add to the fundamental frequency.
- *Custom* for single-event experiment with irregular timing of stimulation.

In the last case, a custom file should be used, which is a raw text file where a list of numbers with proper spaces whound represent some characteristics of the given stimulus; two different sub-options can be chosen: *Custom 1* (*one entry per volume*) and *Custom 3* (*three column format*). In the case of this experiment, driven by specific timing protocols, the Custom 3 option was adopted, shaped with a text file of three column, where: the first number in each triplets indicates the timing of the onsets (in s), the second one the duration and the last one the value of the input during that period (usually this value is left as 1).

Then, the convolution option allows to establish which form to give to the Haemodynamic Response Function (HRF) convolution that will be applied to the given waveform. The possible options are: *none* (if the original waveform does not need any convolution), *gaussian*, *gamma* (i.e. normalisation of the probability density function of the Gamma function) and *double Gamma HRF*, that indicates functions arising from the mixture of two gamma fuctions: one standard positive gamma function and a small, delayed gamma, which should model the late undershoot.

After the setting of the explanatory variable, the *Contrast value* should be set as well. Due to the simplicity of the model, one contrast was considered appropriate for the production of the final Z image. The final design matrix representation, reported in Figure 33, is shown in terms of two vertical columns: the first one is related to the ungoing of the EV previously set (i.e. the stimulus application, with its duration along time), the second one corresponds to its temporal derivative. On the left-side of the first column, a vertical bar is placed in grey to represent the total amount of time of the experiment: the smaller red bar located from the central side, corresponds to the cut-off period of the High-Pass Temporal Filter established during the pre-processing step.

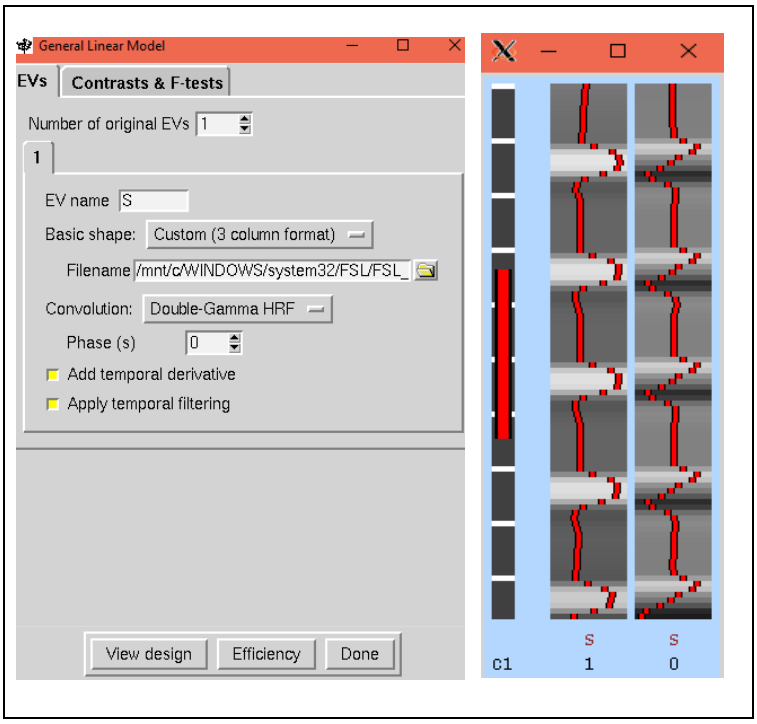

Figure 33 – *General Linear Model (GLM) tab used for the Design Model of the experiment with the correspondent representation:* each EVs indicates a taste stimulus lasting 15s and convolved by a gamma function; the vertical bar placed on the left of the model shows the period of time of the entire experiment (black) and the cut-off period of the High-Pass temporal filter (red); the second column represents the temporal derivative of the first one.

4.2.3.2 Post-Stats

The last tab in the FEAT GUI to be set-up is the Post-Stats, where it is possible to adjust all those parameters needed to determine which voxels are statistically significant for each contrast previously defined in the Pre-Stats place.

Firstly, it is necessary to define the thresholding criteria, that is, the way through which the resulting Z statistic image deriving from the initial statistical test is thresholded to show voxels or clusters of voxels activated at a particular Z significance level. In this section, it is possible to choose among the following:

- *Cluster thresholding*, which uses a Z-statistic threshold to define contiguous clusters. Then, each cluster's significance level is compared with the cluster probability threshold P. At the end, the significant clusters will mask the original Z statistic image to generate colour blobs.
- *Voxel thresholding*, a maximum height thresholding is carried out, based on the so-called Gaussian Random Field Theory (explained later), so that if a voxel is found above threshold, there should be an effect at that voxel location.
- *Uncorrected*, which means thresholding the uncorrected Z statistic values.
- *None*, if one does not want to apply threshold at all.

The GRF theory is an efficient method used to solve multiple comparison of functional images [69]. As already explained, the purpose of a fMRI analysis is to generate a statistical model that should fit the data, giving model parameters. These parameters are thus used to represent the effect, which can be the task itself or the difference between the task and the baseline. To evaluate if the parameters obtained are reliable enough, a volume of statistic values is generated, characterised of thousands of voxels. In a typical statistical analysis, since the purpose is to decide whether the statistic represents an evidence of the effect under study, usually this is compared to the so-called "*null hypothesis*", that is the hypothesis of non-effect. This means that, if the statistic is not compatible with the null hypothesis, then there will be a significance effect, otherwise if there is a given percentage of results (e.g. 5%), this would represent the chance that a result arises even if there is actually no effect. According to this criterion, it is reasonable that in functional imaging one wants to investigate a given family of voxel statistics of the whole brain and the risk of error related to that group of voxels. This is also known as the Family-Wise Error rate (FEW) and indicates the likelihood that this group of voxels could have arisen by chance. There are many criteria to test a family-wise null hypothesis, such as the "height thresholding" above mentioned, where a certain threshold is used to control the FEW that are linked to the number of tests. One of the most used methods to set this threshold is the so-called Bonferroni correction, which is based on simple probability rules, giving a corrected p value for the voxel of interest. Nevertheless, this method is sometimes considered too conservative, because some fMRI data show a correlation between neighbouring statistic values, leading to obtain fewer independent values in the statistic volume with respect to the number of voxels. Spatial correlation is most of times strictly related to the spatial pre-

processing applied to the fMRI images; for example, in group analysis, in order to compare different brains of different subjects it is necessary to re-align each individual image to a given standard template (i.e. Registration process, already described). This procedure gives a new picture of the re-aligned brains, where the voxels locations are different with respect to the original ones, due to a re-sample that may induces smoothing (which in turn involves averaging over voxels, thus spatial correlation) [69]. Moreover, as already seen, the smoothness of an image can be expressed with the Full Width at Half Maximum (FWHM). Since smoothing means blurring the image and increasing spatial correlation, thus it reduces the number of independent observations. For this reason, it is not so easy to use the Bonferroni correction to analyse smoothed data, issue which instead may be solved by using the Random Field Theory.

The Random Field Theory (RFT) is a recent criterion used for dealing with smooth statistical maps, thus it is considered a reliable way to analyse functional images. The RFT works on the following stages:

1. It firstly estimates the smoothness of the statistical map.
2. Then, it uses the value of smoothness inside an appropriate equation, to obtain, for different thresholds, the so-called *Euler characteristic (EC)*. The EC is a property of the image strictly related to the number of clusters above a given threshold (i.e. it can be seen as the number of blobs in an image after thresholding).
3. Finally, the EC obtained allows to compute the threshold expected.

More in detail, the EC is the number of 3D blobs with Z value higher than the threshold, and depends on the number of *resels,* a term introduced for the first time by Worsley to indicate the number of resolution elements in a statistical map, which in turn can be considered similar to the number of independent observations [70].

In this study, it was optioned a cluster thresholding, with Z threshold equal to 3.1 and cluster P threshold of 0.03

Once that also the Post-Stats tab is set-up, it is possible to proceed by pushing the button Go, which starts this First-Level Analysis.

As already anticipated, all the steps described above are related to the analysis of a single taste of a single subject. Thus, they were then repeated for each taste (water, salty and sweet) a number of time equal to the number of subjects under investigation. When all the Single-Subject Analysis were properly completed, they were used as input for the Group-Analysis (inter-subject analysis).

4.2.4 Multi-Subject Statistical Analysis (Higher-Level)

After the Single-Subject Analysis, it is necessary to group the single feat directories to obtain a final general result for the group of subjects under study. This is possible via the Higher-Level Analysis, which may refer to (1) analysis *across sessions*, or/and (2) analysis *across subjects*. With this purpose, FEAT offers two different ways of modelling:

- *Fixed Effects (FE) Modelling*, that is considered more sensitive to activation, but it ignores cross-sessions variance, so it reports activation with respect to the group of sessions and not for wider population.
- *Mixed Effects (ME) Modelling*, that models the session/subject variability, allowing to extend the results to the wider population from which the session/subject were taken into consideration.

The GLM page provides a list of several multi-subject designs adopted by FSL users, which is continuously updating thanks to Jeanette Mumford and Tom Nichols {29}. Nevertheless, for more complex designs, it is suggestible to manually generate the design files required by FSL.

In order to find among the several experimental designs available on the GLM page, the closest as possible to this experimental procedure, the first selection was made by considering only designs of no-repeated measures, i.e. those ones where there is only one scan per subject. This is mainly because each fMRI data analysed corresponds to the response of the Single-Subject to a given taste, so, if one taste is considered as a single session, the correspondent EV imposed in the Single-Subject Analysis of that functional image will be the single session effect. This means that it is not necessary to implement a Multi-Session Analysis, because each session is analysed with the correspondent response's functional image (instead of having functional images deriving from a multi-session experiment).

Once established this, among the various proposals, the Single-Group Average was considered the nearest to the real one. The Single-Group Average (or One-Sample T-Test) Model, is the simplest possible linear model, where a single group of subjects is modelled, giving as output the mean response.

To implement this design, the first step is to select "Higher-Level Analysis" on the FEAT GUI, and input the First-Level FEAT directories (i.e. the Single-Subject results). In this experiment, for each taste there is a different number of subject (which are only those ones who underwent the 2nd protocol of stimuli): for each stimulus' group, the aim is to compute the mean group effect.

According with this criterion, three different kinds of Group Level Analysis were performed by applying the Single-Group Average experimental design, each one characterised of a different number of subjects (since only those ones who underwent the 2nd protocol were taken into account):

1. Single-Group Average, composed by four subjects, giving the mean *neutral* stimulus response.
2. Single-Group Average, composed by six subjects, giving the mean *salty* stimulus response.
3. Single-Group Average, composed by five subjects, giving the mean *sweet* stimulus response.

According to this, for each stimulus, the following steps were adopted:

- Firstly, after having chosen "Higher Level Analysis" in the FEAT GUI, from the lower-level FEAT the nifti format files denoted as *"cope images"* were selected as input: each of these corresponds to the Single-Subject Analysis result of a given subject in terms of a thresholded activation image saved as nifti file.
- Then, the Stats tab was setup, by selecting Fixed Effect (FE) higher-level modelling. This implemented a standard weighted fixed effects model, where the degrees-of-freedom were computed by summing the effective degrees-of-freedom for each input from the 1st Level Analysis and then by subtracting the number of Higher-Level regressors.
- At this point, the Full Model Setup was setup, by imposing a number of EVs equal to the number of subject for that specific taste stimulus; for example, the neutral stimulus responses analysed in the 1st Level Analysis were four (each related to one subject's response), thus in the Full Model Setup of the Single-Group Average (Higher-Level Analysis) four EVs were selected, each one representing the statistical results of the response of one subject to the neutral stimulus. Then, one contrast was imposed (C1), so to obtain as output the Group Mean Response for that stimulus.
- Finally, a Post-Stats tab also in this case was implemented, by selecting Cluster as thresholding method, with Z threshold equal to 2 and P threshold equal to 0.05.

5. RESULTS

Once FEAT finishes one run, it finds the directory name associated with the 4D fMRI data, to create a related *".feat"* directory, where all the outputs are saved. Each step of the analysis is associated to a given results that can be found inside the directory. All the results are shown in the so-called "report.html" file, placed in the *.feat* folder, through which it is also possible to monitor the progress of the analysis until the end of the process.

5.1 Pre-Statistical Results

The Pre-Stats results allow the user to understand if the pre-processing step was properly performed, by looking at the estimated translation/rotation displacements associated to the functional data. More in detail, the .html report shows firstly a brief summary of the pre-processing steps applied from MCFLIRT, such as all the parameters previously chosen to perform the motion and slice-timing correction, as well as the spatial smoothing and the temporal filtering. Then, three graphical results are shown for each input data: *estimated rotations* (rad), *estimated translations* (mm), *estimated mean displacement* (mm). All of them represent the realignment parameters reported by MCFLIRT for rotation and translation motion correction, each one described for the x,y and z axis and reported as functions of the fMRI input volumes. In order to correctly check these results, a good rule is considering any sudden motion greater than half of a voxel size as an object of further investigation.

In this work, all the subjects' data reported motion correction parameters within the neglectable range. In Figure 34, 35 and 36 it is possible to see an example for each taste, where all the peaks noticeable are in the order of 10^{-1} mm and therefore considered acceptable.

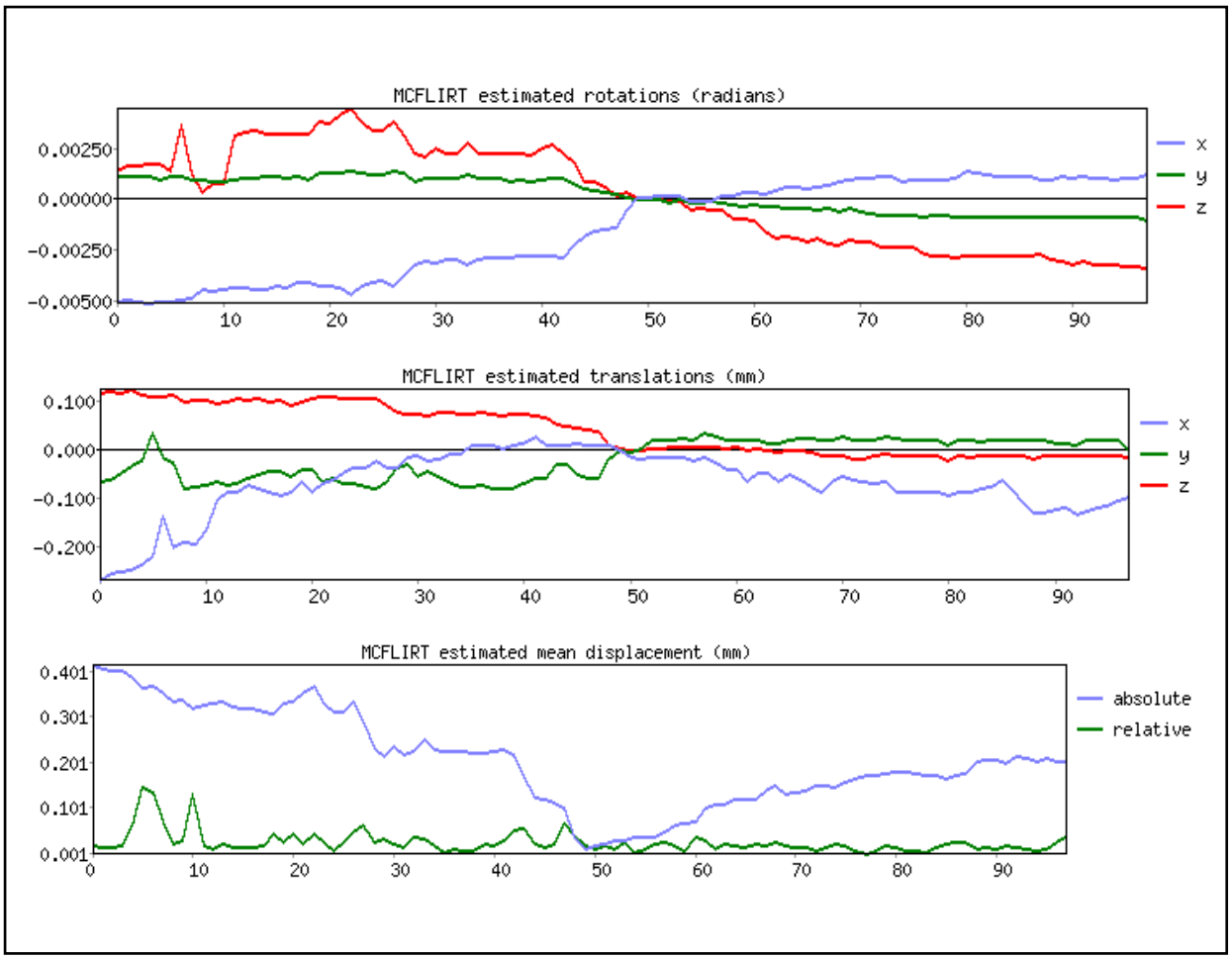

Figure 34 – *The displacement detected in subject S3 of Water Stimulus Group.*
The above panel indicates the rotation movement around the three axes, expressed in radians (rad). The middle panel indicates the rotation movement along the axes, expressed in millimetres (mm). The final panel indicates the mean displacements (mm). It is possible to notice a mean displacement either at the initial or to the final volumes, even though the magnitude is such to be considered negligible.

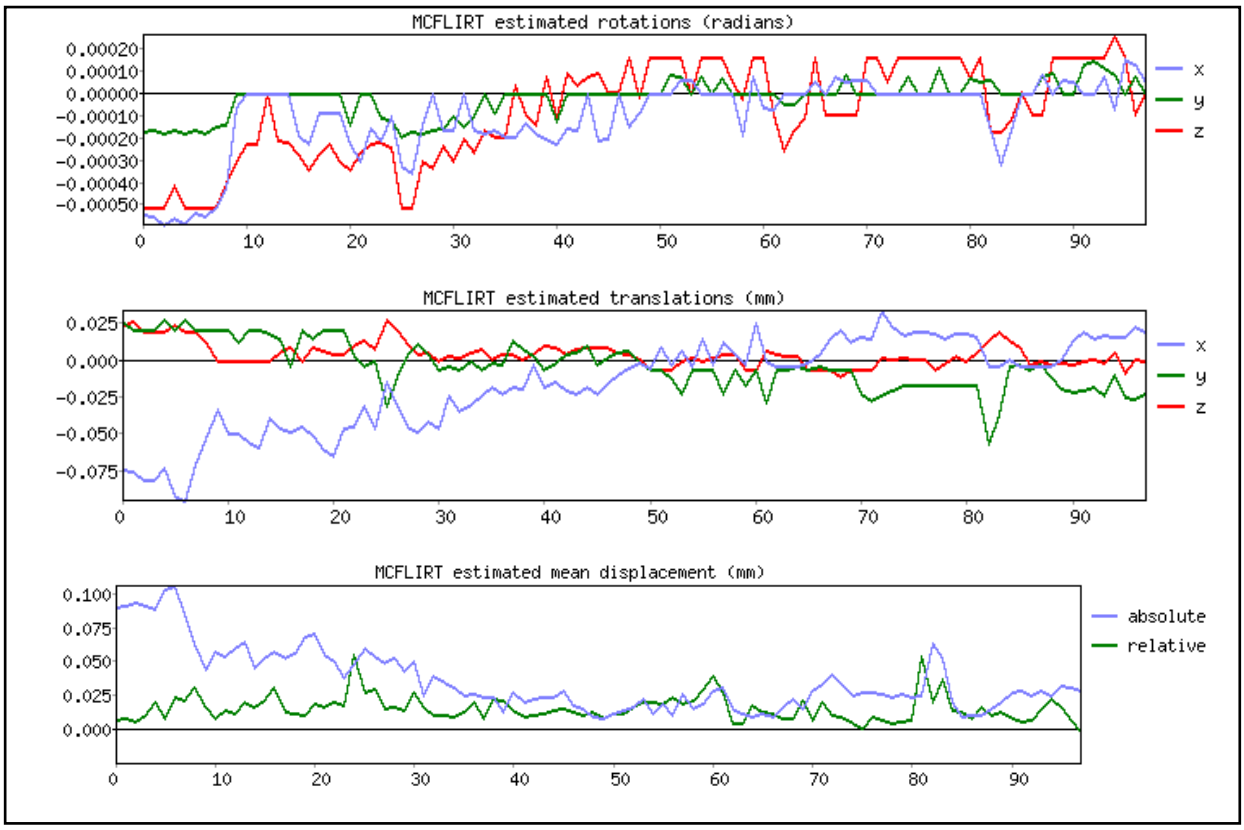

Figure 35 - *The displacement detected in subject S2 of Salty Stimulus Group.*
The above panel indicates the rotation movement around the three axes, expressed in radians (rad). The middle panel indicates the rotation movement along the axes, expressed in millimetres (mm). The final panel indicates the mean displacements (mm). It is possible to notice an initial (negligible) mean displacement, which progressively goes to zero.

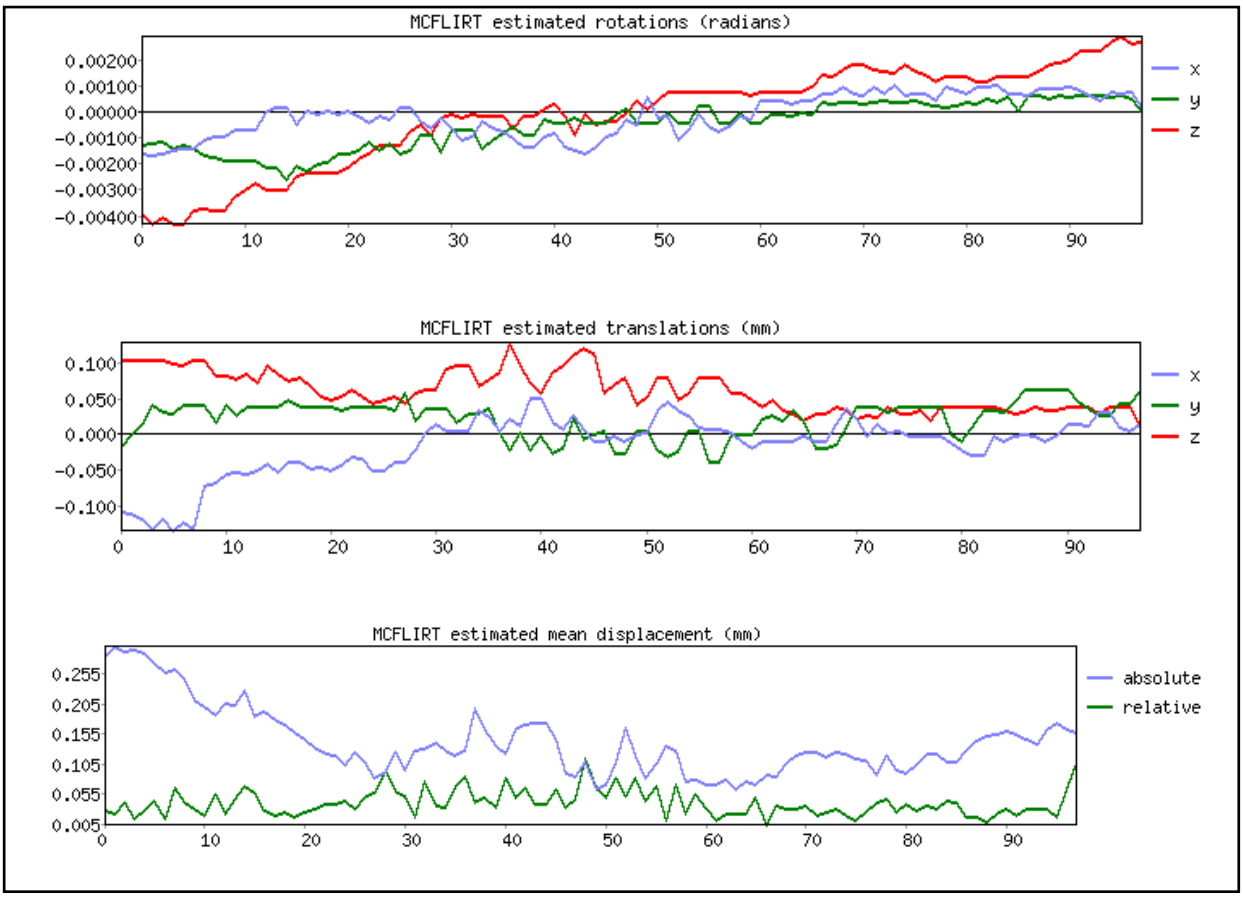

Figure 36 - *The displacement detected in subject S4 of Sweet Stimulus Group.*
The above panel indicates the rotation movement around the three axes, expressed in radians (rad). The middle panel indicates the rotation movement along the axes, expressed in millimetres (mm). The final panel indicates the mean displacements (mm). It is possible to notice an initial displacement, which progressively goes to zero. Even though the mean displacement maintains magnitude values greater than zero, the estimation can be considered negligible.

5.2 Single-Subject Analysis Results

5.2.1. Stats Results

The first statistical result gives the representation of the Model Design specified by the user during the setting-up of FEAT, for each subject's taste response. As can be noticed in the example shown in Figure 37, the Stat report page offers an illustration of the Design Matrix (previously described), where the red line under the regressor EV(=S) should reproduce the time-series of the voxel that is responsive to that stimulus, and the white bars represent the HRF convolved with the onset of each trial for that condition.

An additional image here is the “Covariance matrix and design efficiency”, with the effect size needed to estimate each contrast at a given Z threshold. In this representation, each square indicates any correlation between the different regressors, in terms of squares coloured according to a grey scale (where white indicates the best correlation and black the worst one). Since the diagonal represent each of the conditions correlated with itself, it should be characterized of only white squares, while the other squares are coloured with a grey-scale colour according to the efficiency percentage. At the end of this image, the effect required is reported, in terms of percent signal change to obtain an effect which will pass the specified Z-threshold (i.e. the percentage signal changes necessary to detect that contrasts). This value is usually considered acceptable if below than 2%, as can be noticed in Figure 37, which gives as an example the Model Design with the correspondent Covariance Matrix and Design Efficiency of subject S4 of Sweet Response Group.

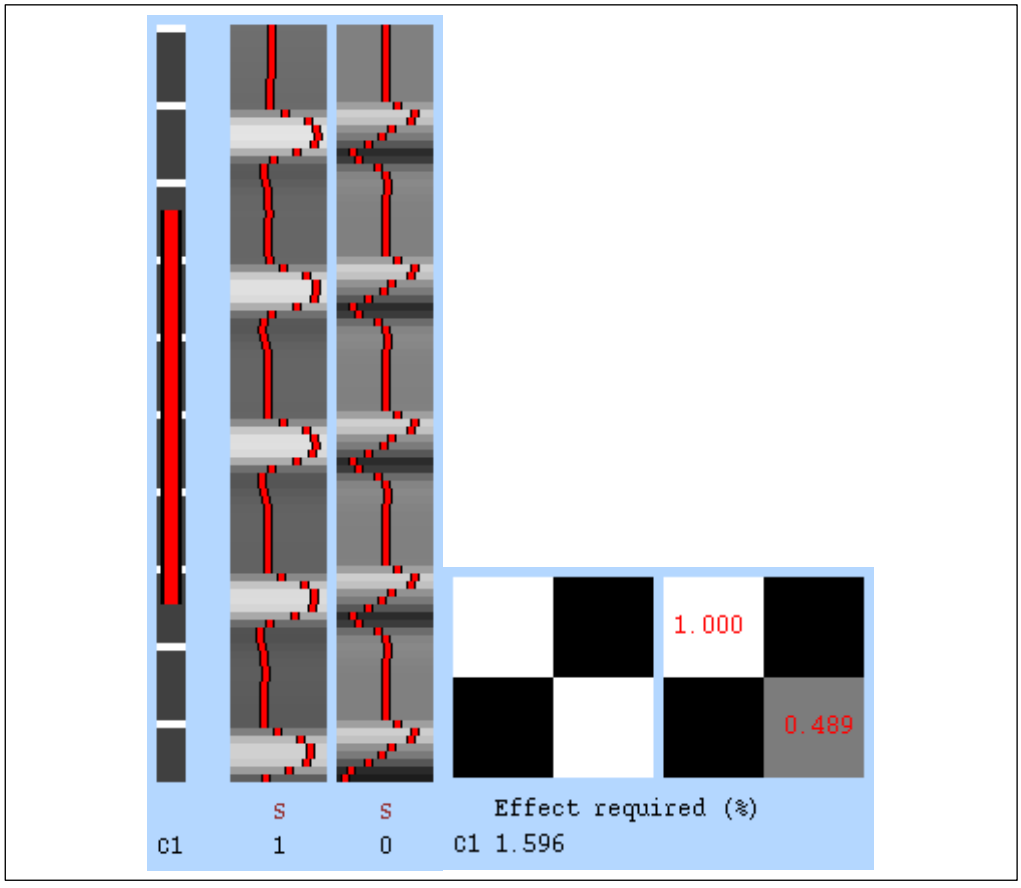

Figure 37 - *Statistical image results for subject S4 of Sweet Response Group.*
On the left, the Matrix Design set in the Stat tab of the FEAT gui, where S indicates the regressor established (i.e. the Stimulus), while C1 indicates the contrast associated to that kind of regressor. On the right, the Covariance Matrix associated to the regressor, together with the design efficiency reported as percentage of the effect required. As can be noticed, since the percentage of the contrast is below 2%, the result can be considered acceptable.

5.2.2. Registration and Normalization Results

The FEAT report html file offers the possibility of checking how good the Co-registration and Normalization processes have been via three main representations:

- The functional to high-res representation shows the functional image overlapped to the correspondent structural 2D image and vice versa (Figure 38, first panel).
- The high-res to standard representation shows the structural 2D image overlapped to the standard MNI template and vice versa (Figure 38, second panel).
- The functional to standard representation shows the functional image overlapped to the standard MNI template and vice versa (Figure 38, third panel).

The co-registration of the functional images to the 2D anatomical ones was successful for all the subjects for each taste. The normalization of the high-res anatomical image to the standard template was considered optimal in most cases, with exception of some subjects in which a slight upward translation of the structural image with respect to the MNI template was detected. This observation can be reflected as a consequence to the functional to standard representations.

In Figure 38, an example of successful co-registration and normalization process is reported, referred to the functional data of subject S2 belonging to the Sweet Stimulus Group.

In Figure 39, it is possible to notice the translation occurring during the normalization of the anatomical image to the standard space, which consequentially affects the normalization of the functional image to the MNI template. The example reported is from subject S4 of the Sweet Stimulus Group.

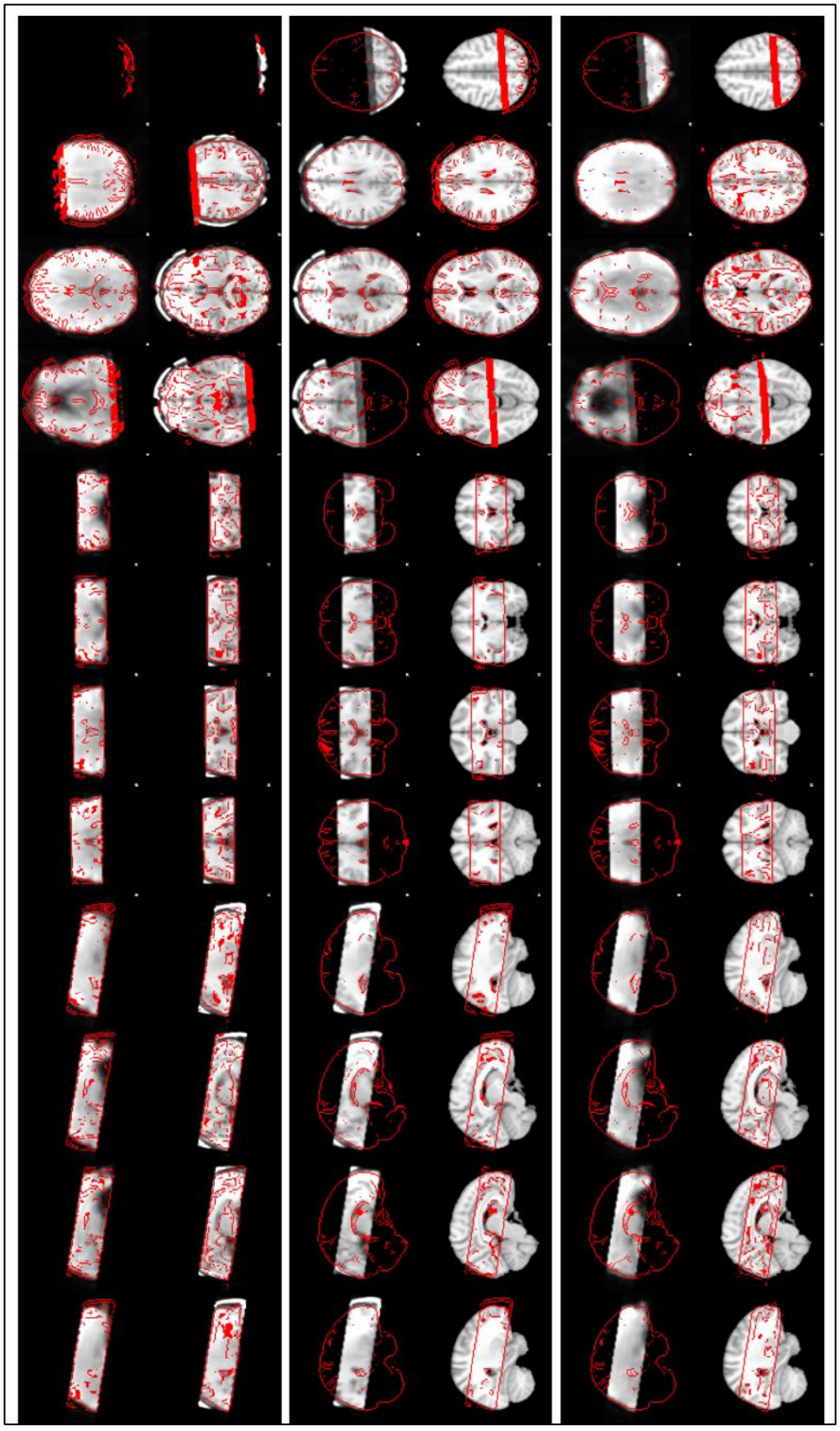

Figure 38 – *Registration and Normalization results for subject S2 of Sweet Stimulus Group.*
From left to right: the first panel shows the functional images (grey brain, first row) co-registered to the 2D anatomical image (redline), and vice versa in the second row; the second panel shows the 2D anatomical image (grey brain, first row) with respect to the red standard MNI template (redline), and vice versa in the second row; the third panel shows the functional image (grey brain) normalized with respect to the standard MNI template (redline), and vice versa in the second row.

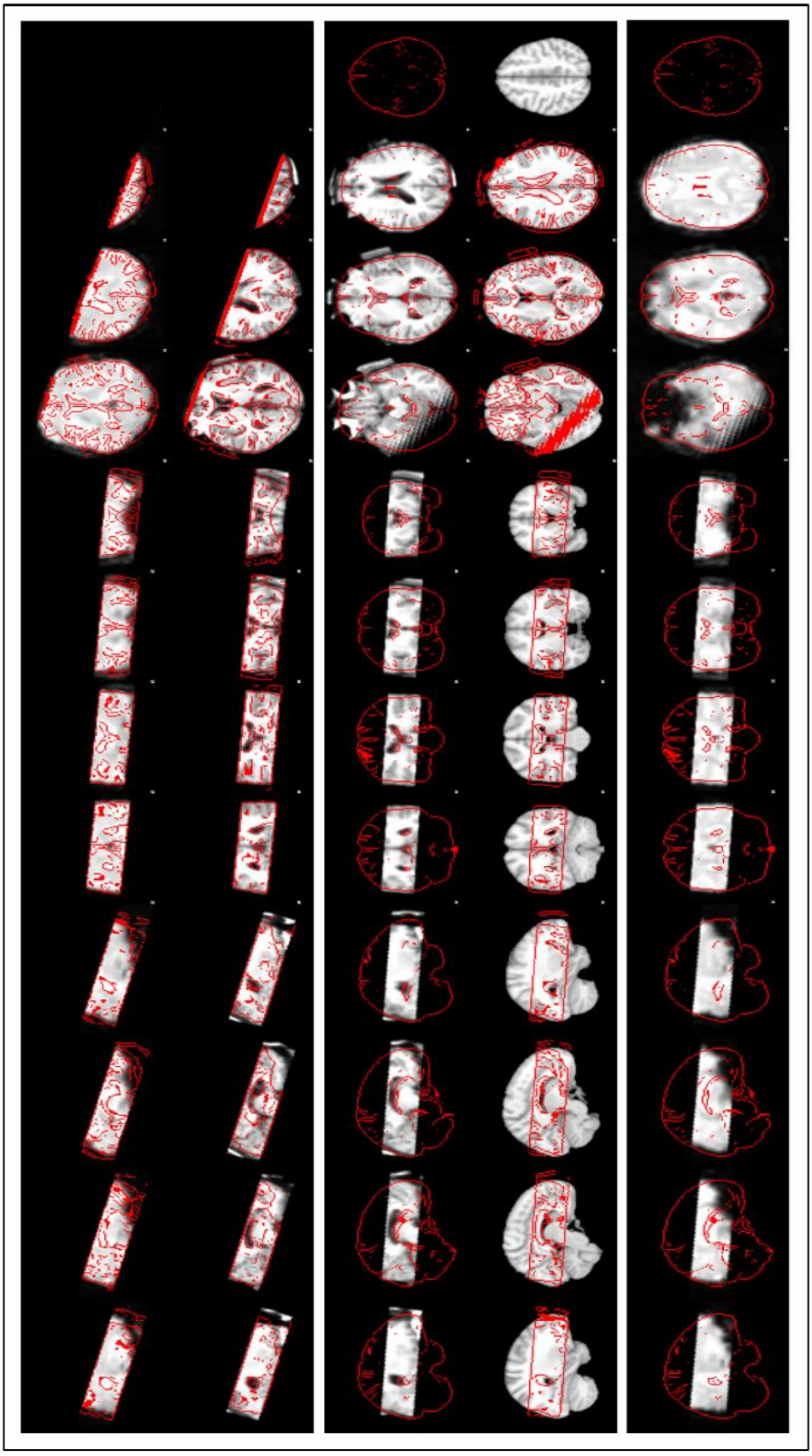

Figure 39 – *Registration and Normalization results for subject S4 of Sweet Stimulus Group.*
From left to right: the first panel shows the functional images (grey brain, first row) co-registered to the 2D anatomical image (redline), and vice versa in the second row; the second panel shows the 2D anatomical image (grey brain, first row) with respect to the red standard MNI template (redline), and vice versa in the second row; the third panel shows the functional image (grey brain) normalized with respect to the standard MNI template (redline), and vice versa in the second row.

5.2.3. Post-Stats Results

As final statistical result, FEAT generates a thresholded activation image for each contrast previously set in the Model Design tab. This is represented as a series of contrast activation maps, each one related to a specific correspondent brain slice of the given subject.

Furthermore, the html report gives a set of time-series plots for data vs model for peak Z voxels. The main FEAT report web page contains a single plot for each pre-set contrast: in the case of cluster-based thresholding, clicking on this image takes to the more significant clusters' list, which are reported according to both the voxel space and the Standard MNI Space. In this way, an initial check can be performed, to understand if the activation maps look like what is expected to be. After this initial check, it is possible to better visualize the resulting activation maps by opening on FSLeyes the correspondent COPE (Contrast Of Parameter Estimates) images placed inside the *.feat* directory.

An example of thresholded activation maps resulting from the Single-Subject Analysis of the same subject S2 in three different taste stimulation sessions, with correspondent time-series plot of the activated voxel is reported in Figures 40, 41 and 42. Although the gustative stimulus induces a bilateral cortical activation, in this thesis the attention was given to the ipsilateral activation voxels. This because the main pathway from taste receptors to the primary gustatory cortex is ipsilateral, and therefore more consistently observed.

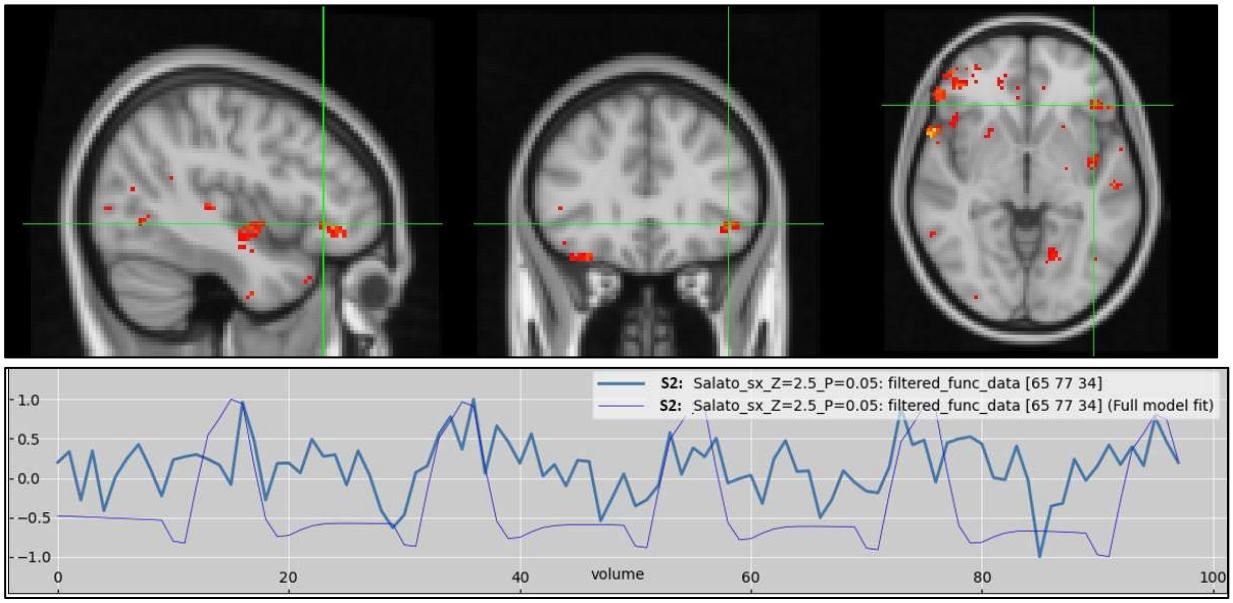

Figure 40 – *Ipsilateral cortical activation of subject S2 after salty stimulus visualized via FSLeyes. From left to right: sagittal plane (x canvas) representation, coronal plane (y canvas) representation and axial plane (z canvas) representation.* The more significant voxel related to the gustative information response is pointed by the green cursor, in correspondence of coordinates (-41,29,4) in MNI space, or (-40,25,0) in TALAIRACH space, indicating an ipsilateral activation within the primary gustatory cortex. According to the radiological convention, left hemisphere is on the right.

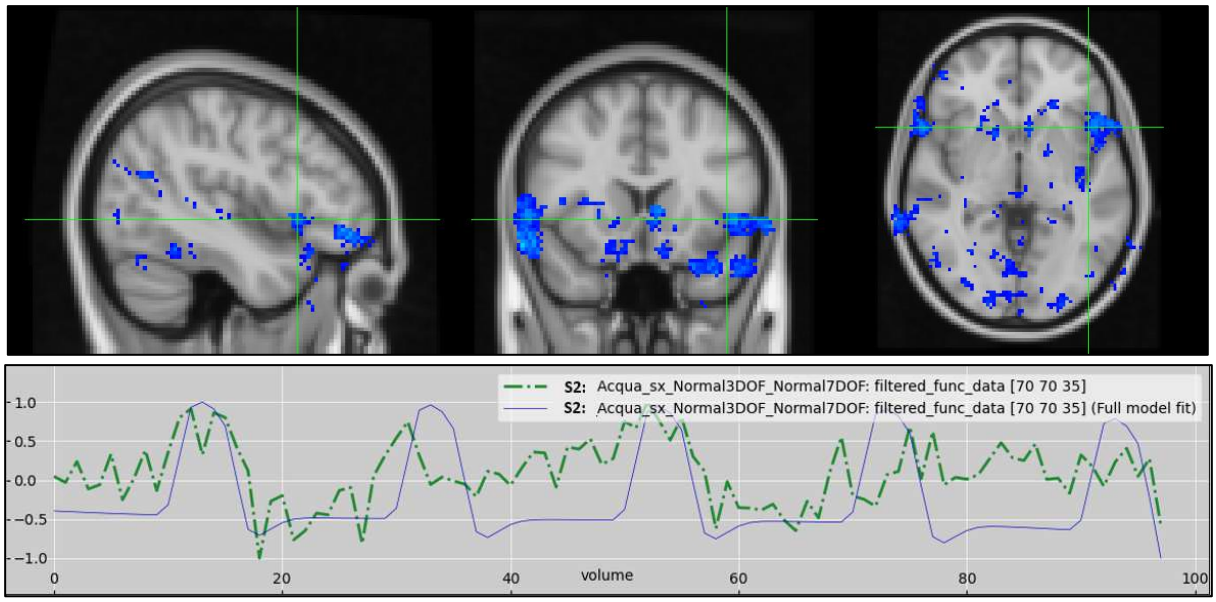

Figure 41– *Ipsilateral cortical activation of subject S2 after water stimulus visualized via FSLeyes. From left to right: sagittal plane (x canvas) representation, coronal plane (y canvas) representation and axial plane (z canvas) representation.* The more significant voxel related to the gustative information response is pointed by the green cursor, in correspondence of coordinates (-41,11,1) in MNI space, or (-43,15,-2) in TALAIRACH space, indicating an ipsilateral activation within the left-insula. According to the radiological convention, left hemisphere is on the right.

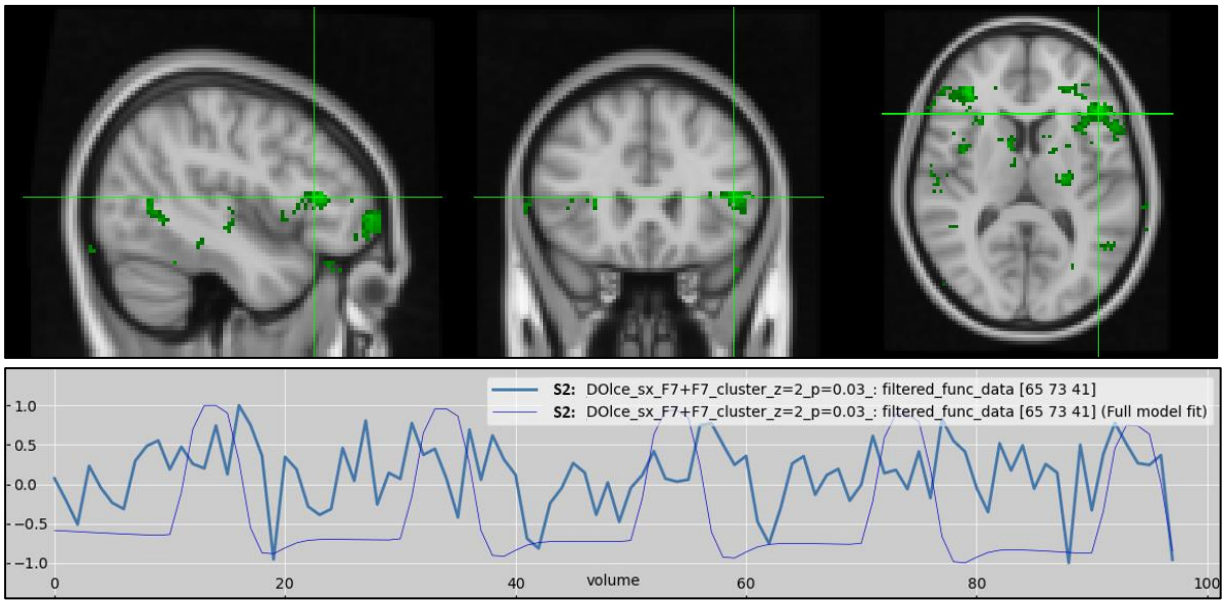

Figure 42 – *Ipsilateral cortical activation of subject S2 after sweet stimulus visualized via FSLeyes. From left to right: sagittal plane (x canvas) representation, coronal plane (y canvas) representation and axial plane (z canvas) representation.* The more significant voxel related to the gustative information response is pointed by the green cursor, in correspondence of coordinates (-41,23,10) in MNI space, or (-39,21,11) in TALAIRACH space, indicating an ipsilateral activation. According to the radiological convention, left hemisphere is on the right.

5.3 Group-Analysis Results

The Multi-Subject analysis report gives the thresholded activation maps represented across different brain slices of the average response of each given stimulus. As for the Single-Subject Analysis, it is possible to visualize the coordinates of the most significant voxels (or cluster) in the voxel or standard space. The COPE.nii files related to the averaged activation responses are then collected within a new folder denoted with whatever name previously set and followed by *".gfeat"*. By visualizing these results on FSLeyes, it was then possible to individuate for each significant cluster coordinate the correspondent location within the brain MNI template. The final representation showing the ipsilateral activation of each taste stimulus is reported in the following Figures 43, 44 and 45, with the correspondent MNI coordinates in description.

In Table 4 it is possible to see the MNI coordinates of the main cortical areas where neural activation due to gustative stimulation was detected in Group Analysis, with the correspondent translation in Talairach Space. Even though only the ipsilateral side was investigated, for completeness also the presence of the contralateral one was verified.

Stimulus	***Tailarach Space***		***MNI Space***	
	Contralateral GI	*Ipsilateral GI*	*Contralateral GI*	*Ipsilateral GI*
Salty	33,18,11	-37,13,4	35,20,7	-38,16,2
Neutral	33,18,10	-37,16,5	35,20,8	-38,19,3
Sweet	42,24,1	-36,12,4	42,24,-3	-38,15,6
	Contralateral SI	*Ipsilateral SI*	*Contralateral SI*	*Ipsilateral SI*
Salty	55,-17,10	-52,-34,26	58,-17,19	-54,-35,26
Neutral	46,-32,-1	-53,-32,28	48,-31,-6	-55,-33,28
Sweet	52,-14,13	-47,-27,26	55,-13,11	-47,-28,26
	Contralateral MI	*Ipsilateral MI*	*Contralateral MI*	*Ipsilateral MI*
Salty	47,-7,9	-41,-3,4	50,-6,6	-43,-1,1
Neutral	42,-6,8	-35,-10,7	45,-5,5	-37,-9,5
Sweet	37,-12,14	-38,-15,12	39,-11,12	-40,-14,10

Table 4 – *MNI coordinates of the main cortical activated areas resulting from the Group Analysis, with the correspondent translation in Talaiarach Space*. Even though only the ipsilateral side was investigated, for completeness also the presence of the contralateral one was verified.

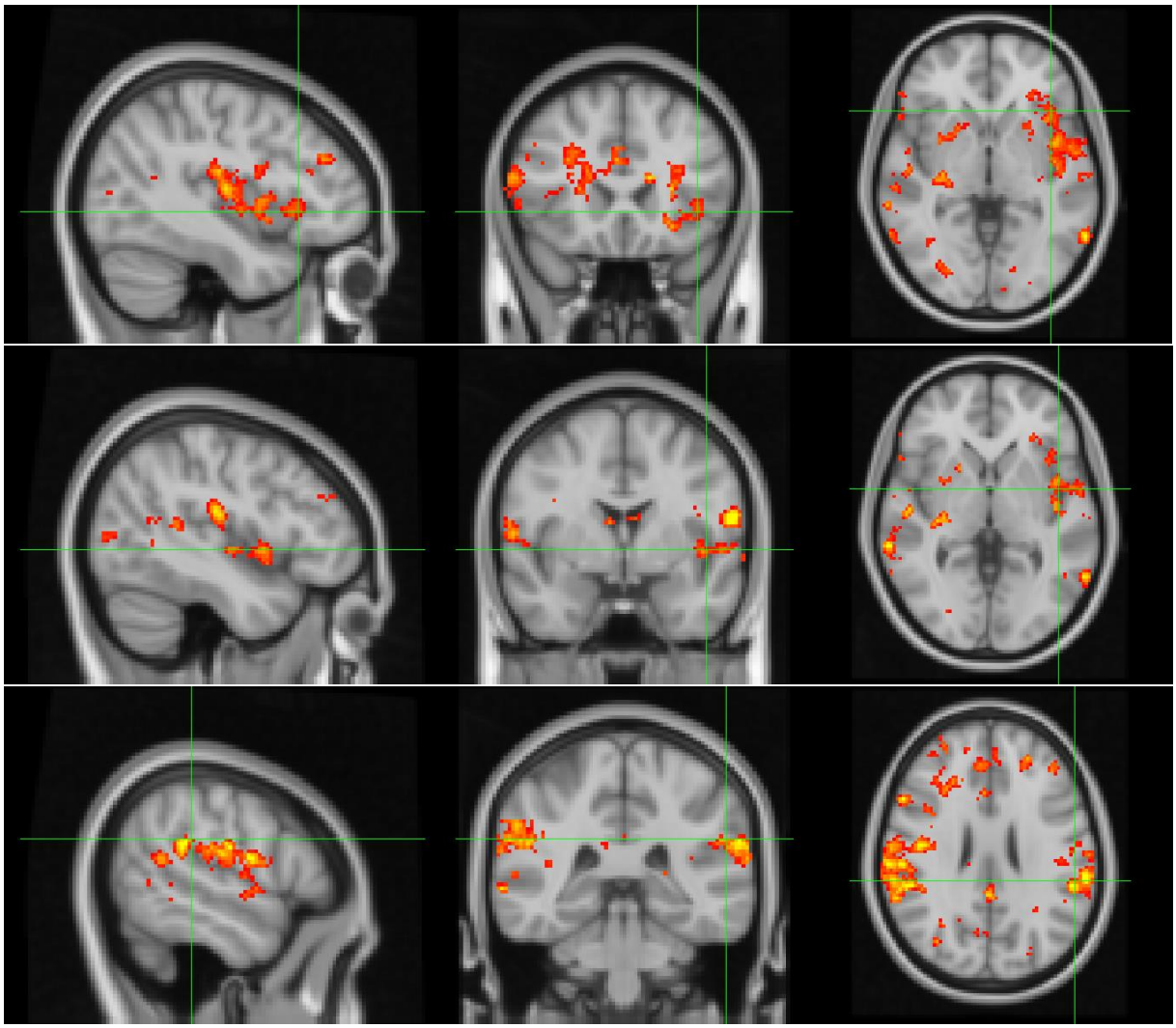

Figure 43 – *Averaged ipsilateral cortical activation elicited by salty stimulus of taste receptors in the healthy subjects of the Group Analysis.* In the top panel, the activated voxels are detected within the primary gustatory cortex (-38,15,6). In the middle panel, activation is detected in the middle-insula (50,-6,6). In the bottom panel, activation is detected in the ipsilateral primary somatosensory cortex (SI) (-54,-35,26). Z statistical values go from red (lower values) to yellow (higher values).

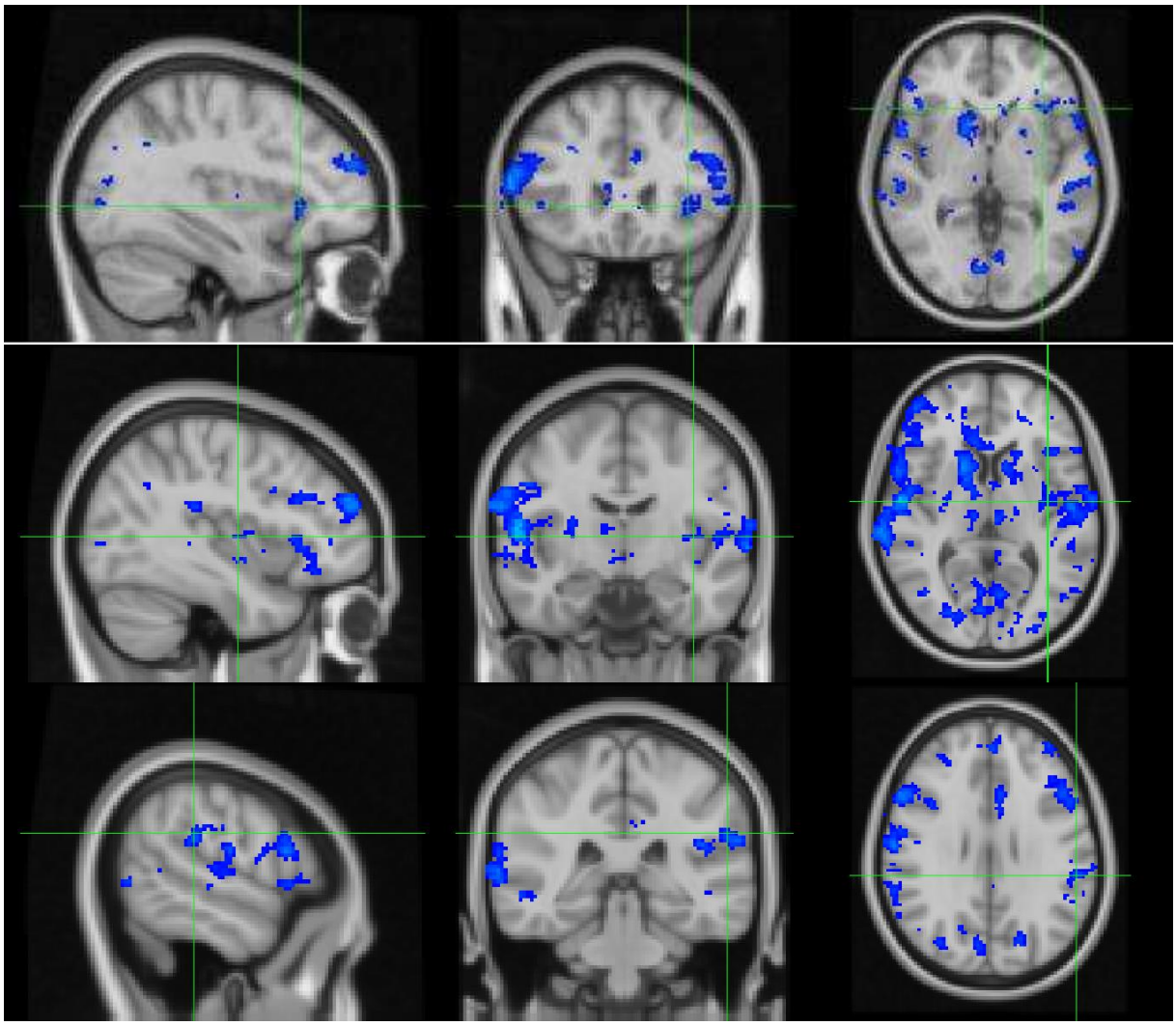

Figure 44 – *Averaged ipsilateral cortical activation elicited by neutral stimulus of taste receptors in the healthy subjects of the Group Analysis* In the top panel, the activated voxels are detected within the primary gustatory cortex,(-38,19,3). In the middle panel, activation is detected in the middle-insula (-37,-9,5). In the bottom panel, activation is detected in the ipsilateral primary somatosensory cortex (SI) (-55,-33,28). Z statistical values go from dark blue (lower values) to light blue (higher values).

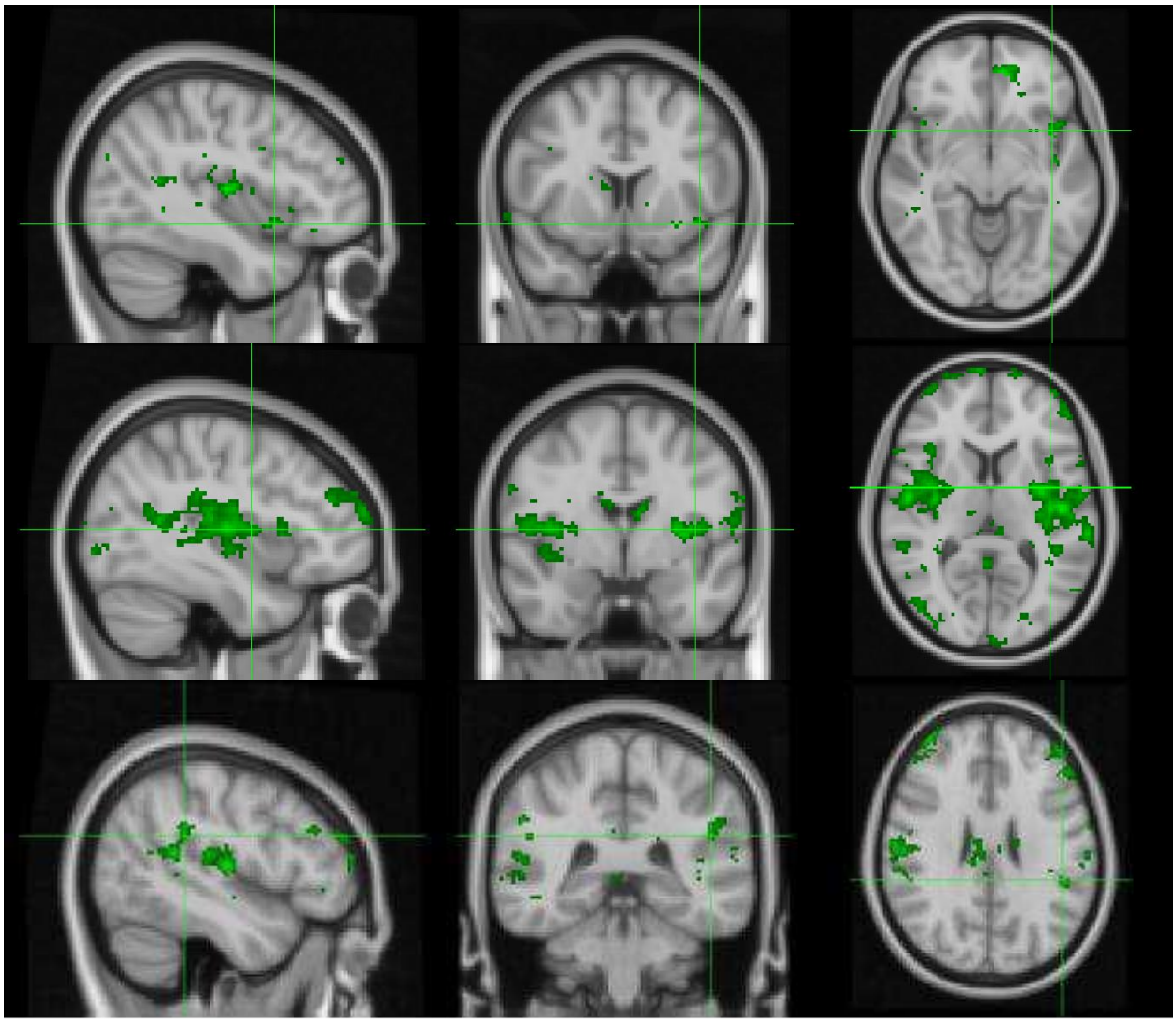

Figure 45 – *Averaged ipsilateral cortical activation elicited by sweet stimulus of taste receptors in the healthy subjects of the Group Analysis* In the top panel, the activated voxels are detected within the primary gustatory cortex (-38,15,6). In the middle panel, activation is detected in the middle-insula (-40,-4,10). In the bottom panel, activation is detected in the ipsilateral primary somatosensory cortex (SI) (-47,-38,26). Z statistical values go from dark green (lower values) to light green (higher values).

A final observation to be considered is related to the contralateral neural activation that can be detected as brain response to the tactile tongue stimulation given by the cotton pad during the experiment. Indeed, most of the participants showed a bilateral neural activity within the inferior part of the parietal lobe, in the primary somatosensory cortex, with predominance in the contralateral side with respect to where the stimulus was given (in this case, in the right side). An example of this neural activity for each taste stimulus group is reported on Figure 46.

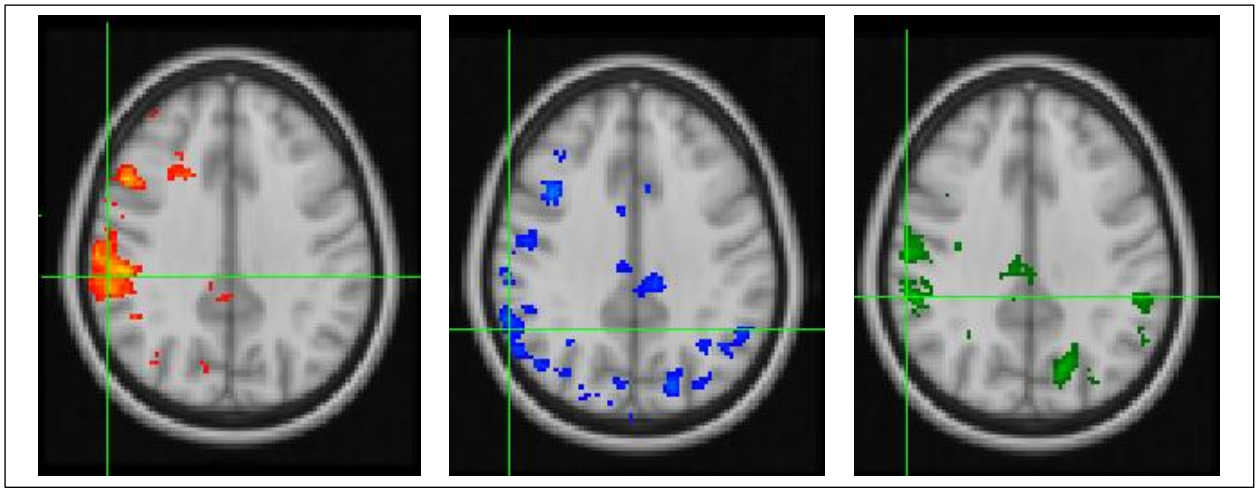

Figure 46 – *Contralateral tactile tongue representation in the primary somatosensory cortex, after salty (left), water (center) and sweet (right) stimulations of the left hemi-tongue.*

Finally, the z-thresholded activation maps obtained from each Group Analysis were exported given as input inside MRIcroGL software, where each image file was used as overlay onto a standard MNI template {30}. Here, a selection of the most significant cluster for each overlay was performed and each result was overlapped to the others, allowing to obtain a chemiotopic map representation of neural activity within the primary gustatory cortex onto the standard MNI152, visible on Figure 47.

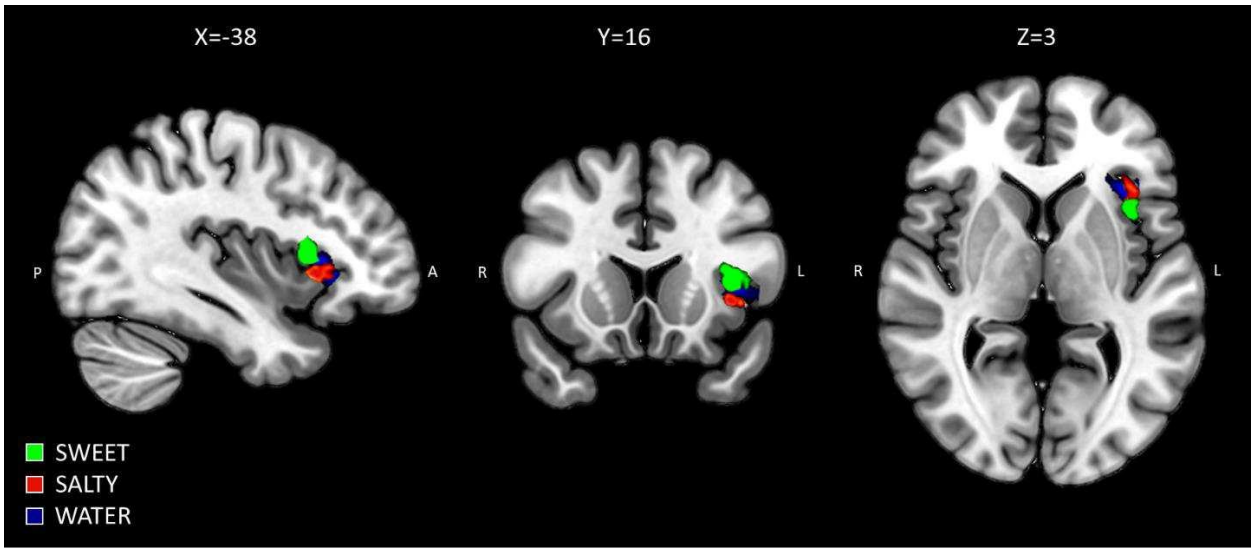

Figure 47 – *Chemiotopic map representation of salty (red), neutral (blue) and sweet (green) gustative stimulations of the left hemi-tongue.* According to the radiological convention, left hemisphere is on the right.

6. DISCUSSION

The aim of this Thesis was to investigate the ipsilateral neural cortical activation elicited by gustative stimulus given to the left hemi tongue, based on statistical analysis of task fMRI data executed by using the FEAT tool of FSL software.

The analysis was performed considering 7 of the initial total subjects, who underwent the taste experiment by adopting the 2nd protocol of stimulus administration. Since each taste session (for the same subject) had been performed separately from the others, not all of them had been executed with the same protocol. Therefore, only three individuals provided three different taste sessions each performed according to the 15s task protocol. More in detail:

- The neutral stimulus analysis was administered to four subjects (S1, S2, S3, S4).
- The salty stimulus analysis was administered to four subjects (S1, S2, S4, S5)
- The sweet stimulus analysis was administered to six subjects (S1, S2, S3, S4, S5, S6, S7).

Even though the results in most cases showed a bilateral activation (as suggested from the literature), this study focused on the ipsilateral cortical activation, that is known to be predominant for taste stimulations [3]. Therefore, since only left hemi tongue stimuli were considered, a greater attention was given to the analysis of the left side of the cortex. The results showed in most cases neural activations within cortical areas known to be involved in the primary processing of gustative information. More precisely, within the ipsilateral gustatory area, the ipsilateral primary somatosensory cortex and the ipsilateral middle insula, as can be noticed in Table 4 and Figures 43, 44 and 45.

A particular attention has to be given to the role of water as taste stimulus, which is a concept still under debate. Even though it has been often used in taste experiments as neutral stimulus, nowadays it is more considered as an independent taste stimulus [3], and for this reason it was reported as a taste in this study. Nevertheless, even though the activated cortical areas were those expected, in this case the z-stat value related to these activations was found lower than the other two stimuli. A possible reason of this might be related to the intensity of the taste stimulus, which in case of water administration may be less intense than salt or sweet.

In general, this fMRI results confirmed the expected ipsilateral activation of the middle insula and the primary gustatory cortex with salt, water and sweet stimulations applied in combination with a tactile stimulus to the left-side of the tongue. At the same way, also neural activation due

to tactile tongue stimulation was detected, with predominance in the contralateral side to the stimulus, as suggested in previous studies [2, 3]

Technical considerations and limits of the presents study

Some important technical considerations about this study can be explicated.

- A first limit of this statistical analysis was related to the normalization of the axial section's acquisitions. As many studies suggest, this is a critical process that, in case of task-fMRI analysis, completely condition the final results in terms of spatial localization. This issue is more emphasized when the purpose is looking for very small activation areas, as in this work. Therefore, it is often suggested to use high resolution cortical registration methods to improve the spatial correspondence across individual brains, as demonstrated in Prinster et al. [71]. In this work, the exclusive FSL usage was not completely successful in terms of spatial normalization, principally due to the incapacity of the software to perform a reliable registration in case of "*few fMRI slices*" (i.e. the field of view is small along the Z direction), either with the subject's structural image or directly to the standard space. The recommendation provided by the software in this case to obtain a good result is to take during the experiment a single whole-brain "functional" image, that should normally be the same kind of the initial functional image (4D input), but covering the whole brain (i.e. the initial fMRI image should be a subset of slices of the "whole-brain" functional image). In this way:
  1. a first co-registration of the fMRI data is performed to the *whole-brain functional image*,
  2. then, the whole-brain functional image is co-registered to the usual *high-res T1 weighted structural image*,
  3. finally, the high-res structural image is normalized with respect to the *standard.*

  By combining the transformation matrices resulting from these co-registrations, at the end it is possible to properly normalize the initial functional 4D input with respect to the standard space. Nevertheless, in the case of this study, it was not possible to use a whole brain functional image, which made the registration process more challenging with respect to whole-brain registrations. Among the different trials performed, the best results were obtained with that one using an initial external registration via FLIRT (already described in Methods). In this way, after the external registration an initial re-alignment of the functional data could be obtained, then re-defined by repeating a second registration within the FEAT

gui. By the way, only some of the 21 functional dataset (seven subjects, three tastes each) reached an optimal realignment and normalization, whereas the other ones gained the same orientation of the standard template, but with a minimal translation in the inferior-superior direction, that should have been affect the final statistical results from a in terms of punctual coordinates, even though the statistical analysis showed neural activations in the same cortical areas detected in previous studies (e.g. [3,5,9,15-18,20,22,23,71]).

- Another crucial topic to be considered is related to the kind of standard template used to perform the normalization process. Even though most of the task fMRI studies take as reference the Talairach Space, the FSL software library does not provide this kind of standard template. Therefore, this study was conducted by firstly considering the MNI152 template as reference, and then converting the resulting coordinates into the Talairach Space via the MNI2Talairach online tool. Nevertheless, as already anticipated in chapter 4, the conversion from MNI to Talairach Space is a critical process which leadsint to some errors related to the differences between these two types of standard templates. Many studies (e.g. [68]) have discussed about the crucial disparity between coordinates from brain spatially normalized using MNI templates with respect to those ones of the Talairach standard, and this difference varies according to the brain location, leading to confusion during comparisons. The mni2tal matlab tool (previously mentioned) generally reduces the mni-tal disparities for inferior brain areas but increases differences for the anterior, posterior and superior parts. Furthermore, the coordinate disparity changes also for different brain templates within the same fitting method, which means that using two different MNI templates (such as the MNI152 and the MNI305) within FSL, will lead to different results. Due to the current lack of an optimal mni2tal converter, results occurring from this study were mostly evaluated by considering the cortical area of the activation, rather than the specific correspondence between the resulting MNI coordinates and their conversion in Talairach space.

Intervariability and intravariability

A final consideration regards the inter-variability and intra-variability aspects of the final localization results.

- Previous studies had difficulties to demonstrate a chemiotopic organization of taste cortical processing in humans, presumably due to inter-individual anatomical variability of the primary gustatory cortex response [71]. Also in this case, even though the Single-Subject

Analysis satisfied the expectations in terms of gustative areas localization, the specific coordinates localized for each individual differed across subjects. Moreover, intervariability was indentified in terms of z-statistical intensity of the activation voxels, which was different across subjects, suggesting that different individuals perceive the same intensity of a given taste differently, as reported in many studies (such as [9]).

- For what concern the intra-variability pattern, it was also observed differences in terms of intensity of activation of different tastes within the same single-subject. More in detail, salty stimulus responses were characterized of a more intense neural activation, followed by the sweet and finally the neutral stimulus response. By the way, this might be also due to the fact that neurons that are tuned on a given taste, can respond differently according to the concentration of that taste, as suggested by [9].

Conclusion

The oral cavity and in particular the tongue give rise to many sensitive inputs from different receptors, which provide the brain of information about retronasal smell, taste, tactile and thermal sensation. The combination of all these information determines what is commonly known as "flavor". Due to the integration of these different sensitive inputs, an interesting objective has been to perform an experiment such to isolate as much as possible the only gustative contribution, with the purpose of identifying the correspondent cortical activation area. In order to achieve this aim, functional magnetic resonance images of healthy subjects were acquired, while experiencing different taste administration via a specific protocol designed such that only the eventual tactile stimulus might interfere with the gustative one. Then, the fMRI data were pre-processed and statistically analysed via the FEAT tool provided by the FSL software library. Results coming from the Single Subject and Group Analysis confirmed the expected ipsilateral activation of the anterior and middle insula and the primary gustatory cortex after different taste stimulation, together with the predominant contralateral tactile representation.

Some suggestions for future studies might be the following:

- ✓ In case of axial sections fMRI acquisitions to be investigated using FEAT from FSL software, it would be more practical to work provided of at list a single whole-brain functional image, with same technical characteristics of the functional sections; in this

way, each axial functional image would be firstly co-registered to the whole-brain functional image and then to the high-resolution structural image. This two-step co-registration performed prior to the normalization would allow to achieve the best alignment of the functional image to the standard template.

- ✓ If it is necessary to collect results in both MNI and Talairach spaces, it is crucial to adopt a reliable MNI-to-Talairach converter, which should take into account all the variances between MNI and Talairach Spaces, as well as the differences between the two types of MNI standard template (MNI-305 and MNI-152) that can be chosen from the various available software (such as SPM or FSL).

Bibliography

[1] D.G. Laing, A. Jinks - Flavour perception mechanisms; Trends in Food Science & Technology (1996), 7: 387-389

[2] B. Cerf-Ducastel, P. Van De Moortele, P. MacLeod, D. Le Bihan, A. Faurion - Interaction of Gustatory and Lingual Somatosensory Perception at the Cortical Level in the Human: A Functional Magnetic Resonance Imaging Study; Oxford University Press (2001), 371-383

[3] G. Mascioli, G. Berlucchi, C. Pierpaoli, U. Salvolini, P. Barbaresi, M. Fabri, G. Polonara – Functional MRI cortical activation from unilateral tactile-taste stimulation of the tongue; Physiology & Behaviour (2015), 221-229

[4] Martini, Timmons, Tallitsch – Anatomia Umana (Quarta edizione), EdiSES (2010)

[5] D.M. Small – Taste representation in the human insula; Brain Struct Funct (2010), 214: 551-561

[6] J.R. Gibbons, N.M. Sadic - Neuroanatomy, Neural Taste Pathway; Treasure Island (FL): StatPearls Publishing (2022)

[7] C.R. Noback, N.L. Stromiger, R.J. Demarest, D.A. Ruggiero – The Human Nervous System, Structure and Function (Sixth Edition); Humana Press (2005)

[8] I.E. De Araujo, S.A. Simon – The gustatory cortex and multisensory integration; Int J Obes (Lond) (2009), 33(Suppl 2): S34–S43

[9] M. A. Schoenfeld, G. Neuer, C. Tempelmann, K. Schübler, T. Noesselt, J.M. Hopf, H.J. Heinze – Functional Magnetic Resonance Tomography correlates of taste perception in the human primary taste cortex; Neuroscience (2004), 127: 347-353

[10] D.M. Small, D.H. Zald, M. Jones-Gotman, R.J. Zatorre, J.V. Pardo, S. Frey, M. Petrides – Human Cortical Gustatory Areas: A review of functional neuroimaging data; NeuroReport (1999), 10: 7-14

[11] K. Sakamoto, H. Nakata, M. Yumoto, R. Kakigi – Somatosensory processing of the tongue in humans; Frontiers in Physiology (2010), Integrative Phsysiology, Article 136

[12] L.C. Triarhou – Cytoarchitectonics of the Rolandic operculum: morphofunctional ponderings; Brain Structure and Function (2021), 226: 941 – 950

[13] J.M. Breza, K.S. Curtis, R.J. Contreras – Temperature Modulates Taste Responsiveness and Stimulates Gustatory Neurons in the Rat Geniculate Ganglion; J Neurophysiol (2006), 95: 674 – 685

[14] P. Haggard, L. De Boer – Oral somatosensory awareness; Neuroscience and Biobehavioral Revies (2014), 47: 469 – 484

[15] R. Vincis, A. Fontanini – Central taste anatomy and physiology; Handbook of Clinical Neurology (2019), 164, Chapter 12: 187 – 203

[16] E. Iannilli, N. Noennig, T. Hummel, A.M. Schoenfeld – Spatio-temporal correlates of taste processing in the human primary gustatory cortex; Neuroscience (2014), 273: 92 – 99

[17] E. Iannilli, V. Gudziol – Gustatory pathway in humans: A review of models of taste perception and their potential lateralization; J Neuro Res. (2018), 97(3): 230 – 240

[18] K. Onoda, M. Ikeda, H. Sekine, H. Ogawa – Clinical study of central taste disorders and discussion of the central gustatory pathway; J Neuro Res. (2012), 259:261 – 266

[19] M. Pandurangan, I. Hwang – Systemic Mechanism of Taste, Flavour and Palatability in Brain; Appl Biochem Biotechnol (2015), 175: 3133 – 3147

[20] D.M. Small – Flavor is in the brain; Physiology and Behavior (2012), 107: 540 – 552

[21] R.J. Stevenson, L.A. Miller, K. McGrillen – The lateralization of gustatory function and the flow of information from tongue to cortex; Neurophysiologia (2013), 51:1408 – 1416

[22] D.M. Small, G. Bender, M.G. Veldhuizen, K. Rudenga, D. Nachtigal, J. Felsted – The Role of the Human Orbitofrontal Cortex in Taste and Flavor Processing; New York Academy of Sciences (2007), 1121: 136 – 151

[23] J. Chikazoe, D.H. Lee, N. Kriegeskorte, A.K. Anderson – Distinct representations of basic taste qualities in human gustatory cortex; Nature Communications (2019), 10: Article 1048

[24] E.A. Disbrow, L.B.N. Hinkley, T.P.L. Roberts – Ipsilateral Representation of Oral Structures in Human Anterior Parietal Somatosensory Cortex and Integration of Inputs across the Midline; The Journal of Comparative Neurology (2003), 467: 487 – 495

[25] B. Cerf, D. Lebihan, P.F. Van de Moortele, P. Mac Leod, A. Faurion – Functional Lateralization of Human Gustatory Cortex Related to Handedness Disclosed by fMRI Study; Annals N.Y. Academy of Sciences (1998), 855: 575 – 578

[26] Y. Tamura, Y. Shibukawa, M. Shintani, Y. Kaneko, T. Ichinohe – Oral structure representation in human somatosensory cortex; NeuroImage (2008), 43: 128 – 135

[27] M.L. Blankenship, M. Grigorova, D.B. Katz, J.X. Maier – Retronasal Odor Perception Requires Taste Cortex but Orthonasal Does Not; Current Biology (2019), 29: 62 – 69

[28] B.G. Green – Studying Taste as a cutaneous sense; Food Quality and Preference (2002), 14: 99 – 109

[29] D.E. Harlow, L.A. Barlow – Embryonic Origin of Gustatory Cranial Sensory Neurons; Dev Biol. (2007), 310: 317 – 328

[30] S. Obiefuna, C. Donohe – Neuroanatomy, Nucleus Gustatory; Treasure Island (FL): StatPearls Publishing (2022)

[31] P.E. Ludwig, V. Reddy, M. Varacallo – Neuroanatomy, Central Nervous System (CNS); Treasure Island (FL): StatPearls Publishing (2021)

[32] L. Thau, V. Reddy, P. Singh – Anatomy, Central Nervous System; Treasure Island (FL): StatPearls Publishing (2021)

[33] H. Basinger, J.P. Hogg – Neuroanatomy, Brainstem; Treasure Island (FL): StatPearls Publishing (2022)

[34] I. Chen, F. Lui – Neuroanatomy, Neuron Action Potential; Treasure Island (FL): StatPearls Publishing (2022)

[35] S.D. Roper, N. Chaudhari – Taste buds: cells, signals and synapses; Nat. Rev Neurosci. (2017), 18: 485 – 497

[39] G.H. AlJulaih, S. Lasrado – Anatomy, Head and Neck, Tongue Taste Buds; Treasure Island (FL): StatPearls Publishing (2022)

[37] C. Spence – The tongue map and the spatial modulation of taste perception; Current Research in Food Science (2022), 5: 598 – 610

[38] K. Thomas, K. Minutello, J. M Das – Neuroanatomy, Cranial Nerve 9 (Glossopharyngeal); Treasure Island (FL): StatPearls Publishing (2022)

[39] O. Singh, J. M. Das – Anatomy, Head and Neck, Jugular Foramen; Treasure Island (FL): StatPearls Publishing (2022)

[40] M. Al-Chalabi, V. Reddy, I. Alsalman – Neuroanatomy, Posterior Column (Dorsal Column); Treasure Island (FL): StatPearls Publishing (2022)

[41] M. Al-Chalabi, V. Reddy, I. Alsalman – Neuroanatomy, SpinoThalamic Tract; Treasure Island (FL): StatPearls Publishing (2022)

[42] K.H. Jawabri, S. Sharma – Physiology, Cerebral Cortex Functions; Treasure Island (FL): StatPearls Publishing (2022)

[43] J.D. Nguyen, H. Duong – Neurosurgery, Sensory Homunculus; Treasure Island (FL): StatPearls Publishing (2022)

[44] A. Faurion, B. Cerf, P.F. Van De Moortele, E. Lobel, P. Mac Leod, D. Le Bihan – Human taste cortical areas studied with functional magnetic resonance imaging: evidence of functional lateralization related to handedness; Neuroscience Letters (1999), 277: 189 – 192

[45] S. Nacy, S. Kbah, H.A. Jafer, I. Al-Shaalan – Controlling a Servo Motor Using EEG Signals from the Primary Motor Cortex; published on ResearchGate (2016)

[46] I.E.T. De Araujo, M.L. Kringelbach, E.T. Rolls, P. Hobden – Representation of Umami Taste in the Human Brain; J. Neurophysiol (2003) 90: 313-319

[47] K. MacMahon, G. Cown, G. Galloway – Magnetic Resonance Imaging: The Underlying Principles; Journal of Orthopaedic & Sports Physical Theraphy (2020)

[48] L. Pauling, C.D. Coryell – The Magnetic Properties and Structure of Hemoglobin, Oxyhemoglobin and Carbonmonoxyhemoglobin; Proceedings of the National Academy of Sciences (1936), 22 (4): 210-216.

[49] S. Ogawa, T.M. Lee, A.R. Kay, D.W. Tank – Brain magnetic resonance imaging with contrast dependent on blood oxygenation; Proceedings of the National Academy of Sciences (1990), 87: 9868-9872.

[50] O.J. Arthurs, S. Boniface – How well do we understand the neural origins of the fMRI BOLD signal?; TRENDS in Neurosciences (2002), 25 (No. 1): 169.

[51] J.C. Gore – Principles and practice of functional MRI of the human brain; The Journal of Clinical Investigation (2003), 112: 4-9.

[52] R.C. Oldfield – The assessment and the analysis of handedness: the Edinburgh inventory; Neurpsychologia (1971), 9(1): 97 – 113

[53] S. Aglioti, G. Tassinari, M.C. Corballis, G. Berlucchi – Incomplete gustatory lateralization as shown by analysis of taste discrimination after callosotomy, J. Cogn. Neurosci (2000), 12: 238 - 245.

[54] S. M. Aglioti, G. Tassinari, M. Fabri, M. Del Pesce, A. Quattrini, T. Manzoni, G. Berlucchi – Taste laterality in the split brain; Eur. J. Neurosci, (2001); 13: 195 – 200.

[55] J.Q. Yang, R. Wang, Y. Ren et al. – Neuromorphic Engineering: From Biological to Spike-Based Hardware Nervous Systems; Wiley (2020), 32(52): 2003610

[56] J.Q. Yang, R. Wang, Y. Ren et al. – Neuromorphic Engineering: From Biological to Spike-Based Hardware Nervous Systems; Wiley (2020), 32(52): 2003610

[57] M.Z. Yildiz – Effects of Mechanical and Temporal parameters on tactile psychophysical responses; Published on ResearchGate (2013)

[58] M. Witt – Anatomy and development of the human taste system; Elsevier B.V. (2019), 164: 147 – 171

[59] M. Jenkinson, C.F. Beckmann, T.E.J. Behrens, M.W. Woolrich, S.M. Smith - FSL; Neuroimage (2012), 62:782 - 790

[60] R.A. Poldrack, J.A. Mumford, T.E. Nichols – Handbook of Functional MRI Data Analysis – Cambridge University Press (2011)

[61] M. Smith – Fast Robust Automated Brain Extraction; Human Brain Mapping (2002); 17: 143 – 155

[62] O. Esteban et al. – FMRIPrep: a robust preprocessing pipeline for functional MRI; Nat Methods (2019), 16(1): 111 – 116

[63] A.C. Evans, D. Collins, S. Mills, E. Brown, R. Kelly, T. Peters – 3D statistical neuroanatomical models from 305 MRI volumes; Nuclear Science Symposium and Medical Imaging Conference (1993), 3: 1813–17

[64] M. Jenkinson, S.M. Smith – A global optimisation method for robust affine registration of brain images; Medical Image Analysis (2001), 5(2):143-156

[65] M. Jenkinson, P.R. Bannister, J.M. Brady, and S.M. Smith – Improved optimisation for the robust and accurate linear registration and motion correction of brain images; NeuroImage (2002), 17(2):825-841

[66] P. Jezzard, P.M Matthews, S.M. Smith – Functional Magnetic Resonance Imaging: An Introduction to Methods; Oxford University Press (2001), 75(1): 6 – 12

[67] D.B. Parker, Q. Razlighi – The Benefit of Slice Timing Correction in Common fMRI Preprocessing Pipelines (2019), 13:821.

[68] J.L. Lancaster, D. Tordesillas-Gutiérrez, M. Martinez, F. Salinas, A. Evans, K. Zilles, J.C. Mazziotta, P.T. Fox – Bias between MNI and Talairach coordinates analyzed using the ICBM-152 brain template; Human Brain Mapping (2017), 28 (11): 1194-1205.

[69] M. Brett, W. Penny, S. Kiebel – An Introduction to Random Field Theory (2003)

[70] K.J. Friston, C.D. Frith, P.F. Liddle, R.S.J. Frackowiak. Comparing functional (PET) images: The assessment of significant change; Journal of Cerebral Blood Flow and Metabolism (1991), 11:690–699.

[71] A. Prinster, E. Cantone, V. Verlezza, M. Magliulo, G. Sarnelli, M. Iengo et al. – Cortical representation of different taste modalities on the gustatory cortex: A pilot study; PLoS ONE (2017), 12(12): e0190164.

Sitography

{1} McGraw Hill Medical site – Anatomy of the Brain
https://accessmedicine.mhmedical.com/content.aspx?sectionid=202020846&bookid=2478&Resultclick=2

{2} ScienceDirect site – Cerebrum
https://www.sciencedirect.com/topics/neuroscience/cerebrum

{3} SlidePlayer site – Human Anatomy 13 Part 1: The Central Nervous System
https://slideplayer.com/slide/9288904/

{4} Openstax CNX site – Principles of Biology, Chapter 27, Nervous System
https://cnx.org/contents/24nI-KJ8@27.4:pMqJxKsZ@10/Nervous-System

{5} Cleveland Clinic site – Neurotransmitters
https://my.clevelandclinic.org/health/articles/22513-neurotransmitters

{6} StatPearls site – Cranial Nerves
https://www.ncbi.nlm.nih.gov/books/NBK549830/figure/article-26421.image.f3/?report=objectonly

{7} EnM (Endocrinology and Metabolism) site – Recent Advances in Understanding Peripheral Taste Decoding: 2010 to 2020
https://www.e-enm.org/journal/view.php?doi=10.3803/EnM.2021.302

{8} Cleveland Clinic – Health Library, Thalamus
https://my.clevelandclinic.org/health/body/22652-thalamus

{9} NIH (National Institute of Neurological Disorders and Stroke) – Brain Basics: The Life and Death of a Neuron *https://www.ninds.nih.gov/health-information/public-education/brain-basics/brain-basics-life-and-death-neuron*

{10} Healthline – An Easy Guide to Neuron Anatomy with Diagrams
https://www.healthline.com/health/neurons

{11} TeachMeAnatomy – The Trigeminal Nerve (CN V)
https://teachmeanatomy.info/head/cranial-nerves/trigeminal-nerve/

{12} TeachMeAnatomy – The Facial Nerve (CN VII)
https://teachmeanatomy.info/head/cranial-nerves/facial-nerve/

{13} TeachMeAnatomy – The Vagus Nerve (CN X)
https://teachmeanatomy.info/head/cranial-nerves/vagus-nerve-cn-x/

{14} Queensland Brain Institute – Action Potentials and synapses
https://qbi.uq.edu.au/brain-basics/brain/brain-physiology/action-potentials-and-synapses

{15} Scientific American, Making sense of taste
https://www.scientificamerican.com/article/making-sense-of-taste-2006-09/

{16} Wiley Online Library: Magnetic Resonance Imaging: Physical Principles and Sequence Design, Second Edition
https://onlinelibrary.wiley.com/doi/book/10.1002/9781118633953
{17} National Institute of Biomedical Imaging and Bioengineering (NIH) site: Magnetic Resonance Imaging (MRI)
https://www.nibib.nih.gov/science-education/science-topics/magnetic-resonance-imaging-mri

{18} Radiology key – Fastest Radiology Insight Enging site
https://radiologykey.com/magnetic-resonance-basics-magnetic-fields-nuclear-magnetic-characteristics-tissue-contrast-image-acquisition/

{19} BrainKart site – Radiology – Magnetic Resonance Imaging
https://www.brainkart.com/article/Magnetic-Resonance-Imaging_25293/.)

{20} MRI Questions site – Question and Answers in MRI
https://mriquestions.com/does-boldbrain-activity.html

{21} MRIcron official site:
https://www.nitrc.org/projects/mricron

{22} The Center of Morphometric Analysis site (Harvard Medical School)
https://cma.mgh.harvard.edu/

{23} The McConnell Brain Imaging Centre site
http://www.bic.mni.mcgill.ca/ServicesAtlases/HomePage).

{24} FLIRT – FSL User Guide
https://fsl.fmrib.ox.ac.uk/fsl/fslwiki/FLIRT/UserGuide

{25} MNI2Talairach matlab converter: *https://it.mathworks.com/matlabcentral/fileexchange/87047-mni2atlas*

{26} MNI2Talairach BioImage Suite Tool: *https://bioimagesuiteweb.github.io/webapp/mni2tal.html*

{27} BrainMap: the MNI and Talairach atlas: *https://brainmap.org/training/BrettTransform.html*

{28} Stats – GLM (General Linear Model)) – FEAT User Guide
https://fsl.fmrib.ox.ac.uk/fsl/fslwiki/FEAT/UserGuide#Stats_.28First-level.29

{29} GLM – Experimental Designs for Group Analysis – FEAT User Guide
https://fsl.fmrib.ox.ac.uk/fsl/fslwiki/GLM#Experimental_Designs_-_No_repeated_measures

{30} MRIcroGL software – NTRC site
https://www.nitrc.org/projects/mricrogl

Ringraziamenti

A conclusione di questo elaborato, vorrei ringraziare chi ha contribuito alla sua realizzazione.

Il primo ringraziamento va alla mia relatrice Mara Fabri, che con infinita disponibilità mi ha seguito durante tutto il percorso di tirocinio e stesura della tesi.

Ringrazio inoltre le mie correlatrici Laura Burattini ed Ilaria Marcantoni, per il massimo supporto ricevuto e per avermi dato la possibilità di svolgere questo tirocinio presso il Dipartimento di Ingegneria dell'Informazione.

Ho il piacere di ringraziare anche chi non ho conosciuto in prima persona, ma senza i quali non avrei mai potuto svolgere questo lavoro. Queste persone sono il Prof. Gabriele Polonara, direttore della Neuroradiologia dell'Ospedale Regionale di Torrette e responsabile dell'apparecchiatura di Risonanza Magnetica, e Luigi Imperiale e Lucio Montesi, Tecnici di Neuroradiologia, che hanno provveduto all'acquisizione ed al salvataggio dei dati.

Grazie ad Elena, che, con la sua disponibilità e solarità, mi ha permesso di capire quanto sia importante la solidarietà e il supporto reciproco.

Un ringraziamento particolare va alla mia famiglia e ad Eugenio, per tutte le volte che hanno creduto in me molto più di quanto io non credo in me stessa.

Grazie a tutti i miei coinquilini, ciascuno dei quali mi ha regalato un pezzo di sé, e mi ha permesso di conoscere meglio un pezzo di me.

Infine, ringrazio Eleonora, Emanuele, Giulia e Melisa. Siete stati la mia seconda famiglia. Grazie.